Nanoparticle delivery of anti-tuberculosis drugs

Formulation and testing of clofazimine containing nanoparticles using a zebrafish embryo tuberculosis model

Håkon Høgset

Department of Biosciences

Faculty of Mathematics and Natural Sciences

UNIVERSITY OF OSLO

February 2016

Acknowledgements

First, I would like to thank professor Gareth Griffiths for accepting me in his group and for giving me the opportunity to work in an encouraging and stimulating environment. I would also like to give a big thanks to Federico Fenaroli, my co-supervisor, who instructed, supported and challenged me throughout this project. Thanks also to Martin Speth, Jon Hildahl and Urska Repnik, who have all provided me with great help during the cell work in this thesis. I am also grateful to all former and present members of the Griffiths group, Lasse Evensen, Patrick L. Johansen, Signe Løvmo, Lilia Ulanova, Carina Vibe, Jørgen Benjaminsen and Shahla Bagherifam.

Thanks also to Bård Mathiesen and Håken Christensen for help and support running the zebrafish facility. My appreciation goes to Barbara Claro for helping me with the DLS measurements and interpretations, and thanks to Steven Wilson for helping us with the HPLC measurements. Great thanks also go to Ana Tavara and Montse Bargalló for assisting us with zebrafish embryos throughout the project. I am also grateful to PCI Biotech who provided us with chitosan particles for this work.

My final thanks go to all my friends and family who have supported me during the project. I am very grateful for my parents who always helped and supported me; special thanks must go to my father Anders who has given me invaluable feedback during the process. Finally, yet importantly, I want to thank my wonderful girlfriend Line who also is my most important friend and motivator.

Oslo, February 2016

Håkon Høgset

Abstract

Tuberculosis is an infectious disease that, despite the introduction of antibiotics over 50 years ago still causes more than 1.3 million deaths per year. The last decades have seen the emergence of multi-drug resistant tuberculosis (MDR-TB) bacteria that require treatments lasting up to 2 years and the use of more toxic and less effective drugs than in the treatment of drug-susceptible tuberculosis. Improving the treatment against MDR-TB is therefore of uttermost importance. Clofazimine (CFZ) is an anti-leprosy drug that is currently used as a last resort in treatment of MDR-TB. Despite conflicting reports on its effect, recent studies have associated CFZ with highly effective treatment of MDR-TB. CFZ treatment leads to massive skin and tissue drug accumulation and formation of intracellular inactive drug deposits. This is likely to hamper the treatment effect, and also causes visible skin discoloration in treated patients. Improved delivery of CFZ at the infection site could therefore potentially both enhance the therapeutic effect and reduce the side effects of the drug.

Animal studies using different drug-loaded polymeric nanoparticles (NP) have shown that they localise at tuberculosis infection sites and lead to an enhanced therapeutic outcome. In this work, we wished to develop a NP treatment approach with CFZ. Firstly, we tested several ways to formulate polymeric CFZ-NP. Using nanoprecipitation, we managed to find conditions for encapsulation of CFZ into the biocompatible polymer poly (lactic-co-glycolic) acid (PLGA). By refining the encapsulation technique, we found a way to reproducibly formulate PLGA-CFZ NP in a narrow size-range well suited for studies in biological systems. In macrophages, the encapsulated CFZ behaved strikingly different from CFZ in its free form. Thus, the PLGA-CFZ NP were present in the macrophages as large aggregations with a prolonged retention in the cells. Importantly, the PLGA-CFZ NP demonstrated drastically reduced macrophage toxicity as compared to the free drug. The therapeutic effect of the PLGA-CFZ NP was tested against *Mycobacterium marinum* infections in a zebrafish embryo tuberculosis model. Although a tendency towards a therapeutic effect was seen in some experiments, the overall therapeutic outcome was unclear. The most promising result was obtained by combining treatment with PLGA-CFZ NP with the tuberculosis first-line drug rifampicin, and such combination regimens is a promising approach that should be explored in further studies.

Selected abbreviations

BCG	Bacille Calmette-Guérin
BSA	Bovine serum albumin
CFU	Colony forming units
CFZ	Clofazimine
CLDI	Crystal-like drug inclusions
CV	Crystal violet
DABCO	1,4-diazabicyclo[2.2.2]octane
DAPI	4',6-diamidino-2-phenylindole
DCM	Dichloromethan
DMSO	Dimethyl sulfoxide
Dpi	Days post infection
Dpt	Days post treatment
ETH	Ethambutol
FCS	Fetal calf serum
FDA	American food and drug administration
INH	Isoniazid
M.m	*Mycobacterium marinum*
M.tb	*Mycobacterium tuberculosis*
M-CSF	Macrophage colony-stimulating factor
MDR-TB	Multi-drug resistant tuberculosis
MIC	Minimum inhibitory concentration
MOI	Multiplicity of infection
NP	Nanoparticles
OD_{600}	Optical density at 600 nm
PBS	Phosphate buffered saline
PFA	Para-formaldehyde
PLGA	Poly(lactic-co-glycolic) acid
PVA	Polyvinyl alcohol
PVP	Polyvinyl pyrrolidone
PZA	Pyrazinamid
Rcf	Relative centrifugal force

RIF	Rifampicin
rpm	Revolutions per minute
RPMI	Roswell park memorial institute cell medium
TB	tuberculosis
TEM	Transmission electron microscopy
THF	Tetrahydrofuran
Tween 80	Polyoxyethylene (20) sorbitan monooleate
v/v	Volume/volume
WHO	World Health organization
XDR-TB	Extensively-drug resistant tuberculosis

Table of Contents

1 Introduction

1.1 Tuberculosis

1.1.1 Tuberculosis and man

Tuberculosis (TB) is a disease that has afflicted humans through all of their modern history, and it was known already to Hippocrates (Daniel 2006). Even though effective modern health care systems have made TB a treatable disease, its presence is still very pronounced in many countries. Thus, 1.3 million people die from TB infections each year, and an estimated 8.6 million people get newly infected every year (WHO 2013). Also, as many as 2.2 billion people carry a latent TB infection, with a 10% chance of developing active disease throughout lifetime – resulting in a large reservoir of TB (WHO 2013).

A major breakthrough in the understanding of TB came when its causative agent, the bacillus *Mycobacterium tuberculosis* (*M.tb*) was unveiled in 1882, when Robert Koch famously demonstrated its role in the infection in a lecture to the Berlin Physiological Society (Koch 1932, Schluger 2005). After Koch's discovery followed decades of progress towards fighting TB. Clemens Freheirr von Pirquet discovered a positive immune reaction after subcutaneous injection of tuberculin – a protein derivative from *M.tb*. Further improvements on this finding led to the development of the tuberculin skin diagnostic test (TST) in the 1930's. TST is still in use today and makes it possible to diagnose latently infected individuals (Daniel 2006). In the same period, Albert Calmette and Camille Guerin at the Pasteur Institute developed the BCG-vaccine by attenuating *Mycobacterium bovis*, a close relative of *M.tb* (Daniel 2006). This vaccine has been used until today although it is mostly effective against childhood TB, and has little effect against adult TB (Verma and Grover 2009).

Man's stance against TB improved even more with the discovery and development of antibiotics. In 1944 Waksman and Schatz discovered streptomycin, the first drug with an evident effect against TB (British research council, 1948) and, in the following years, several new drugs were introduced to treat TB. Among these were rifampicin (RIF), isoniazid (INH), pyrazinamide (PZA) and ethambutol (ETH) which eventually led to the development of the current drug regime (Mitchison and Davies 2012), were

these four drug are administered together over a period of 6 months. However, as will be further discussed below (chapter **1.2.1**) this treatment regime is in many ways sub-optimal, meaning that TB still represents a major health problem on a global basis.

1.1.2 Tuberculosis pathogenesis

TB is an airborne disease that is transmitted through coughing and sneezing from an infected individual. Small droplets containing as few as one single bacterium can enter the alveoli of a non-infected individual, and one such droplet is enough to provoke an infection (Wells, Ratcliffe et al. 1948, Dannenberg 2006). In the alveoli, the bacteria are ingested by alveolar macrophages, which constitute the first-line defence against particles and infectious agents in the lungs. Alveolar macrophages are usually highly activated, and effectively kill intruding bacteria. However, if the macrophage fails to do so, the bacteria can multiply intracellularly and eventually destroy the macrophage (Dannenberg 2006). New, non-activated macrophages are recruited from the blood stream and they ingest the released bacteria (Russell 2007) (**Figure 1.1**). Because they are not activated, these macrophages do not efficiently kill the bacteria, and *M.tb* can grow exponentially inside them (Dannenberg 2006). During this process more macrophages are recruited and infected and uninfected macrophages start clustering together, marking the beginning of the tubercle bacterial lesion called the granuloma (Davis, Clay et al. 2002).

The adaptive immune system responds slowly to TB infection and an adaptive immune response is usually not effective until after 2-3 weeks (Cooper 2009). Recruitment of adaptive immune cells to the granuloma usually coincides with the end of the bacterial exponential growth (Russell, Cardona *et al.* 2009). Macrophages containing bacteria start to die, and many of the granulomas then develop a necrotic caseum core into where the bacteria are released. The necrotic core is hypoxic and bacteria often do not grow well there (Rustad, Sherrid et al. 2009). Hence, unless the bacteria are taken up by new non-activated macrophages their growth is arrested (Dannenberg 2006). However, the bacteria are not killed and the bacterial lesion enters a stalemate between the bacteria and the immune system. Thus, if the necrotic core gains access to the vasculature, and thereby oxygen, the bacteria can

start growing again, and can be released to the outside world via the airways to infect new individuals (Grosset 2003).

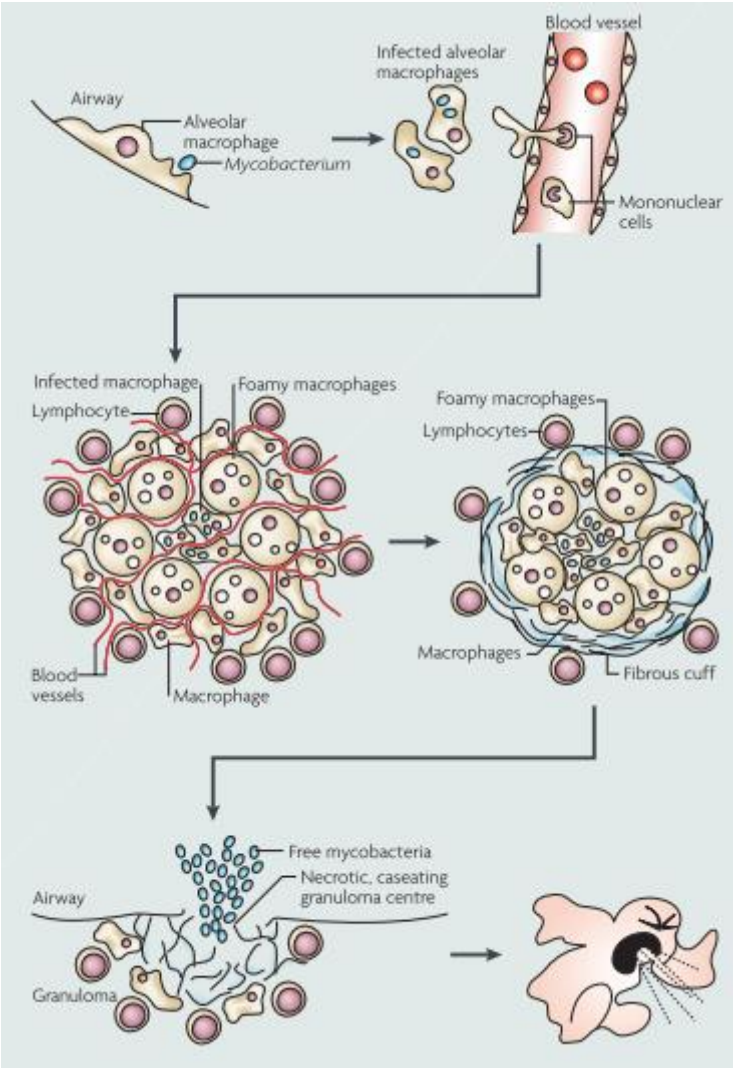

Figure 1.1: A schematic drawing of the pathogenesis of TB including the formation of the granuloma. The figure is taken from Russell (Russell 2007)

1.1.3 Granulomas - the interaction between pathogen and host

Granulomas are formed by aggregation of immune cells into well-organized structures that the body uses as an attempt to control an infection. The formation of granulomas is a hallmark feature of TB and much effort has been put into understanding their role in tuberculous pathology. The early granuloma progression is characterized by differentiation of macrophages into granuloma-specific

morphotypes. These include inter-digitated epithelioid cells, multi-nucleated giant cells (Ramakrishnan 2012), and most notably foamy macrophages filled with lipid droplets (Russell, Cardona et al. 2009) **(Figure 1.1)**. The outer part of the granuloma is often formed by lymphocytes recruited after the onset of the adaptive immune response. As the granulomas progress, they become increasingly more compact and organized. Sometimes a fibroblast-rich fibrous cuff develops around the granuloma, giving it a stratified appearance in histological sections (Leong, Dartois et al. 2010).

Originally thought to be solely a static, host defensive mechanism, the granuloma is now considered to have a more complex and dynamic role in TB pathogenesis. Granulomas can be formed without the aid of adaptive immunity (Davis, Clay et al. 2002), and work on mycobacterial infection in zebrafish by the group of Ramakrishnan has demonstrated that granulomas can contribute to dissemination of the disease, mainly by seeding new granulomas by infected macrophages (Davis and Ramakrishnan 2009).

Human granulomas show great variety and they progress or heal as individual entities (Flynn, Chan et al. 2011). In some granulomas, the immune system gets the upper hand and the bacteria are killed. The granulomas then heal and resolve, leaving a fibrous scar. The granulomas can also fail to heal and remain active. This can lead to a breakdown of the granulomas and release of active virulent bacteria into the bronchioles where they may spread. The third possibility is that the granulomas develop into latent granulomas, containing viable, but non-active, bacteria. This is thought to be the most frequent outcome and gives a latent tuberculous infection that can be reactivated at a later stage.

1.1.4 Latency and secondary tuberculosis

Patients who develop the active form of TB on the first encounter with *M.tb* are said to suffer from primary TB. Much more likely, however, is it that the first infection leads to a latent TB, in fact, as much as 90 % of primary TB cases recover spontaneously (Hunter 2011). Latent TB is defined as a positive tuberculin test without any other signs of active pathology (Barry, Boshoff et al. 2009). Persons with a latent TB have a 5-10% chance of reactivation, leading to active TB later in life; and this, so-called secondary TB, is thought to be the reason for as much as 80% of the active TB cases

in the world (Hunter, Jagannath et al. 2007). Why and how TB is reactivated is not known, but it is thought that most cases are caused by reactivation of inactive bacteria rather than re-infection (Andrews, Noubary et al. 2012). The reactivation involves a high number of foamy macrophages and takes place in the upper lobes of the lungs (Russell, Cardona et al. 2009). Secondary TB may also cause caseous necrosis and eventually release of bacteria. If the necrotic regions break into the bronchioles bacteria can be coughed out and transmitted; thereby completing the TB infection cycle **(Figure 1.1)**.

1.1.5 *Mycobacterium tuberculosis* inside the macrophage

M.tb has major parts of its lifecycle inside macrophages, and the ability to enter and replicate inside these cells is critical for the bacteria. *M.tb* mainly enters macrophages by phagocytosis and can bind to and enter the cells through many different cell surface receptors. Among these are mannose receptors, CD14 binding receptors, scavenger receptors and Fc-γ receptor, (Ernst 1998). Because of the phagocytic uptake process, the bacteria will at least initially be localised in phagosomes inside the infected cell. Phagosomes are vacuoles in the early endocytic pathway that go through a process of maturation and fusion with other endocytic vacuoles. In this process, they gradually become more acidic and bactericidal; and after fusion with lysosomes they are referred to as phago-lysosomes, which are highly active in bacterial killing (Flannagan, Cosio et al. 2009). However, *M.tb* has the ability to arrest phagosome maturation before the phago-lysosome stage and thereby keep the vacuolar pH at 6.2 to 6.4 where bacterial killing is not efficient. Various lipids in the bacterial cell wall and other factors somehow contribute to this maturation arrest process, which is still poorly understood (Sturgill-Koszycki, Schlesinger et al. 1994). Nevertheless, it is agreed that this process somehow protects the bacteria from an immediate immune response (Russell 2001).

After entering the macrophages, *M.tb* dramatically changes its metabolism and switches its carbon source from sugars to fatty acids. This change is associated with decreased growth and decreased killing *in vitro* (Rohde, Veiga et al. 2012). *In vivo*, *M.tb* uses its cell wall lipids to manipulate the host macrophages to develop into fat-containing, so-called foamy macrophages (Peyron, Vaubourgeix et al. 2008) (**Figure**

1.1). These foam cells often contain many bacteria and, as mentioned above, play a critical role in the development of secondary TB (Russell, Cardona et al. 2009).

Thus, *M.tb* is well adapted to survive inside the macrophage and can manipulate the intracellular environment to facilitate its survival, in a way that contributes to the overall pathogenesis.

1.2 Tuberculosis treatment and the emergence of drug resistant tuberculosis

1.2.1 The first-line drugs

Medical treatment of TB is difficult and requires daily administration for at least 6 months of four different antibiotics: Rifampicin (RIF), Isoniazid (INH), pyrazinamide and ethambuthol (ETH). All these four drugs are given during the first two months of treatment, while only RIF and INH are administered for the last four months. RIF, INH and ETH are mainly active against actively growing mycobacteria (Sarkar and Suresh 2011). RIF targets the β-subunit of the DNA-dependent RNA-polymerase, while INH is a pro-drug that must be acted upon by a bacterial enzyme (Kat G); (Brennan 2008) INH inhibits fatty acid synthesis in fast growing populations of mycobacteria. ETH is included as a supportive drug to minimize INH resistance, and like INH it works against fast-growing populations of mycobacteria by inhibiting cell wall synthesis (Brennan 2008). The mechanism of action of PZA is less well characterized than for the other three first-line drugs, but PZA is included in the first line regimen because of its effect against mycobacteria with low metabolic activity **(see also 1.2.3)** (Hu, Coates et al. 2006, Zhang, Yew et al. 2012). Thus, Inclusion of PZA reduces the occurrence of relapse (Fox, Ellard et al. 1999) and this has been attributed to its activity against slow growing bacteria that are not killed by the 3 other drugs. The current first-line drug regimen has a high success rate with drug-sensitive *M.tb* when the patient strictly complies with the daily doses. However, the prolonged and intensive treatment often leads to patient non-compliance, with an increased chance of relapse, and even more serious, an increased chance of selection for drug resistant bacteria. Despite the obvious challenges with the current drug regimen, the

last 50 years has seen almost no development of new TB drugs, with bedaquiline and delaminid as the only notable exceptions (Zumla, Gillespie et al. 2014)

1.2.2 Multi-drug resistant tuberculosis

The introduction of antibiotics has had a huge impact on survival rates in TB patients and the present cure rate is close to 90%, when the chemotherapy is strictly complied to (WHO 2013). However, the emergence of drug resistant *M.tb* is a major, and growing, concern in the TB field today. TB is considered multi-drug resistant (MDR-TB) when *M.tb* bacteria are resistant to the two first-line drugs RIF and INH (Dheda, Gumbo et al. 2014). In 2012, 450,000 new TB cases were considered to be MDR-TB, making up approximately 5% of the total new infections globally. However, the estimated number of deaths due to MDR-TB was 170,000, reflecting the severity of its emergence (WHO 2013). Multi-drug resistant *M.tb* develops from drug-susceptible *M.tb* by acquiring mutations in genes needed for the functioning of the drugs. These genes can either code for the drug target itself or for proteins needed to process the drug before it becomes active (Sacchettini, Rubin et al. 2008). Incomplete treatment caused by patient non-compliance is considered the main reason for the emergence of MDR-TB.

Successful therapy of MDR-TB is dependent on second-line antibiotics (**Table 1.1**), and this treatment is much more complicated and prolonged than the treatment for drug-susceptible TB (Zumla, Nahid et al. 2013). Thus, second-line treatment can easily last 2 years; and it is also very expensive. In addition, most of the second-line drugs are more toxic than the first-line drugs (Shim and Jo 2013). Taken together, this makes the predicted outcome of the treatment of MDR-TB much less favourable than for drug-susceptible TB. The need for such an extensive treatment also underscores the inherent difficulty of treating TB, even with effective antibiotics. Thus, finding ways to shortening the treatment is a main goal in TB research today. In many countries, extensively drug resistant TB (XDR-TB) has also become a problem. These bacteria have the same resistance as MDR-TB but are in addition resistant also to several second-line drugs (see **Table 1.1**). By consensus, XDR-TB should also be resistant to any of the fluoroquinolones in group 3 and any of kanamycin, amikacin or capreomycin in group 2 (Dheda, Gumbo et al. 2014)

First-line anti-TB drugs

Group 1. Oral: isoniazid (H/Inh), rifampicin/rifampin (R/Rif), pyrazinamide (Z/Pza), ethambutol (E/Emb), rifapentine (P/Rpt) or rifabutin (Rfb).

Second-line anti-TB drugs

Group 2. Injectable aminoglycosides: streptomycin (S/Stm), kanamycin (Km), amikacin (Amk). Injectable polypeptides: capreomycin (Cm), viomycin (Vim).

Group 3. Oral and injectable fluoroquinolones: ciprofloxacin (Cfx), levofloxacin (Lfx), moxifloxacin (Mfx), ofloxacin (Ofx), gatifloxacin (Gfx).

Group 4. Oral: *para*-aminosalicylic acid (Pas), cycloserine (Dcs), terizidone (Trd), ethionamide (Eto), prothionamide (Pto), thioacetazone (Thz), linezolid (Lzd).

Third-line anti-TB drugs

Group 5. Clofazimine (Cfz), linezolid (Lzd), amoxicillin plus clavulanate (Amx/Clv), imipenem plus cilastatin (Ipm/Cln), clarithromycin (Clr).

Table 1.1: The table shows the WHO recommended TB drugs and how they are categorized. The first-line drugs include the standard four drug regimen used against drug-susceptible TB. MDR bacteria are resistant to RIF and INH. XDR bacteria are in addition resistant to either of the second-line drugs, Stm, Km or Amk in group 2 and any of the injectable fluoroquinolones in group 3. CFZ, the main focus of this thesis is currently a third-line drug in group five. Table adapted from Zumla *et al.* (Zumla, Nahid et al. 2013)

1.2.3 Drug-persistent tuberculosis

In addition to the problems with multi-drug resistance, TB treatment is frequently also hampered by so-called drug-persistent *M.tb* bacteria. These are bacteria, that despite being genetically drug-susceptible, acquire a tolerance to the drugs (McDermott 1958, Zhang 2014). This drug-tolerance is reversible and is often called phenotypic drug-resistance, to distinguish it from the better-known, irreversible genetic drug-resistance described above. The mechanisms and the terminology of drug persistence is somewhat disputed, but in this thesis, the word drug persistence will be applied to all bacteria with an increased drug tolerance, that do not have known genetic drug resistance.

M.tb are slow growing, they replicate only every 24 h, and are thought to exist in different metabolic states during an infection; and it has been speculated that the metabolic state of *M.tb* influences its drug tolerance. A dormant i.e. non-replicating metabolic state can, for example be induced by oxygen depletion (as occurs in the granuloma), and it has been demonstrated that oxygen depletion can induce persistence in mycobacteria *in vitro* (Wayne 1976). Apart from PZA the first-line drugs target only replicating bacteria and the first-line treatment therefore works

poorly against non-replicating bacteria. Since PZA seems to be able to attack dormant bacteria the finding that inclusion of PZA in the drug-regime significantly reduces the recovery time seems to support the idea that there is a link between dormancy and persistency (Zhang, Yew et al. 2012).

Several genes have been found to be important for the dormant metabolic state, e.g. McKinney *et al.* showed that the *M.tb icl2* gene coding for isocitrate lyase, the gating protein of the glyoxylate cycle, was needed during dormant metabolism. Mutations in the isocitrate lyase gene disrupt the glyoxylate cycle and severely hampers *M.tb*'s ability to survive inside the macrophages (McKinney, Honer zu Bentrup et al. 2000). Importantly, this demonstrates that even if the dormant state mostly hampers treatment it is not without potential targets for new drugs. For instance, Metronidazole was shown to have no effect against actively growing *M.tb*, but can effectively kill dormant *M.tb* under anaerobic, dormant conditions (Wayne and Sramek 1994).

A lot of attention has also been given to bacterial efflux pumps, and such pumps are thought to play a major role in drug persistence (Szumowski, Adams et al. 2013). Efflux pumps can actively pump drugs out of the bacterial cytoplasm and thereby prevent them from killing the bacteria. This is potentially a very harmful form of drug persistence because it allows the bacteria to maintain an active replicating metabolism. Thus, work done in the group of Ramakrishnan has shown that actively replicating mycobacteria are found also during extensive drug treatment, and that these bacteria were shown to have an up-regulated expression of many efflux pumps (Adams, Takaki et al. 2011).

1.3 New strategies for TB treatment

As also discussed above there are several reasons why TB is so hard to eradicate and this relates not only to the bacteria themselves, but also to the pathology of TB. For one thing, *M.tb* has a thick and waxy cell wall that is almost impermeable to hydrophilic compounds (Jarlier and Nikaido 1994, Brennan and Nikaido 1995). In addition, the high viscosity and thickness of the cell wall also makes it a barrier also to lipophilic drugs (Liu, Barry et al. 1996).

Another problem is that *M.tb* resides in granulomas that are often poorly vascularized. Furthermore, a large fraction of the bacteria in a developed granuloma

is found in the necrotic core, so to reach these bacteria, the drug must diffuse into the necrotic core where they often have low penetrance (Dartois 2014). Thus, the plasma concentration of anti-TB drugs are not considered to be predictive of the drug concentration at the infection sites and drugs administered through the systemic route often fail to reach the bacteria in high enough concentrations to eradicate them (Dartois 2014). This issue was underscored when it was demonstrated that three of the first-line drugs, INH, RIF and PZA, had markedly lower exposure in the granulomas than in the plasma of TB infected rabbits (Kjellsson, Via et al. 2012). However, it must be emphasized that granulomas show great heterogeneity in the same individual, and while some granulomas may be vascularized, others are not (Capuano, Croix et al. 2003, Flynn, Capuano et al. 2003). Thus, the pharmacokinetics of a drug will vary greatly between different granulomas (Dartois 2014). This problem should not be underestimated and some authors believe that this “kinetic variability” and the sub-therapeutic concentration it causes is the main reason for the development of drug-resistant bacteria (Dheda, Gumbo et al. 2014).

The issues related to the current treatment regimens, and especially the emergence and spread of MDR-TB, have made it very important to find alternative TB treatment regimens (reviewed in (Zumla, Gillespie et al. 2014)). Several new drugs are currently being tested for TB treatment, but the development, documentation and approval of new drug molecules is always a slow and expensive process (DiMasi, Hansen et al. 2003). Another, possibly quicker and easier strategy is re-purposing of old drugs that are already clinically approved for treating other diseases, or that are in little use due to other causes, such as difficulty in administration or high toxicity (Savoia 2015). Linezolid and moxifloxacin are two of the most promising re-purposed drugs for TB treatment, and another interesting alternative is clofazimine, as will be discussed further below in section **1.3.3** (Zumla, Nahid et al. 2013). Whatever strategy chosen, the continued effort to eradicate TB must build on the increased knowledge about the complexity of TB treatment discussed above.

1.3.1 Tuberculosis animal models

For the development of new therapies, good animal models are of outmost importance. An animal model should reflect the pathology of human disease in the best possible way, but it is also important to develop models where the testing of

different treatments is fairly easy and rapid, making it possible to screen through a variety of drugs in order to be able to define the best options for further development.

TB is studied in several mammalian models, but none of them completely resembles the human TB; maybe reflecting the fact that in nature *M.tb* only infects humans (Russell 2013). The mouse, *Mus musculus* is a commonly model that is susceptible to both *M. bovis* and *M.tb*. However, the mouse models fail to develop the organised, caseating granulomas found in infected humans and its relevance has therefore been questioned (Via, Lin et al. 2008). Guinea Pig, *Cavia porcellus* is highly susceptible to both *M.bovis* and *M.tb* and unlike in mice, the infection does develop caseous necrosis. However, guinea pigs lack the heterogeneity of human tuberculous lesions and this model does not develop the latent stage that occurs in 90% of *M.tb* infected human (Padilla-Carlin, McMurray et al. 2008).

Rabbit, *Oryctolagus cuniculus*, can be infected with both *M. bovis* and *M.tb*, and for both species infection is followed by rapid bacterial growth. *M.bovis* infection in rabbits leads to extracellular bacterial growth, followed by a rapid spread of bacteria, which is usually fatal. *M.tb* on the other hand is normally well controlled and the infection seldom kills the rabbit (Converse, Dannenberg et al. 1998, Dannenberg 2006). TB infected rabbits develop a more heterogeneous spectre of bacterial lesions, which makes it a relevant model for drug drug-delivery studies. The Cynomologus macaque, *Macaca fasicularis*, is a non-human primate and it is considered the TB model that best recapitulates the human pathology (Capuano, Croix et al. 2003). However, the macaque model is expensive and its use is controversial and subject to substantial ethical issues.

Common to all the mammalian TB models is the fact that if one wants to investigate the localisation of the bacteria; this can only be done by histology, after sacrificing the animal. This makes it impossible to analyse the development of the infection in real-time, meaning that details of the developing mycobacterial infection may easily be missed. Intra-vital microscopy, such as multi-photon microscopy has been used to monitor selected tissues in some mouse experiments, but this is far from routine (Egen, Rothfuchs et al. 2008, Egen, Rothfuchs et al. 2011).

1.3.2 Zebrafish tuberculosis model

The zebrafish (*Danio Rerio*) is a teleost fish, which because of its short generation time and transparent embryonal and larval stage is a highly rated, and increasingly used, experimental animal. Zebrafish are cheap and easy to keep, and many modified strains and genetic tools are available. Zebrafish was introduced to the scientific community in 1973 by Georg Streisinger, who used it to study early embryonic development (Li, Huang et al. 2013). Since then, its use has expanded and zebrafish models are now deployed in many branches of biological research such as cancer, neuro-physiology and toxicology (Wyart and Del Bene 2011, Peterson and Macrae 2012, White, Rose et al. 2013). Over the past decades, zebrafish has also become a popular infection model, especially for bacterial diseases (Meijer and Spaink 2011). When fully developed, zebrafish has possesses innate and adaptive immune system, with many similarities to the human immune system (Lugo-Villarino, Balla et al. 2010).

1.3.2.1 Tuberculosis studies in zebrafish

The zebrafish embryo model for TB was established by Ramakrishnan's group in 2002 and it has given important insight to the TB field (Davis, Clay et al. 2002). A special advantage of this model is the optically transparency of zebrafish embryos, that has made it the only TB model where host-pathogen interactions can be studied real-time in a live animal, and at high resolution.

Zebrafish is a natural host to the aquatic pathogen *Mycobacterium marinum* (*M.m*), which is a close relative of *M.tb* (Tonjum, Welty et al. 1998). *M.m* is a natural host of both fish and ectoderms and has a wider spectrum of hosts than the *M.tb* (Cosma, Swaim et al. 2006, Tobin and Ramakrishnan 2008). Although capable of causing infections in humans, *M.m* grows optimally between 30-33 $^{\circ}$ C and the bacteria therefore only produces superficial lesions in humans and does not normally cause systemic infections. *M.m* infection in adult zebrafish leads to an infection with a pathology that resembles the human granulomas (Swaim, Connolly et al. 2006). It has also been shown that *M.m* infection of adult zebrafish can lead to a latent infection. This infection can later be re-activated using γ-radiation (Parikka, Hammaren et al. 2012). Thus, the pathology *of M.m* infection captures several aspects of human TB, and during infection, *M.m* can also arrest phago-lysosomal

fusion in macrophages. (Cosma, Sherman et al. 2003, Tobin and Ramakrishnan 2008).

During early stages of development, the zebrafish embryo has a rudimentary immune system consisting of macrophages and neutrophils, and does not develop active lymphocytes until 20 days post infection (Herbomel, Thisse et al. 1999, Langenau, Ferrando et al. 2004). This makes the zebrafish embryo an especially good model for studying the initial interactions between the innate immune system and mycobacteria. Experiments where *M.m* was injected into the vasculature of the zebrafish embryo showed that macrophages can take up bacteria and form granulomas prior to the development of adaptive immunity (Davis, Clay et al. 2002). Later, in similar experiments it was shown that mycobacteria exploit newly recruited macrophages to disseminate the infection. Similar to what is envisioned for human TB; uninfected macrophages arriving at the infection site ingest extracellular bacteria before carrying the bacteria to a new site where they seed a new granuloma. (Davis and Ramakrishnan 2009). Also, studies of treatment of *M.m* infection in zebrafish embryos have shown similar effects of the commonly used anti-tuberculosis drugs as the effects seen in human infection (Adams, Takaki et al. 2011). Taken together these findings suggest that zebrafish embryos could be a good model for studying new treatment strategies for human TB.

1.3.3 Nanocarrier mediated drug delivery - a novel approach to tuberculosis treatment

Administration of drugs by systemic routes is very convenient, but also has several inherent problems. Thus, many drugs have an unfavourable biodistribution, leading to low accumulation at the diseased site, and an inferior therapeutic effect (Panchagnula and Thomas 2000). Drugs can also accumulate in off-target tissues or cells, often leading to toxic or other unwanted effects. In addition, many drugs are rapidly cleared from the blood through either the liver or the kidneys, meaning that frequent administration is necessary to achieve a therapeutic drug concentration in the blood (Chertok, Webber et al. 2013).

These problems led Paul Erlich over a hundred years ago to envision “the magic bullet” - a “drug package” that could selectively target the disease and cure it, without affecting the rest of the body. One approach for generating such magic bullets is the

use of so-called nanocarriers (Couvreur and Vauthier 2006). Nanocarriers are nanometre-sized chemical structures designed to deliver drugs inside a body. The definition of a nanocarrier varies between different authors, but in this thesis, a broad definition will be applied and nanocarriers will cover drug delivery systems with diameters 1-1000 nm, following the suggestion of Nicloas et al. (Nicolas, Mura et al. 2013). The principle of a nanocarrier is that chemical compounds are used to encapsulate or bind a drug, generating a structure that will alter the behaviour of the drug in the body in an advantageous way. Encapsulation of the drug can be done in several ways and some examples are shown in **Figure 1.2**.

Nanocarriers can offer several advantages compared to the systemic delivery of free drugs. For one thing, the drugs are often associated with the nanocarriers in a manner that protects them from rapid degradation or excretion. The nanocarriers and the drug can then gradually dissociate, leading to slow and sustained release and thus reduce the number of administrations needed (Couvreur and Vauthier 2006). In addition, depending on the nanocarrier, it is also possible to add chemical groups (such as receptor ligands) to the nanocarrier surface and thereby improve their affinity for receptors on specific cells or organs. This can increase the nanocarrier's localisation at the diseased site and thereby lead to targeting of the drug. Targeting can lead to both an enhanced treatment effect and reduced off-target effects, especially reduced toxicity (Kamaly, Xiao et al. 2012, Nicolas, Mura et al. 2013).

Because of the great potential of nanocarrier therapy, the last decades have seen the development of a vast spectre of different nanocarriers. These can be divided into different classes depending on their chemical constituents and formulation (**Figure 1.3**) and further into subclasses depending on their shape and interaction with the drug (**Figure 1.2**).

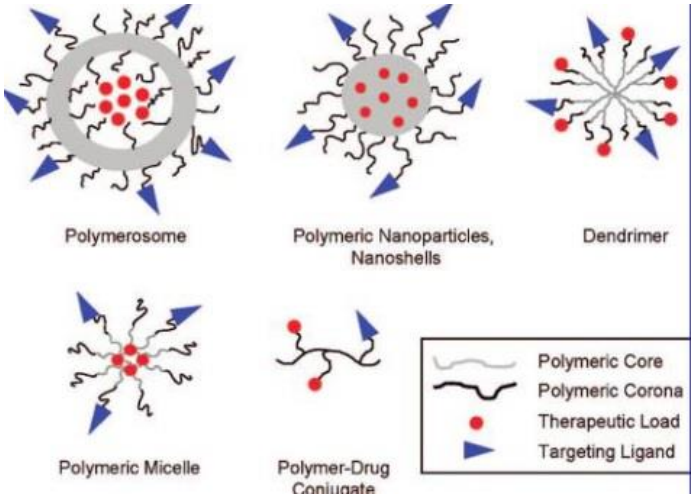

Figure 1.2: Structure of the most commonly used polymeric nanocarriers, which is the type of nanocarrier used in this thesis. An example of a nanoparticle (NP) is shown the middle of the top row. In nanoparticles the drug is entrapped in the polymer used to form the NP. The figure is taken from Alexis *et al.* (Alexis, Pridgen et al. 2008).

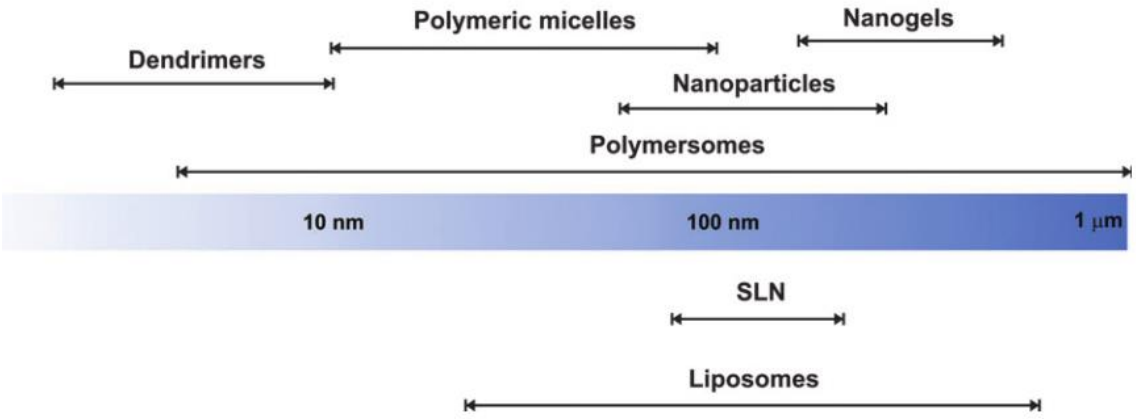

Figure 1.3: An overview of nanocarriers and their size range. Above the scale bar are the polymeric nanocarriers, and below the scale bar the lipid based nanocarriers. The categorization is based on the shape and structure of the nanocarrier. Nanoparticles, which are used in this thesis, are polymeric nanocarriers. SLN denotes solid lipid nanocarriers. Adapted from Nicolas *et al.* (Nicolas, Mura et al. 2013)

The first nanocarriers to be developed in the 1960's were the lipid based liposomes, and some such carriers have been approved for clinical use e.g. to treat cancer or fungal infections (Allen and Cullis 2013). Later many different chemical structures have been explored for nanocarrier development, but the rest of this thesis will focus on polymeric nanocarriers, and in particular nanoparticles. The use of polymers to make what is called nanoparticles (NP) was developed during the 1970's (Langer and Folkman 1976), and NP have been studied extensively since that time, mainly because they offer improved drug loading and *in vivo* stability, e.g. as compared to liposomes. During the preparation of NP, the polymer forms a matrix that entraps the drug (see **Figure 1.2**). By using polymers that are biodegradable and non-toxic NP can be developed so that they, at least in theory, can be used without significant side effects.

Successful NP-based therapy requires a detailed understanding of the interactions between the nanoparticle and the body. The properties of NP, and also their behaviour in the body, are influenced by their shape, size, charge and composition (Alexis, Pridgen et al. 2008, Kumari and Yadav 2011, Kamaly, Xiao et al. 2012). For instance nanocarriers with a size >200 nm are efficiently taken up by phagocytic cells (Desjardins and Griffiths 2003). Positively charged carriers are also taken up more rapidly because they interact with the negatively charged cell membrane (Frohlich

2012). In contrast, NP with a hydrophilic surface are taken up slowly and can usually circulate for a longer time in the blood than hydrophobic NP (Gref, Minamitake et al. 1994). This is very important in many approaches for NP-based therapies where it is crucial to avoid uptake in liver phagocytic cells, that would otherwise rapidly remove the NP from the circulation, so that they do not reach their target (Alexis, Pridgen et al. 2008).

1.3.4 PLGA-nanoparticles as possible tuberculosis therapeutics

The prolonged and difficult treatment of TB discussed above has led several researchers to investigate the potential of using NP-based therapy to treat the infection. Among these studies, the most notable results have come from studies using PLGA NP (Griffiths, Nystrom et al. 2010). PLGA poly (lactic-co-glycolic acid) is a biocompatible polymer that can easily be degraded by hydrolysis *in vivo* (Shive and Anderson 1997) and it has also been approved for various uses by the American Food and Drug Administration (FDA).

The fact that *M.tb* resides inside macrophages makes the nano-therapy approach to TB different from many other nano-therapies (for instance cancer), where avoidance of macrophage attention is one of the main challenges when engineering NP. For TB treatment, to the contrary, uptake of NP by macrophages can potentially facilitate the direct delivery of drug-loaded NP to the infection site, making this approach especially attractive as a therapeutic option.

Studies in cell culture have demonstrated that phagocytosis of NP-encapsulated TB drugs leads to an increased intracellular concentration of the drugs. This has been shown *in vitro* for both INH and RIF (Anisimova, Gelperina et al. 2000) (Yoshida, Matumoto et al. 2006). Encapsulation of RIF into PLGA also increased the bactericidal effect of RIF against BCG *in vitro*, compared to free administered RIF (Yoshida, Matumoto et al. 2006). Later *in vitro* experiments using the fluorescent dye coumarin-6 loaded into PLGA-NP have demonstrated that phagocytosed PLGA-NP end up in lysosomes where they are slowly degraded (Kalluru, Fenaroli et al. 2013). Even though mycobacteria reside in early endosomes and therefore in a different compartment from the NP, *in vitro* experiments showed that RIF loaded PLGA-NP

eradicated BCG from macrophages more efficiently than free administered RIF (Kalluru, Fenaroli et al. 2013).

Gopal Khuller and his group in India assessed the *in vivo* effect of PLGA-NP treatment of TB in several studies. A key information from these studies is that using PLGA-NP to deliver anti-TB drugs both increases the bioavailability of the drugs and reduces the number of doses needed for complete eradication of the infection. For three of the first-line drugs (RIF, INH and PZA), single doses of PLGA encapsulated drug led to increased and prolonged drug concentration in plasma of guinea pigs, when they were compared to the same dose of free administered drug (Sharma, Pandey et al. 2004). Later it was shown that 3-5 doses of PLGA beads with co-encapsulated RIF and INH could give the same treatment effect as 45 daily doses of free-administered RIF and INH and sterilize the lung and spleen of *M.tb* infected guinea pigs (Sharma, Sharma et al. 2004). Similar results have also been obtained in *M.tb* infected mice (Pandey, Sharma et al. 2003)

However, the *in vivo* behaviour of PLGA-NP during TB treatment had not been well characterized in the studies by Khuller and others. By adapting the zebrafish TB model described above, our group was able to start studying the *in vivo* dynamics of the PLGA-NP in the zebrafish embryo. The transparency of the zebrafish makes it a very useful model system for studying the *in vivo* distribution and behaviour of NP. Thus, important insight to the PLGA-NP treatment of TB was provided when it was shown that polymeric NP passively target macrophages and co-localize with the site of infection already after 1 day in zebrafish embryos (Fenaroli, Westmoreland et al. 2014). Strikingly, it was observed that macrophages could carry PLGA-NP injected into the vasculature across the blood-brain barrier if *M.m* was injected in the hindbrain ventricle. This demonstrated that macrophages can work as vehicles for NP delivery to the infection site. In the same report it was shown that NP encapsulated RIF was more effective than free drug to treat *M.m* infection in zebrafish. (Fenaroli, Westmoreland et al. 2014). These experiments gave empirical evidence to the proposed mechanism for NP-based treatment against TB and the results suggest that targeting of macrophages could be an important principle in the future of TB nano-therapy.

1.3.5 Clofazimine as a potential anti-tuberculosis therapeutic

Clofazimine (CFZ) (**Figure 1.4**) is a riminophenazine antibiotic that was synthesised and described during the 1950s in several publications by Vincent Barry and colleagues as a potential TB drug. (Barry, Conalty et al. 1956, Barry, Belton et al. 1957). Later work, however questioned CFZ's efficacy against *M.tb* as its effect varied widely across the different animal models (Barry and Conalty 1965); and the subsequent development of more potent TB drugs made CFZ largely superfluous in the TB treatment. Later however, CFZ was shown to be effective against a different mycobacterium, namely the leprosy-causing *Mycobacterium leprae*, and CFZ is still used routinely for leprosy treatment (Noordeen 2016).

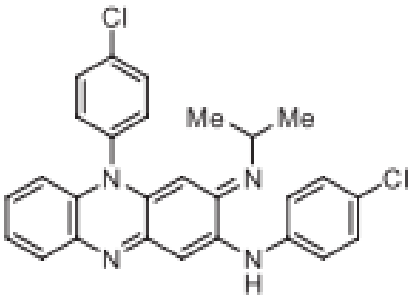

Figure 1.4: The molecular structure of clofazimine. Figure adapted from Brennan (Brennan 2008).

Despite the 60 years that have passed since CFZ was first described the effects of the drug are still poorly understood, and this has placed it in the periphery of the MDR-TB treatment alternatives. CFZ is today among the WHO listed TB drugs, but the unknown effect has given CFZ a current status as a third-line, group five drug (**Table 1.1**). In particular, CFZ has an unknown mode of action, which in combination with the varying results in animal models described above, has led to disputes about whether CFZ has any effect at all against TB *in vivo*.

However, in 2010 Van Deun *et al.* published a meta-study of treatment of MDR-TB affected patients suggesting that CFZ inclusion in MDR-TB treatment could have a great effect on treatment outcome (Van Deun, Maug et al. 2010). Together with the well-demonstrated effect of CFZ against MDR-TB isolates *in vitro*, this so-called

"Bangladesh study" has led to a renewed interest in CFZ. Thus, several studies have been done to investigate the potential of CFZ in TB, as well as MDR-TB, treatment. Two of the more promising results have come from studies done in the group of Jacques Grosset demonstrating that inclusion of CFZ had a substantial effect in killing of INH-resistant *M.tb* in mice (Grosset, Tyagi et al. 2013). Later, they also showed that exchange of CFZ for ETH in the four-drug first-line therapy reduced the duration of treatment by 2 months in mice (Tyagi, Ammerman et al. 2015).

CFZ has several characteristics that, if it were confirmed to be effective against TB *in vivo*, would make it a very useful drug. A very attractive feature of this drug is that, at least *in vitro*, it is also active against non-replicating bacteria, making it potentially useful against the slow growing persisters discussed in section **1.2.3.** Thus, *In vitro* CFZ has been shown to be effective against hypoxia-induced drug tolerant bacteria (Grant, Kaufmann et al. 2012), and this seems to be the case also *in vivo* (Xu, Lu et al. 2012*)*. CFZ has a low frequency of adverse effects when used in MDR-TB treatment and is cheap compared to many other MDR-TB drugs (Gopal, Padayatchi et al. 2013). The importance of this financial aspect cannot be underestimated given that TB is predominantly a disease of poorer countries.

A general consideration in the use of CFZ is its extreme hydrophobicity. CFZ has a measured log P of 7.1 which makes it practically insoluble in water (Brennan 2008). (Log P is a measurement of the how a compound is distributed between an oil phase of octanol and a water phase. The log P is then the $\log_{10}$ of the octanol/water ratio). CFZ is mild proton acceptor with a $pK_a = 8.51$, making CFZ more soluble under acidic conditions, but so far this has not been exploited in the practical use of CFZ. The high hydrophobicity leads to difficulties in administering this drug. CFZ is generally administered orally, but the current way of using CFZ leads to massive accumulation in skin and fatty tissues in humans. CFZ also has a very slow degradation rate in the human body and its half-life is estimated to about 70 days (Brennan 2008). CFZ is a red coloured dye and accumulation in skin lead to skin discolouration; although this effect is reversible it has been reported to cause inconvenience for patients and two suicides have been reported as being a consequence of this phenomenon.

A few investigators have tried to identify the mode of action of CFZ. Van Rensburg *et al.* reported that CFZ was only effective against Gram-positive and mycobacterial

species of bacteria (Van Rensburg, Joone et al. 1992). They concluded that CFZ works by destabilizing the bacterial membrane potential. A different hypothesis, originally put forth by Vincent Barry (Barry, Belton et al. 1957) is that CFZ kills bacteria by generating reactive oxygen species (ROS). CFZ is known to have redox properties and *in vitro* experiments in *Mycobacterium smegmatis* suggested that CFZ is reduced by the bacterial enzyme type II NADH dehydrogenase (NDH-2) in a process that generates ROS (Yano, Kassovska-Bratinova et al. 2011). Similar results were shown in *M.tb* (Lechartier and Cole 2015*)* and in both studies the effect of CFZ could be diminished by adding high concentrations of menaquinone, the enzymatic co-factor which is the natural substrate for NDH-2.

Recent findings have shown that *in vivo* CFZ accumulates in macrophages into large, intracellular, membrane-bound, crystal-shaped aggregates. These so-called crystals-like drug inclusions (CLDIs) are hypothesised to be a protective response to a potentially toxic drug (Baik and Rosania 2012, Baik, Stringer et al. 2013). *In vitro*, where such inclusions have not been found, higher doses of CFZ have been described as being toxic to macrophages (Yoon, Sud et al. 2015). What impact these CLDIs may have on treatment is yet to be known.

The comprehensive skin and tissue accumulation observed during CFZ-treatment suggests that the biodistribution may be sub-optimal, and this may play a role in the often variable results from CFZ treatment. Thus, encapsulation of CFZ in NP could be very interesting option for enhancing the efficacy and utility of the drug. In spite of this, the literature on nano-therapy using CFZ is sparse, and there is, to my knowledge, no therapeutic studies done using polymeric CFZ NP. Two studies have investigated CFZ with liposomal nanocarriers against *Mycobacterium avium,* and *M.tb* infections in mice. Against *M. avium*, doses of 5 mg/kg and 10 mg/kg CFZ in liposomes reduced the CFU-counts in lungs, spleen and liver of the infected mice (Mehta 1996). Against *M.tb,* a dramatic reduction in CFU-counts could be obtained, likely because the CFZ-liposomes, by lowering CFZ toxicity, allowed for a much higher injected dose (100 mg/kg liposomal CFZ, as compared to 5 mg/kg free CFZ) (Adams, Sinha et al. 1999). These two studies are also the only experiments were CFZ was injected directly into the blood of animals; and also the only two studies that report severe toxic side effects from CFZ on the experimental animals. In a more recent experiment, CFZ micro-particles were prepared by spray-drying and

administered through the aerosol route in *M.tb* infected mice. This increased the therapeutic effect in the lungs compared to orally administered CFZ. However, in this study, neither treatments had any therapeutic effect on the spleen (Verma, Germishuizen et al. 2013). The potential of CFZ NP in TB treatment is therefore still unclear, but since several studies have given promising results it is interesting to further explore this treatment approach.

2 Aims of the work

The aims this master thesis was to: i) Develop a protocol to encapsulate CFZ in polymeric NP. ii) Compare the behaviour of CFZ-NP and free CFZ *in vitro* in order to identify and quantitate differences in toxicity, uptake and retention of CFZ. iii) Assess the therapeutic effect of CFZ-NP *in vivo* and investigate whether nanoparticle encapsulation can enhance the effect of CFZ TB treatment. The *in vitro* experiments were performed using a murine macrophage model and the *in vivo* experiments were performed using the zebrafish *M.m* infection model.

3 Materials and methods

3.1 Encapsulation of Clofazimine in nanoparticles

3.1.1 Single emulsion solvent evaporation method

The single emulsion solvent evaporation method was adapted from Kalluru *et al.* (Kalluru, Fenaroli et al. 2013). In this method, sonication is used to make NP by emulsification of a mixture of one organic phase and one aqueous phase that are non-miscible (Kamaly, Xiao et al. 2012). A polymer and a hydrophobic drug are dissolved in an organic solvent to make the organic phase. The aqueous phase is usually prepared with an amphiphilic surfactant, which helps in shaping the NP and make them more water-soluble. Sonication provides energy that forces the two phases to be mixed, and this creates the emulsification where nano-sized droplets of the oil-phase forms inside the water phase. The surfactant stabilizes these droplets in the water and prevents them from aggregating. After sonication, the emulsified solution is put to stir so the organic solvent can evaporate **(Figure 3.1)**.

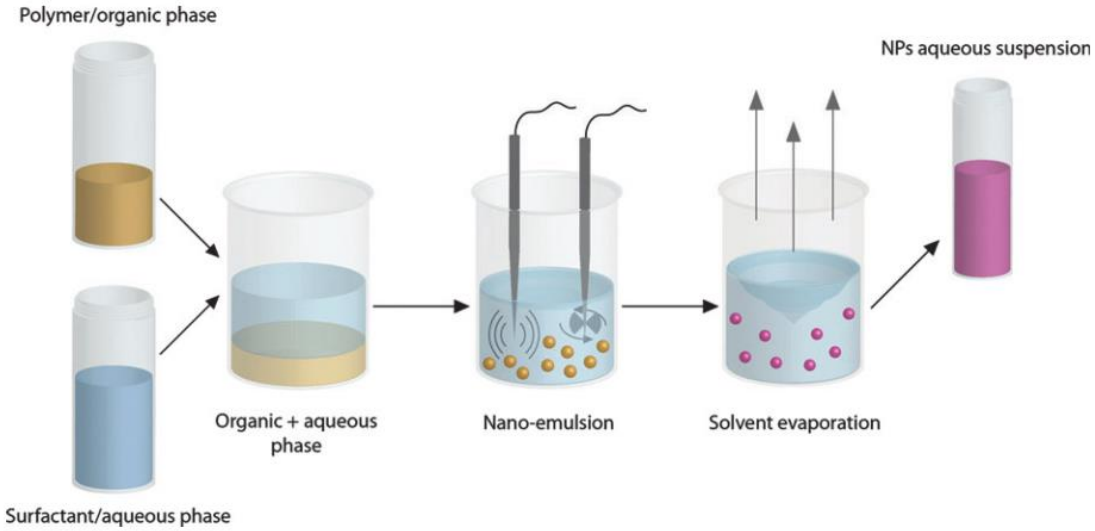

Figure 3.1: Schematic drawing of the single emulsion solvent evaporation method. Figure taken from Nicolas *et al*. (Nicolas, Mura et al. 2013)

Procedure:

We used the polymer PLGA Resomer® RG 502 (purchased from Evonik Röhm GmbH, Darmstadt, Germany) with 50 % lactic acid and 50% glycolic acid (50:50).

100 mg PLGA and 100 mg clofazimine (Sigma-Aldrich, St. Louis, MO, USA) were dissolved in 10 ml dichloromethane (DCM; Sigma-Aldrich, St. Louis, MO, USA) to make the organic phase. The organic phase was then stirred overnight in a 100 ml Erlenmeyer flask that was tightly sealed with a lid and parafilm, to avoid evaporation.

The aqueous phase was prepared with either 1 % (w/V) or 4 % (w/V) polyvinyl alcohol (PVA), (Alfa Aesar, Ward Hill, MA, USA). This solution was heated to 90 °C with moderate stirring for 45 minutes to dissolve all of the PVA crystals. The heating was turned off and the solution was left stirring overnight.

Before mixing the two phases, the aqueous phase was filtered through a 0.22 µm filter to remove any PVA aggregates. 20 ml of the aqueous phase was transferred to a 100 ml glass beaker before adding 10 ml of the organic phase, and this mixture was immediately emulsified by sonication for 3 mins at 450 watt (60%) using a tip sonicator (Power 750 Watt, Sonics & Material Inc., Church Hill Road, Newtown, USA). After sonication, the emulsified solution was divided into two 50 ml Erlenmeyer flasks, covered with aluminium foil that had been prepared with a 2 mm^2 hole, and put to stir overnight. The small hole in the aluminium foils allows for gentle evaporation of DCM and prevents the evaporation process from breaking the NP.

Complete evaporation was detected by the absence of smell from DCM. After evaporation, the NP were washed in sterilized Milli-Q water to remove any excess PVA and unbound drugs. Washing was done by ultracentrifugation using an SW32 Ti rotor (Beckman Coulter, Fullerton, CA, USA) at 15 000 rpm for 30 min and repeated 3 times. Between each washing step, the NP pellet was thoroughly re-suspended in Milli-Q water. The pellet formed after the third wash was re-suspended in 2.5 % trehalose (Sigma-Aldrich, St. Louis, MO, USA) solution, then frozen in liquid nitrogen and freeze-dried over-night using a Freezone 2.5 Freeze-dryer, (Labconco, Kansas City, MO, USA). The trehalose works as a cryo-protectant, and prevents disruption of the NP during the process.

3.1.2 Nanoprecipitation method

Nanoprecipitation is a faster and easier method for NP formation than the single emulsion solvent evaporation method and is therefore a better suited approach when screening for optimal encapsulation conditions of a specific cargo. Nanoprecipitation is performed using a water-miscible organic solvent to dissolve the cargo and the polymer, and an aqueous solution, usually consisting of only deionized water, but it is also possible to prepare the aqueous phase with an emulsifier. The solvent, containing the polymer and the cargo, is added dropwise to the aqueous solution, while under stirring, and as the solvent diffuses into the aqueous medium, the polymer precipitates and NP are formed instantly, presumably with the hydrophobic drug being encapsulated in the hydrophobic core of the particle (see **Figure 3.2**) (Nicolas, Mura et al. 2013). Nanoparticle formation can be seen by a change of colour in the aqueous solution, which usually turns opaque upon NP formation. When the solution is saturated, larger precipitates start to form. The gradual addition of the solvent makes it easier to observe and control NP formation, to avoid precipitation, and to determine at what drug and polymer concentrations the larger precipitates starts to form.

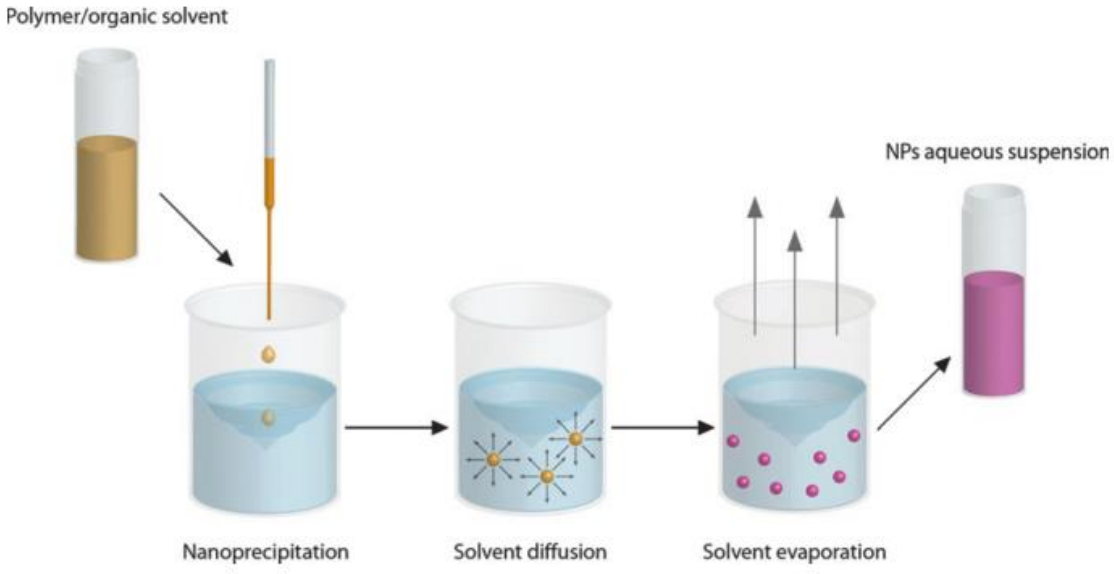

Figure 3.2: Schematic drawing of the nanoprecipitation method. Figure is taken from Nicolas *et al.* (Nicolas, Mura et al. 2013).

Procedure

Clofazimine (Sigma-Aldrich, St. Louis, MO, USA) and PLGA were dissolved at different concentrations and ratios, using 1 ml of either dimethyl sulfoxide (DMSO) (Sigma-Aldrich, St. Louis, MO, USA) or Tetrahydrofuran (THF) (VWR, international AS, Norway). The aqueous solution was prepared using Milli-Q water and either PVA or Tween 80 as surfactants. The surfactant concentrations were varied through the experiment (see **Table 4.3** and **4.4**). After mixing the solvent, the PLGA and clofazimine together, the mixture was vigorously vortexed for 1 min and subsequently sonicated in a water bath for 2-3 minutes until all clumps and aggregates were broken. The sonicated solutions were added to 1 ml syringes coupled to either 23 G or 27 G needles. The DMSO solutions were slightly more viscous than the THF solutions so they were added through 23 G needles in order to have a proper and steady flow through the needle. The organic solvent solutions were then added drop-wise into the aqueous solution at a speed of approximately 200 µl/min. The THF solution was left stirring overnight to facilitate the evaporation of the solvent. The DMSO solution was left stirring for a few hours. The NP were then collected, washed and freeze-dried as described for the single emulsion method (see **3.1.1**).

3.1.3 Chitosan nanoparticle self-assembly

Chitosan is a chitin-derived polymer that is produced by removing an acetate moiety form chitin through hydration in concentrated alkali. The physical and chemical properties of chitosan depend on its molecular weight and the grade of deacetylation, and this also determines its biocompatibility. Chitosan is mainly degraded through enzymatic catalysis. Chitosan NP can be prepared by many different strategies including ionic cross-linking, precipitation techniques or self-assembly if the chitosan polymer is amphiphilic (Wang, Zeng et al. 2011).

In our experiments, we employed the latter method using a *meso*-tetraphenylporphyrin (TPP)-substituted chitosan polymer (Gaware, Hakerud et al. 2013), provided by PCI Biotech AS (Oslo, Norway) (**Figure 3.3**). TPP is a lipophilic compound and, in an aqueous solution the TPP side groups will form hydrophobic interactions. These allow the chitosan polymers to self-assemble into nano-sized particles by forming a core-shell structure where the TPP constitutes the hydrophobic

core and the chitosan backbone constitutes the hydrophilic shell. A hydrophobic drug can thus be entrapped in the hydrophobic core in the particle. The TPP-chitosan polymer is soluble in DMSO, one of the solvents that can also be used for CFZ. However, the TPP-chitosan is not soluble in THF.

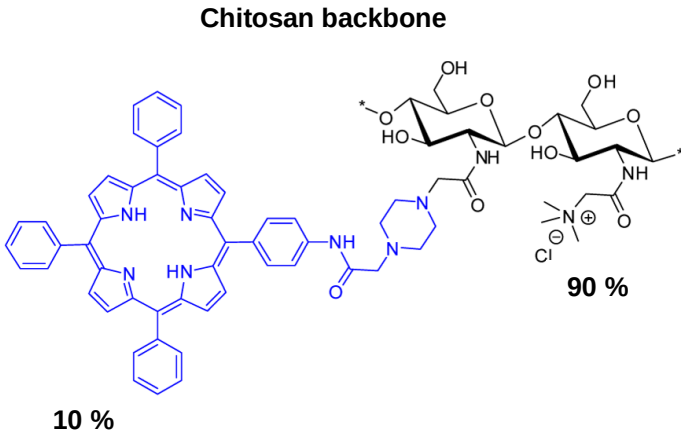

Figure 3.3: Tetraphenylporphyrin-Chitosan nanocarrier. The chitosan backbone was conjugated with tertraphenylporphyrin (blue, 10 %) and trimethylamine (90 %). Figure adapted from Gaware *et al.* (Gaware, Hakerud et al. 2013)

Procedure

1 mg of CFZ and 1 mg of TPP-Chitosan were dissolved in 100 µl of DMSO and sonicated for 2 minutes to break all the aggregates in the solution. The DMSO was diluted by gradually adding 2 ml of Milli-Q water to make the chitosan self-assemble. The procedure was also tried in reverse order and the DMSO-Chitosan-CFZ solution was added to Milli-Q water dropwise in a similar fashion to nanoprecipitation.

3.2 Characterization of PLGA-CFZ nanoparticles

3.2.1 Transmission electron microscopy

Because of their small size (<500 nm), NP are difficult to observe in high resolution in a light microscope. However NP can be visualized using Transmission Electron Microscopy (TEM). An electron microscope uses accelerated electrons to form an

image. Because the electrons have a much shorter wavelength than light, electron microscopy has a higher resolving power and can resolve much smaller objects than light microscopy.

Procedure

A fraction of the freeze-dried NP (either Chitosan or PLGA-CFZ) was dissolved in Milli-Q water in a concentration of 0.5 mg/ml. The NP were then mounted on hexagonal lattice copper, formvar-coated grids by putting a grid on top of a droplet of the NP-solution for 1 minute. The grids were washed gently to remove any unattached NP, by floating it sequentially on 4 droplets of Milli-Q water. After washing, the grids were moved to a droplet of 3% uranyl acetate to give contrast to the sample. After 30 seconds, the grid was removed from the staining droplet, and excess uranyl acetate was gently removed, using a filter paper. The grid was left to dry at room temperature before loading it on an EM sample holder. Imaging was performed in a Philips transmission EM (CM100; Philips, Eindhoven, The Netherlands). The images were recorded digitally with a Quesma TEM CCD camera and iTEM software (Olympus Soft Imaging Solutions, Germany).

3.2.2 Nanoparticle size measurements by dynamic light scattering.

Dynamic light scattering (DLS) is a commonly used method for the characterization of various particles. Particles or molecules in suspension causes laser light to be scattered at different intensities depending on the Brownian motion of the particles. Analysis of the intensity fluctuations can yield the velocity of the Brownian motion, and from this the size of the particles in the suspension can be calculated (Berne and Pecora, 2000).

Procedure

Freeze dried NP were re-suspended in Milli-Q water at a concentration of 0.5 mg/ml. The sample was sonicated thoroughly to make sure to break any NP aggregates. The sample was then transferred to a cuvette and the size was measured by Photon Cross-correlation Spectroscopy (PCCS) method using the Nanophox instrument (Sympatec GmbH).

The nanoparticle size measurements were carried out at the Department of Chemistry at the University of Oslo together with Shahla Bagherifam and Barbara Claro.

3.2.3 Nanoparticle surface charge measurements

The NP surface charge was determined by measuring the electrophoretic mobility of dissolved NP in an applied electric field. These measurements estimate the so-called zeta-potential of the NP. PLGA-CFZ NP were dissolved in a concentration of 1 mg/ml in 0.45% NaCl. This sample was added to a glass cell, PCS1115 capped cuvette. The cuvette has two dip-cell palladium electrodes with 2 mm spacing. The zeta-potential was measured in a Malvern Zetasizer Nano ZS (Malvern Instruments Ltd., Worcestershire, UK) instrument.

The measurements were carried out at the Institute of Pharmacy at the University of Oslo together with Martin Speth.

3.2.4 Determination of nanoparticle drug loading

The clofazimine load in PLGA NP was determined by liquid chromatography-electrospray ionization-mass spectrometry (LC-ESI-MS). Accurately weighed PLGA-CFZ NP samples were dissolved in DMSO to concentrations of 2.0 mg NP/ml. Samples were subsequently diluted in acetonitrile (ACN)/water (65/35, v/v) to 20 µg NP/ml. 5 µl of diluted sample was injected in to a reversed phase LC column (C_{18} stationary phase) coupled to a single quadrupole MS (Waters, Milford, MA). The mobile phase was ACN/water (65/35, v/v). Clofazimine was detected as $[M+H]^+$ = 474.4. The LC peak area was used to calculate clofazimine concentration by means of a calibration curve using external standards. The percentage of clofazimine encapsulated in PLGA was calculated via simple mathematics.

The Clofazimine drug loading analysis was performed in Dr. Steven Wilson's laboratory at the Institute of Chemistry, University of Oslo.

3.3 *In vitro* studies with nanoparticles in mouse macrophages

3.3.1 Isolation of macrophages from mouse bone marrow

All macrophage experiments in this thesis were done using primary bone marrow derived macrophages isolated from C57BL/6 mice. The macrophages were isolated using a protocol adapted from Kalluru *et al.* (Kalluru, Fenaroli et al. 2013). The mice were sacrificed when they were between 4 to 12 weeks old by cervical dislocation, and the mice were soaked in 70% ethanol. Working completely aseptically, the mice were dissected and the femur and tibia were removed and soaked in sterile PBS (Sigma-Aldrich, St. Louis, MO, USA) for roughly 5 minutes. Any remaining mouse tissue that was attached to the bones after dissection was removed by rubbing the bones with autoclaved paper tissue. The cleansed bones were then put in 70 % ethanol and moved to a sterile working hood. The bones were washed in sterile PBS to remove any residual ethanol and then kept in PBS to prevent drying. The ends of the bones were cut with sterile scissors to get access to the bone marrow, where the macrophage precursor cells are found together with other hematopoietic cells. The bone marrow was then washed out of the bone cavity with RPMI 1640 cell culture medium (Lonza, Basel, Switzerland) by using a sterile 5 ml syringe fitted with a 25-gauge needle. The marrow and the medium were collected in a non-treated culture dish and suspended in more cell medium. This suspension was then transferred to a Falcon 50 ml tube and the cells were collected by centrifugation at 400 x rcf for 5 minutes at room temperature. The pellet collected after this step was red coloured and contained both erythrocytes and the macrophage precursor cells – the mononuclear cells. To selectively remove the erythrocytes, the pellet was re-suspended in red blood cell lysis buffer (Sigma-Aldrich, St. Louis, MO, USA). Lysis of the erythrocytes was detected by the medium turning yellow, which took 3-5 minutes. The lysis was stopped by adding fresh RPMI medium, and the cells were collected by centrifugation at 400 x rcf for 5 min at room temperature. After discarding the supernatant, the cells were re-suspended in full primary macrophage cell media, RPMI 1640 supplemented with 10% fetal calf serum (FCS; Sigma-Aldrich, St. Louis, MO, USA), and 50 µM of β-mercaptoethanol (Sigma-Aldrich, St. Louis, MO, USA). To differentiate the monocytes into macrophages, L929 conditioned medium (prepared

in our lab) was added to the RPMI cell medium to a final concentration of 20%. The L929 medium contains murine macrophage colony stimulating factor (M-CSF). The cells were then filtered into a 50 ml Falcon tube through a 70 µm cell strainer (BD Biosciences, Franklin Lakes, NJ, USA). The cells were plated on non-treated culture dishes for 6-7 days to let them differentiate. After differentiation, the cells were collected, re-suspended in FCS with 10% DMSO and kept at –80 $^{\circ}$C.

3.3.2 CCK-8 viability assay

The Cell Counting Kit 8 (CCK-8; Sigma-Aldrich, St. Louis, MO, USA) gives a colorimetric measure of the cell metabolic activity by use of the CCK-8 reagent solution containing a tetrazolium-based salt called WST-8. This salt is reduced by the dehydrogenases of viable cells. The reduction reaction shifts the absorbance of WST-8 and thus the colour of the CCK-8-solution. The shift in absorbance is proportional to the number of viable cells in the solution and can be measured at 450 nm (Ishiyama, Tominaga et al. 1996).

Procedure

Primary murine macrophages were thawed, washed and re-suspended in fresh full antibiotic free RPMI 1640 medium and grown on non-treated culture dishes for 3 days. On the third day, the cells were collected, counted and then diluted to a cell density of $2x10^5$ cells per ml The cells were seeded in transparent 96-wells cell culture plates for 24 hours. We used $4x10^4$ cells per well and one plate per time point in the experiments. After seeding, the cells were settled in a monolayer, and the wells were then washed to remove all unattached cells.

Treatment solutions of PLGA-CFZ NP and free CFZ were then prepared. PLGA-CFZ NP were dissolved directly in full RPMI medium by sonication in a water bath to make a stock solution of NP corresponding to a CFZ concentration of 80µM. Free CFZ was first dissolved in DMSO and then diluted in full RPMI medium to make a stock solution of 80 µM in 1% DMSO. The two stock solutions were further diluted in full RPMI medium to make the treatment groups with lower CFZ concentration. The final treatment solutions had 80, 40, 20, 10, 5 and 2.5 µM of CFZ. Macrophages were treated continuously with these concentrations and the cell medium was changed every third day.

The cell viability was measured at day 1, 3 and 6. The cells were washed twice in PBS before being added 5% (v/v) CCK-8 reagent in clear (phenol red free) RPMI medium. The cells were then incubated at 37 °C for 40 minutes. After incubation, 100 µl was sampled from each well and transferred to a new transparent 96 wells plate. The absorbance was then read at 450 nm for 0.1 seconds in a plate reader (Viktor2, PerkinElmer, Waltham, MA, USA).

3.3.3 Crystal violet viability assay

Cell viability can also be assessed using crystal violet (CV) staining. CV is a dye that interacts with various biological structures, in particular sugar-containing structures such as bacterial peptidoglycans and DNA. CV can also be used to stain eukaryotic cells and the amount of staining in a cell culture is proportional to the number of viable cells. In the CV viability assay, the cells are seeded on a culture dish where they will be firmly attached as long as they are viable. Non-viable cells on the other hand, are no longer able to maintain the active and energy-consuming process of staying attached to the treated surface. Washing in PBS will therefore remove any non-attached and thereby non-viable cells. The remaining cells can be chemically fixed and stained with CV. The fixed cells are thoroughly washed to remove any excess CV, the CV can be extracted using for instance methanol, and the absorbance of the extract can be measured. Because the washing steps remove all unattached cells, the extracted CV will correspond proportionally to the number of cells attached to the surface. These are the cells that were alive before fixation, and CV staining is therefore a direct measure of the number of live cells in a culture.

Procedure.

The CV staining assay was performed on the exact same cells as used in the CCK-8 assay. The cells in the 96 wells plate were fixed for 15 minutes in 4% paraformaldehyde (PFA) in PBS, just after removal of the CCK-8 reagent. After fixation, the cells were washed 3 times in PBS to remove excess PFA. After washing, 50 µl of 0.5 mg/ml CV in 20% ethanol was added to each well and left there for 15 minutes to stain the cells. After staining, the cells were washed thoroughly six times in Milli-Q water and then left to dry upside down on a paper tissue. When the wells were completely dry, 100 µl of methanol was added to each well and the plates were left on an orbital shaker for 5 min at 140 rpm to extract the CV from the cells. 50 µl of

the methanol CV extract was then transferred to a new transparent 96 well plate and analysed by reading the absorbance at 595 nm for 0.1 seconds in a plate reader (Viktor2, PerkinElmer, Waltham, MA, USA).

3.3.4 LAMP-1 antibody labelling of macrophages

Cells were seeded at poly-L-lysine coated glass coverslips in 12 wells cell culture plates for 24 hours. After seeding, the cells were incubated for 3 hours with 20 µM of PLGA encapsulated CFZ. 24 hours later, the macrophages were washed twice in PBS and then fixed for 15 minutes in 4% paraformaldehyde (PFA). The fixed cells were then washed 3 times in PBS.

At the start of the labelling procedure the cells were incubated in of 0.1% glycine in PBS for 10 min to quench the fixative, before the cells were permeabilized using 0.1% Triton X-100 in PBS for 10 min. To reduce non-specific binding the cells were incubated in a blocking solution with 1% bovine serum albumin (BSA) in PBS for 20 min, before being incubated for 30 minutes with the primary antibody (Rat monoclonal antibody specific for mouse LAMP-1, clone 1D4B, Developmental Studies Hybridoma Bank) diluted in 1% BSA. The antibody solution was put in drops of 100 µl on parafilm attached to the bottom of a 15 cm plastic dish and the coverslips were placed with the cells facing down on the antibody drops. Wet paper tissues were put next to the parafilm and the plastic dish was sealed with a lid and parafilm to create and keep a humidified chamber during the entire labelling process.

After labelling with LAMP-1, the coverslips were washed 5 times in PBS before the secondary antibody labelling was performed in the same way as outlined for the primary antibody. The secondary antibody was a goat anti-rat IgG (H+L), conjugated to Alexa 488 (Jackson ImmunoResearch) in 1% BSA. Again, the coverslips were washed 5 times in PBS. To stain the cell nucleus, the coverslips were put on a drop of 0.5 µg/ml DAPI solution in Milli-Q and incubated for 5 min. Immediately after DAPI (Sigma-Aldrich, St. Louis, MO, USA) staining, the coverslips were washed in Milli-Q and dried gently using filter paper. 2 µl of 2% Mowiol (Alfa Aesar, Ward Hill, MA, USA) supplemented with 20 mg/ml DABCO antifade agent (Sigma-Aldrich, St. Louis, MO, USA) were put on a glass slide, the coverslip was firmly placed on top of it with the cells facing down, and the glass slide was moved to the microscope.

3.3.5 Fluorescence microscopy

Fluorescent imaging was performed using an Olympus Fluoview 1000, inverted confocal laser scanning microscope IX81 using a PlanApo 60x/1.42 oil immersion objective (Olympus, Hamburg, Germany).

3.3.6 Flow cytometry

Flow cytometry is a method for high-throughput cell analysis, typically used to identify a subset of cells from a larger population by use of light scattering and fluorescence detection. Usually, the cells to be analysed will have different, or varying fluorescence characteristics, due for instance to differences in antibody labelling, expression of a fluorescent protein or uptake of a fluorescent cargo. Flow cytometry is performed in an apparatus were a dilute suspension of cells is streamed through a nozzle making the cells passing through a laser beam, one at a time. The interaction between the laser light and the cell is detected and this is used to characterize the cell. Scattered light gives information about the cell's size and shape, while the fluorescence can be used to categorize the cell (e.g. by means of antibody binding), and also to give a quantitative measure of the fluorophore associated with the cell. Flow cytometry is a fast method, making it possible to analyse large amounts of cells and many samples in a short time.

CFZ is a naturally fluorescent compound, and thus flow cytometry is well suited for studying CFZ uptake and retention in cells (Keswani, Yoon et al. 2015).

Procedure.

Cells treated with CFZ, in either free or encapsulated form were washed and fixed with 4 % PFA and stored at + 4 °C until they were all analysed at the same time. The flow cytometry was done in a FACS-Calibur (BD Bioscience, New Jersey, USA) using the program Flowing Software 2.5.1. (Turku Centre of Biotechnology, University of Turku, Finland). CFZ was measured in the FL2-channel (red fluorescence). The experiments were performed at The Flow Cytometry Core Facility (FCCF), Oslo University hospital (OUS), Oslo, Norway.

3.4. *In vivo* infection and treatment in zebrafish embryos

3.4.1 Culturing *Mycobacterium marinum*

The following protocol was adapted from Cosma *et al.* (Cosma, Swaim et al. 2006) and (Gao and Manoranjan 2005)

DsRed transformed *M. m* (msp 12::dsRed2, provided by prof. Lalita Ramakrishnan) was kept as frozen stocks at -80 °C. Liquid cultures were prepared 1 week before zebrafish injections to make sure the bacteria were in the exponential growth phase at the start of the experiment. 10 µl of thawed, frozen stock of bacteria was added to 20 ml of a premade liquid growth medium consisting of 18 ml Difco Middlebrook 7H9 broth, and 2 ml OADC (ovalbumin, dextrose, and catalase). The medium was supplemented with 0.02% glycerol and 0.05% Tween 80 to prevent clumping of the bacteria. The *M.m* cultures were grown in a dark room in an incubator at 30 °C with gentle shaking. Usually, the bacteria reach the exponential phase after 5 to 6 days in the incubator. OD_{600} was measured to confirm the growth stage of bacteria and the exponential growth phase corresponded to an OD_{600} ~0,5-1.0 (Comas, Coscolla et al. 2013).

3.4.2 alamarBlue® viability assay

This assay was adapted from Lechartier and Cole (Lechartier and Cole 2015). alamarBlue® is a cell viability assay based on the oxidation-reduction indicator resazurin. alamarBlue® can be used to measure the viability of eukaryotic cells, as well as bacteria. The principle of the assay is that metabolically active cells will convert the non-fluorescent compound resazurin into the strongly red fluorescent compound resorufin. This change in fluorescence can be accurately quantified by measuring the fluorescence at 585 nm in a plate reader. The alamarBlue® assay has been used to evaluate the minimal inhibitory concentration (MIC) of several of the first-line drugs against *M.tb* (Yajko, Madej et al. 1995) and was recently used by Lechartier and Cole (Lechartier and Cole 2015) to determine the MIC of CFZ against in *M.tb*.

Procedure

To assess the MIC of CFZ against *M.m,* bacteria were thawed and grown to the exponential growth phase. The bacteria were then sub-cultured in new media with increasing concentrations of CFZ and left to grow at 30 °C for 4 days. Triplicates of 300 µl of bacteria from each of the CFZ concentrations were incubated for 24 hours in 10% (v/v) alamarBlue® cell viability reagent (Invitrogen) added to mycobacterial growth medium. The fluorescence was then evaluated at 585 nm in a plate reader (SynergyMX, Biotek, VT, USA).

3.4.3 Preparing *Mycobacterium marinum* for micro-injection

Bacteria were harvested no longer than 1 hour before the injection. Prior to harvesting the bacteria, the OD_{600} was measured to confirm that the bacteria were in the exponential growth phase. The bacterial culture was passed twice through a 22-gauge needle before measuring the OD_{600}, as Mycobacteria often form aggregates, which will lead to an erroneously low measurement of the optical density. When the measured optical density was between 0.5 and 1.0, 200 µl of the bacterial culture was collected by centrifugation for 2 min at maximum speed using a table-top centrifuge. After centrifugation, the supernatant was disposed of, and the pellet of bacteria was re-suspended in PBS supplemented with 2 % PVP to make a suspension of OD_{600} equal to 1.0, which corresponds to ~$6x10^7$ CFU/ml (Comas, Coscolla et al. 2013). The PVP was added to prevent bacterial aggregation, which often leads to clogging of the needle used for injection. After re-suspension, the OD_{600} was measured again, and the cell density was adjusted if necessary. An injection volume of 3 nl then corresponds to 180 bacteria and this normally gives an infection that kills the untreated zebrafish control group within 10 to 11 days.

3.4.4 Preparing clofazimine for micro-injection

Clofazimine was weighed and dissolved in DMSO to make a CFZ stock solution of 3.33 mg/ml. This solution was sonicated for 20 seconds to make sure the CFZ was completely dissolved. After sonication, the stock solution was diluted by adding 2% PVP in PBS to make a final solution of 1 mg/ml of CFZ in 30% DMSO. This solution was sonicated for 1 min just before injections. Due to its low solubility, this was the

highest possible concentration CFZ that could be used without clogging the needle used in the zebrafish embryo micro-injections.

3.4.5 Preparing PLGA-CFZ nanoparticles for micro-injection

Freeze-dried PLGA-CFZ NP were stored at 4 °C when not in use. Before injection, NP were dissolved in PBS and sonicated briefly to break all NP aggregates. Concentrations corresponding to up to 10 mg/ml of CFZ could be injected without clogging the needle.

3.4.6 Micro-injections in zebrafish embryos

The injection protocol was adapted from Cosma *et al.* (Cosma, Swaim et al. 2006). Zebrafish embryos were injected with *M.m* at 2 days post fertilization (dpf) and the treatments were injected at 3 dpf. At 2 dpf the zebrafish embryos are sufficiently developed to allow microinjections in the vasculature. The microinjection procedure was the same for PLGA-CFZ NP, free CFZ and bacteria.

Injections were performed using thin borosilicate needles connected to a pressure controller. The needles were made from borosilicate capillaries (outer diameter 1.0 mm, inner diameter 0.78 mm length 100 mm; Harvard, Apparatus, Holliston, MA, USA;) in a Flaming/Brown P-97 micropipette-puller (Sutter, Novato, CA, USA) with the settings: delay 110, heat 610, pull 40, velocity 50 and pressure 500.

The pressure controller (Femojet; Eppendorf AG, Hamburg, Germany) was connected to a flask of N_2 gas. This setup gives firm control of the ejection pressure, the time pulse and the constant pressure during injections. This ensures that the injection volume can be accurately controlled throughout the injection procedure.

The needle was loaded with 5 µl of solution using a micro-loader pipette, before the needle was attached to the pressure controller. The tip of the needle was carefully broken using fine jewellers forceps (Dumont No. 5) and the ejected volume was calibrated in a microscope by measuring the diameter of the released droplet in mineral oil at 60x-magnification. The diameter was measured in arbitrary units marked on the ocular. **Figure 3.4** shows the relation between the volume and the diameter in these arbitrary units at 60x magnification. Altering the pressure, the time pulse or the opening of the glass needle is done adjust the injected droplet to the

right volume (1-8 nl, depending on the exact concentration and content of the solution). As seen in **Figure 3.4** the diameter is most accurately measured between 0.6 and 1.5 units as the curve gets steeper and steeper with increasing diameter.

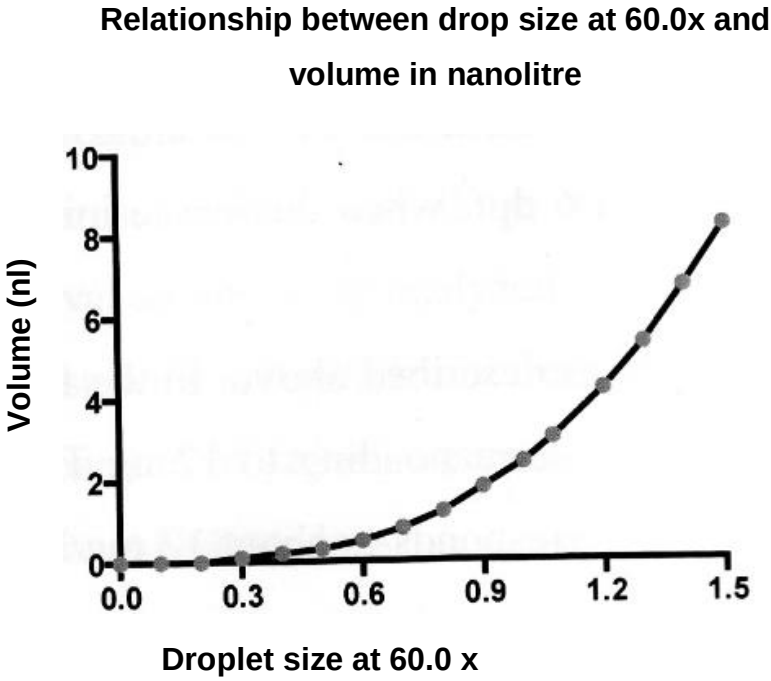

Figure 3.4: The graph shows the relationship between the drop size measured in arbitrary units at 60.0x magnification and the volume of the droplet in nanoliters. Figure adapted from the master thesis of Carina Vibe (University of Oslo 2014).

Prior to injection, zebrafish embryos were sedated in a 230 µg/ml tricaine solution for 1 minute. Sedated embryos were placed on an injection plate of 2% w/v agarose (Sigma-Aldrich, St. Louis, MO, USA) and excess water was gently removed using a transfer pipette and filter paper. The embryos were quickly injected in the caudal vein (**Figure 3.5)** and then immediately put in fresh embryo water for recovery.

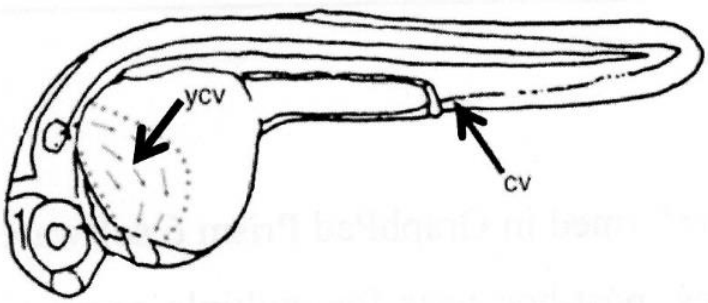

Figure 3.5: Drawing of a zebrafish embryo marked with injection sites. CV is the caudal vein and YCV is the yolk circulation valley. The figure is adapted from Cosma *et al.* (Cosma, Swaim et al. 2006)

3.4.7 Zebrafish husbandry and breeding

Zebrafish were kept in the aquarium facility at the University of Oslo. The fish were kept in tanks at a density of approximately 3 fish per litre of water. The water temperature was kept at 28 °C. The fish had daylight from 8 am to 8 pm and darkness for the remaining 12 hours. At least 10 % of the water was exchanged per day. The conductivity and the pH was measured 3 times per week and nitrite and nitrate levels were measured weekly to control that the water change was sufficient and that the bio-filter degraded the nitrogen waste produced by the fish. The pH was kept between 7 and 8, and the nitrite level was kept below the level of detection using a tetra test kit (Webzoo).

The fish were fed brine shrimps (Silvergrade II Argentimia, argent-labs, USA) once per day and dry-feed pellets (SDS 400) twice per day. An additional fourth feeding was included during breeding since we experienced that this improved the output of eggs. The night before breeding a small plastic box filled with glass marbles was introduced to the aquarium. The marbles stimulate the fish to breed and at the same time protect the eggs from being eaten by other fish. The fish start breeding when the light is turned on in the morning. The fish were left to breed for 2 hours and were not fed until the breeding was over. The marbles were carefully removed and the water in the box was filtered through a sieve to harvest the eggs. The eggs were then washed two times in embryo water and inspected using a Leica M205 FA stereomicroscope (Leica microsystems, Wetzlar, Germany). All dead or diseased eggs were removed. The eggs were distributed into petri dishes with less than 100 eggs per dish and put in an incubator at 28 °C. Embryo water was changed daily and any dead or diseased embryos were removed. At 1 dpf, the eggs were manually dechorionated using

forceps. All experiments were done in the “Casper” zebrafish strain (roy$^{-/-}$; nacre$^{-/-}$, provided by the Norwegian University of Life Sciences, NMBU). These embryos do not develop pigment and therefore remained transparent throughout the experimental period (White, Sessa et al. 2008). This made both injections and the subsequent analyses easier to perform.

3.4.8 Survival experiments in zebrafish embryos

Zebrafish embryos were injected with dsRed *M.m* at 2 dpf and treatment at 3 dpf, as outlined above. After injection, the embryos were allowed to recover overnight and the next day any non-surviving embryos were removed. During the entire experiment, the treatment groups were kept in separate 10 cm dishes and embryo water was changed daily. Every third day the embryos were moved to a new clean petri dish. Every 24 hours all groups were controlled and dead and live fish were counted using a Leica M205 FA stereomicroscope (Leica microsystems, Wetzlar, Germany). Fish with a completely absent heartbeat were considered dead and removed from the dish. Because of the red fluorescence emitted by the dsRed *M.m*-strain used, dead fish could also be controlled for infection by using the red fluorescent channel in the stereo microscope **(Figure 3.6).** This was done for every dead fish to verify that they had been killed by the infection and was not dead due to other causes. The survival experiments were terminated at day 10 or 11 post infection (dpi). At this time point, under normal circumstances, all the embryos in the infected, untreated control group were dead.

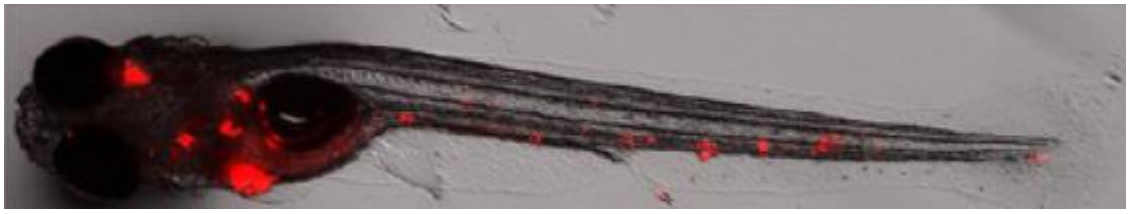

Figure 3.6: Zebrafish embryo infected with dsRed *M.m* The bacterial infection is clearly seen as red spots inside the embryo. Figure is adapted from Fenaroli *et al.* (Fenaroli, Westmoreland et al. 2014)

3.5 Statistics

Survival experiments in infected zebrafish embryos were analysed in GraphPad Prism 6 software (GraphPad Software, La Jolla, CA, USA), using a Kaplan-Meier representation and Log-rank (Mantel-cox) test for pairwise comparison of curves. All other data were analysed in Microsoft Excel where means and standard deviations were calculated.

3.6 Ethical considerations

All animals used in this thesis were kept and treated in full accordance with the local regulations at the University of Oslo. The number of animal used in the experiments was kept to the minimum of what was possible, and all experiments were planned well in advance to make sure no animals were unnecessarily sacrificed.

4 Results

4.1 Formulation of clofazimine nanoparticles

The main goal of this thesis was to develop and test CFZ NP in the zebrafish embryo TB model, and the first major challenge was to find a way to prepare NP containing this drug. Drug entrapment into NP is usually a complicated issue, which often relies on lengthy work performed on a trial and error basis. Prior to this project, my colleagues in the Griffiths' group had spent around 18 months perfecting the method to successfully encapsulate RIF into PLGA (Fenaroli, Westmoreland et al. 2014) and thioridazine into PLGA (Vibe, Fenaroli et al. 2015).

4.1.1 Single emulsion solvent evaporation

The single emulsion solvent evaporation method (as outlined in paragraph **3.1.1**) for making drug-encapsulated PLGA-NP was the standard method used in our laboratory, and had previously been used to encapsulate both RIF and thioridazine. This method was therefore adapted to CFZ using DCM as solvent and PVA as surfactant in the first attempts to make PLGA-CFZ NP. The preparation is summarized in **Table 4.1**.

PLGA 50:50 (mg)	PVA (% w/v) in 20 ml Milli-Q	DCM (ml)	CFZ (mg)
100	1%	10	100
100	4%	10	100

Table 4.1: Summary of components used for single emulsion preparation of PLGA-NP containing CFZ.

The single emulsion solvent evaporation method did not work well for CFZ. During the sonication, PLGA formed a slimy precipitate while CFZ formed needle shaped crystals that could easily be seen in a light microscope (**Figure 4.1**). The crystals varied in size and were too big to be injected in zebrafish. No nanoparticle formation was observed.

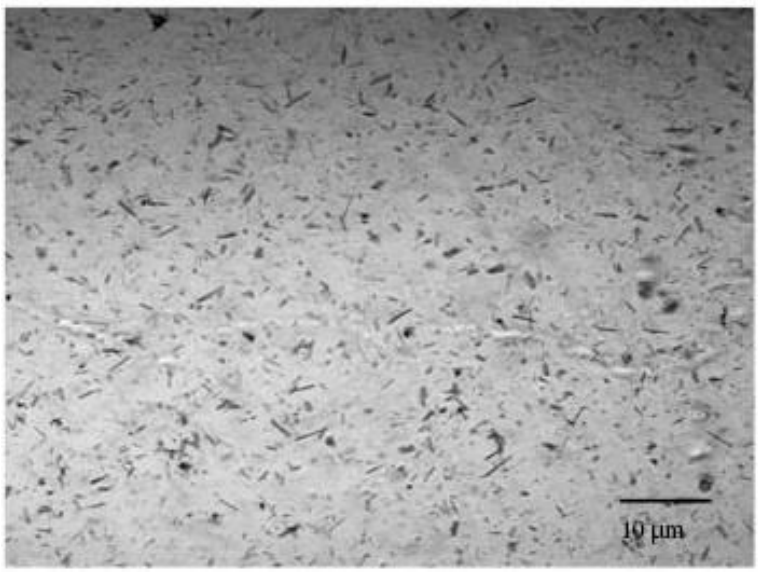

Figure 4.1: Light microscopy of our preparation after an attempt to form PLGA-CFZ NP using the single emulsion solvent evaporation method. Needle shaped CFZ-crystals are easily observed. This sample was prepared with 4% PVA as outlined in Tab. 4.1.

4.1.2. Encapsulation of clofazimine in chitosan nanoparticles

Because the single emulsion method was unsuccessful, we had to try alternative ways to encapsulate CFZ. It was unclear from the single emulsion preparation method whether CFZ could be encapsulated in PLGA and we therefore wanted to also test another type of polymer. In this regard, chitosan polymers modified with hydrophobic TPP side-chains see **Figure 3.3** were interesting because TPP is a very hydrophobic group that makes the chitosan self-assemble into NP in an aqueous solution (Gaware, Hakerud et al. 2013). The idea was that TPP might interact with CFZ and that the chitosan-TPP polymer would entrap also CFZ when they self-assembled. Chitosan and CFZ were co-dissolved in DMSO before Milli-Q water was gradually added to make the chitosan particles self-assemble. The solution was inspected in a Leica DMIRBE microscope (Leica microsystems) to look for aggregates, crystals and NP. After a few rounds of testing, we found that a Chitosan/CFZ ratio of 1:1, giving a final concentration for each of the components of 0.5 mg/ml in 5% DMSO gave a red-coloured transparent solution without any CFZ crystals. However, no NP could be observed by light microscopy, and ultracentrifugation at 15 000 rpm gave no pellet at all. Chitosan NP could however be detected using TEM, with an apparent size of less than 200 nm **(Figure 4.2)**.

Because the Chitosan NP could not be collected with ultracentrifugation they could not be washed, dried and quantified to estimate the efficiency of drug loading (a crucial step for the later use in treatment) with our current set-up. We therefore decided to leave this track without further investigation.

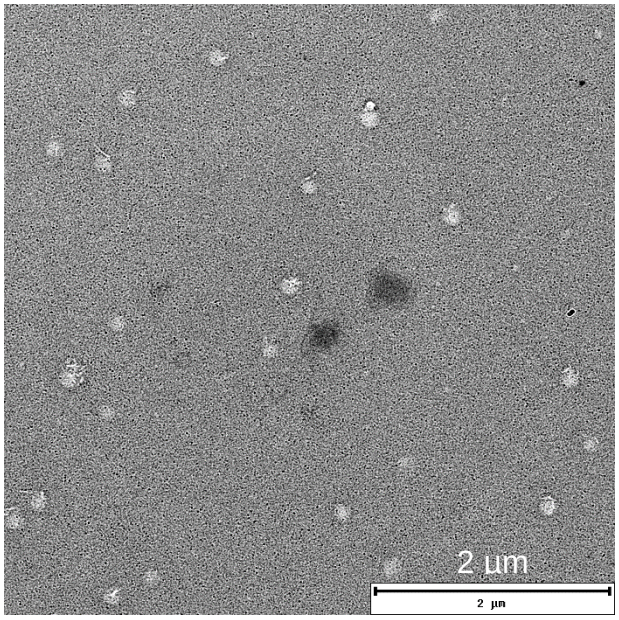

Figure 4.2: TEM of chitosan nanoparticles. Chitosan-CFZ nanoparticles were prepared as described under Materials and Methods, and immediately analysed by TEM. The negatively stained chitosan NP are seen as white spots.

4.1.3 Nanoprecipitation method – screening and optimization

As described above, the initial attempts to encapsulate CFZ in PLGA using the single emulsion solvent evaporation method seemed fruitless, since PLGA and CFZ precipitated separately and no NP were formed. This suggested that PLGA encapsulation of CFZ needed a radically changed approach. We therefore decided to try to prepare PLGA NP containing CFZ *via* nanoprecipitation, a method in which the parameters of NP formation can be finely tuned, and where it is feasible to test a variety of experimental conditions in a relatively short time. Besides being a fast and easy method, nanoprecipitation is also the most suited method for using THF and DMSO, two of the best solvents for CFZ. For preparing the NP, PLGA and CFZ were

co-dissolved in the appropriate solvent and added dropwise to a stirring solution of surfactant dissolved in Milli-Q water. **Table 4.2** summarizes the set up for the initial screening for nanoprecipitation of PLGA and CFZ. The samples were analysed using light microscopy to look for NP, crystals and aggregates. As seen in **Figure 4.3**, it was clear from the microscopy that for NP formation THF was a better solvent than DMSO and that Tween 80 was a better surfactant than PVA.

PLGA:CFZ mg:mg	Solvent (5 % v/v)	Surfactant	Microscopy Evaluation
20:10	THF	1% PVA	No NP - aggregates
20:10	THF	0.5% Tween 80	NP and Crystals
20:10	DMSO	1% PVA	Only crystals
20:10	DMSO	0.5% Tween 80	Only crystals

Table 4.2: The table summarizes the setup for the first nanoprecipitation screen, where different solvents and surfactants were tested in different combinations. In the nanoprecipitation the PLGA and CFZ were dissolved in 1 ml of solvent, and this solution was dripped into 20 ml of water containing the surfactant, as described under Materials and Methods. Evaluations were done by looking at the samples in a Leica DIMBRE microscope.

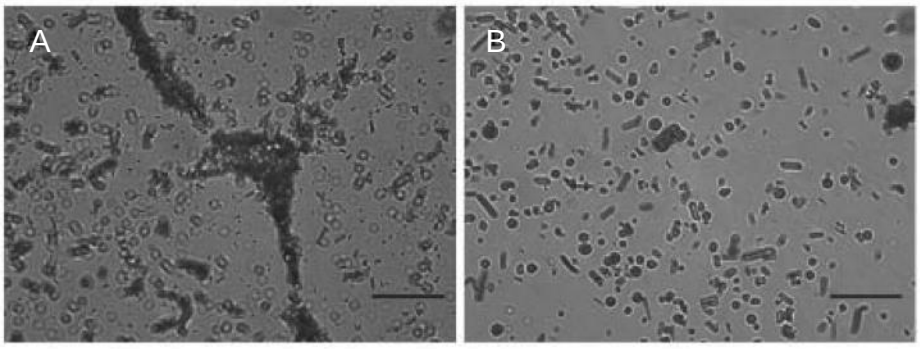

Figure 4.3: Microscopy image done during the nanoprecipitation evaluation using the Leica DMIRBE microscope A**)** The DMSO, 1 % PVA sample. The absence of NP, and the presence of large aggregates or needle shaped drug crystals are seen in the sample. **B)** Shows the THF 0.5 % Tween 80 sample. Round shaped PLGA-CFZ NP are seen together with needle shaped CFZ-crystals. Scale bars 5 µm.

4.1.3.1 Optimization of nanoprecipitation

After identifying an appropriate solvent and surfactant, the next step was to optimize the nanoprecipitation conditions and find a formulation that would give pure NP without any crystal or aggregate formations. In the optimization process, the different parameters had to be varied to find the best combination of the PLGA:CFZ ratio, and the optimal surfactant and solvent concentration. **Table 4.3** summarizes a setup where the ratios and concentrations of PLGA and CFZ were varied.

PLGA end concentration (mg/ml)	CFZ end concentration (mg/ml)	Tween 80 end concentration (% v/v)	THF end concentration (% v/v)	Microscopy evaluation
2	2	0,5	5	Crystals and aggregates
2	1	0,5	5	Crystals and aggregates
2	0,5	0,5	5	Crystals and aggregates
1	1	0,5	5	Crystals and aggregates
1	0,5	0,5	5	NP and crystals

Table 4.3: Summary of nanoprecipitation screen where the ratio and absolute concentrations of PLGA and CFZ were varied. The experiment was performed essentially as described in the legend of Table 4.2. The samples were evaluated using an inverted epifluorescence microscope.

It was found that amounts of PLGA and CFZ of 20 and 10 mg, respectively (in a total volume of 20 ml) gave the most promising results, yielding a mixture of NP and crystals. In order to find conditions to obtain a NP preparation without crystals a new screen was started (summarized in **Table 4.4**). We developed a setup where the final concentrations of PLGA/CFZ (keeping the 2:1 ratio of the substances), THF and surfactant were independently varied. Again, the samples were inspected in the Leica DMIRBE inverted epifluorescence microscope, where crystals, aggregates and NP can easily be distinguished from each other. This third round of screening showed that a sample without any crystals could be formed by increasing the concentration of Tween 80 from 0.5% to 1% in the aqueous fraction. A higher concentration of Tween 80 probably increases the solubility of CFZ in the preparation solution and thereby prevents crystallization. **Figure 4.4** shows examples of PLGA-

CFZ NP formed under nanoprecipitation. Lowering the concentrations also seemed to decrease the size of the particles although this was not quantified. However, a condition that could give pure PLGA-CFZ NP had been successfully determined, allowing the project to progress.

PLGA end concentration (mg/ml)	CFZ end concentration (mg/ml)	Tween 80 end concentration (% v/v)	THF end concentration (% v/v)	Microscopy evaluation
0,5	0,25	0,5	2,5	Crystals and microparticles
0,5	0,25	0,5	5	Crystals and microparticles
1	0,5	0,5	10	50:50 NP and Crystals
1	0,5	1	5	NP aggregates and microparticles
0,5	0,25	1	2,5	Only NP

Table 4.4: Summary of nanoprecipitation screen where the concentrations of PLGA/CFZ, THF and Tween 80 were varied. The experiment was performed essentially as described in the legend to Table 4.2, with the exception that the volume of THF was varied. The samples were evaluated using the inverted epifluorescence microscope.

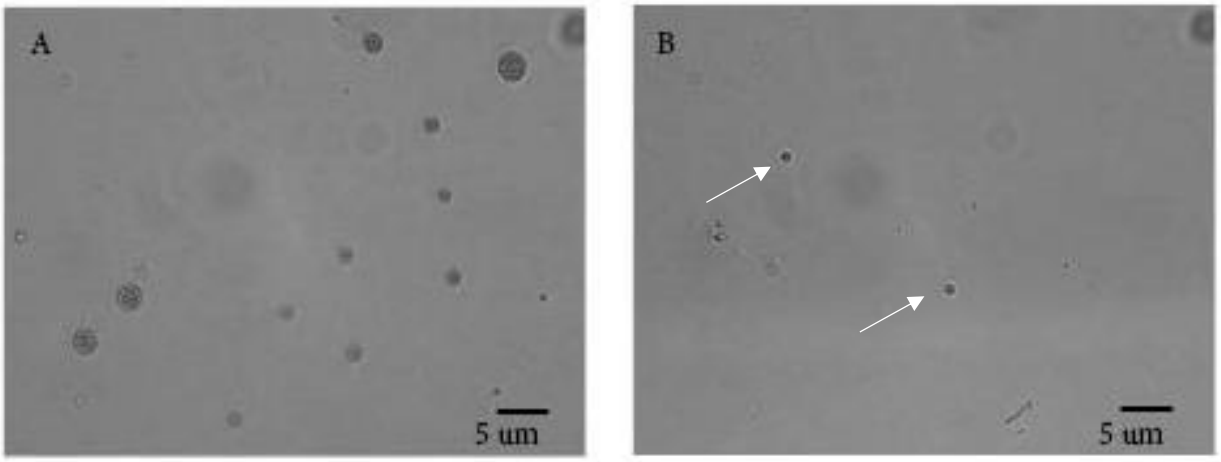

Figure 4.4: Images of nanoprecipitation samples taken with the Leica DIMBRE microscope during the nanoprecipitation evaluation. The two displayed samples were prepared with 1 % Tween 80 **A)** Sample prepared using 1 mg/ml PLGA, 0.5 mg/ml CFZ and 5 % THF Micro -sized PLGA-CFZ. Microparticles were observed. **B)** Sample prepared using 0.5 mg/ml PLGA, 0.25 mg/ml CFZ and 2.5 % THF. Nanoparticles were observed (arrows).

4.2 Nanoparticle characterization

4.2.1 Physical characteristics

Before biological testing of the PLGA-CFZ NP, it was necessary to do a physical and chemical characterization of the NP, since both later experimental set-ups and interpretations of experimental results involving the PLGA-CFZ NP are dependent on knowledge about their physical and chemical characteristics. The mean size, the size distribution, the surface charge and the drug loading are the most critical parameters, and had to be determined before the project could proceed. In addition, at this stage, the stability of the PLGA-NP in water solution was not known and, in particular, we did not know if the NP kept their properties during freeze-drying. If the PLGA-CFZ NP had low stability or could not be freeze-dried, they could not be used in biological experiments.

Table 4.5 summarizes the physical and chemical characteristics of the PLGA-CFZ NP. The mean diameter of the PLGA-CFZ NP dissolved in water was measured before and after freeze-drying by dynamic light scattering (DLS), as described in Materials and Methods. The size of the NP was 353 nm ± 49 before freeze-drying and 328 nm ± 43 after freeze drying, i.e. well within the optimal size range for phagocytosis. The results also showed that the NP had a quite narrow size distribution, something that is also important for the use in and interpretation of biological experiments. The size of the NP was also largely unaffected by the freeze-drying process.

The drug loading in the NP was measured by HPLC, and was found to be 14% w/w. This is lower than the drug loadings that have been achieved for RIF and thioridazine using the single emulsion solvent evaporation method (Fenaroli, Westmoreland et al. 2014, Vibe, Fenaroli et al. 2015). The mean surface charge was measured using a Zetasizer instrument as described in Materials and Methods. The surface charge was slightly negative -1.7 ± 0.3, and significantly less negative than what was found for PLGA-RIF and PLGA-TZ (Fenaroli, Westmoreland et al. 2014, Vibe, Fenaroli et al. 2015).

NP-components	Diameter ± SD (nm) before freeze-drying	Diameter ± SD (nm) after freeze-drying	Zeta-potential (mV)	Drug loading (%,w/w)	Yield (mg)
PLGA 50:50, 1% Tween 80	353 ± 49	328 ± 43	-1.7 ± 0.3	14	17

Table 4.5: Summary of the characterization of the PLGA-CFZ NP prepared by nanoprecipitation.

Re-suspended freeze-dried NP were imaged using transmission electron microscopy and fluorescence microscopy, and representative results are shown in **Figure 4.5**. The TEM confirmed the size- measurements by the dynamic light scattering methods, and also demonstrated that the PLGA-CFZ NP kept their shape after freeze-drying. In addition, the images revealed that the NP had a tendency to aggregate (**Figure 4.5 B** and **C**). In the fluorescence microscopy imaging, the drug loading can be readily although roughly visualized, as CFZ is naturally fluorescent at several wavelengths (Keswani, Yoon et al. 2015).

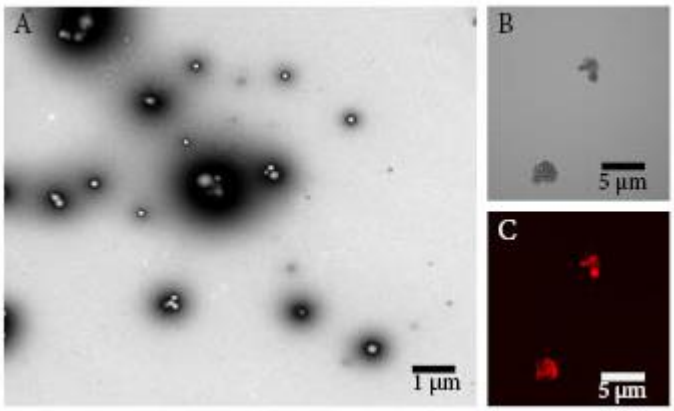

Figure 4.5: A) Representative TEM image of the PLGA-CFZ NP. **B)** Transmission light microscopy image of PLGA-CFZ NP. **C)** The same sample as in B seen in the red fluorescence channel in the inverted Olympus Fluoview 1000 microscope.

4.3 PLGA-CFZ nanoparticle behaviour in macrophages

The characterization of the PLGA-CFZ NP suggested that the NP were suited for biological testing. In order to understand the interaction of PLGA-CFZ NP with macrophages we decided to test them *in vitro* on mouse bone marrow-derived macrophages. The uptake, stability and retention of the NP in the cells were the key parameters we sought to evaluate first.

4.3.1 Intracellular localization of PLGA-CFZ nanoparticles

Previous experiments in our group had shown that PLGA NP loaded with the green fluorescent dye coumarin-6 were rapidly taken up by macrophages and that the NP co-localised with lysosome markers after 1 hour of internalization (Kalluru, Fenaroli et al. 2013). The PLGA-CFZ NP were however prepared differently from those made from the PLGA-coumarin-6. In particular, PLGA-CFZ NP were prepared with Tween 80 as a surfactant as compared to the PVA used in Kalluru *et al*. CFZ or Tween 80 exposed on the surface of the PLGA-CFZ NP could lead to a different interaction with the cell plasma membrane and possibly change the uptake route. It was therefore possible that the PLGA-CFZ NP could be localized to a different intracellular compartment from what had been observed for the other PLGA-NP.

When the PLGA-CFZ NP were characterized, it became clear that CFZ-loading gave the NP a slight red fluorescence (**Figure 4.5**). This made it possible to directly visualize the NP in a fluorescence microscope. Initial data showed that macrophages, at least to some extent, could take up the PLGA-CFZ NP (data not shown). This uptake is likely to happen by phagocytosis, meaning that the NP would enter the cells inside a phagosome. The normal destination for phagocytosed material is the lysosomes (Flannagan, Cosio et al. 2009), so we thought that this would also be the case for PLGA-CFZ NP. To investigate the intracellular localization of the NP we labelled the macrophages with the LAMP-1 antibody (as described in **section 3.3.4**), and studied the localization of the NP by fluorescence microscopy. LAMP-1 (lysosomal-associated membrane protein 1) is a trans-membrane protein enriched in late endosomes and phagosomes, but not in early or intermediate endosomes.

LAMP-1 antibody labelling should therefore selectively mark late endosomes and phagosomes (Flannagan, Cosio et al. 2009).

As shown in **Figure 4.6** it is clear that the PLGA-CFZ NP were internalized by the macrophages **(A**, **B**, **D**) and that CFZ was visible as large red spheres inside the cells (**A**, **D**). The large size of the nanoparticle spheres made it difficult to do a detailed evaluation of their localization inside the cell and to see co-localization with the LAMP-1 antibody. In addition, it was also difficult to conclude on possible co-localisation because the NP also exhibited weak green fluorescence that made it difficult to distinguish between the NP and the secondary antibody used in the sample (**Figure 4.7**). In addition, the primary macrophages are dense with lysosomes making co-localization hard to determine (**Figure 4.6 C**).

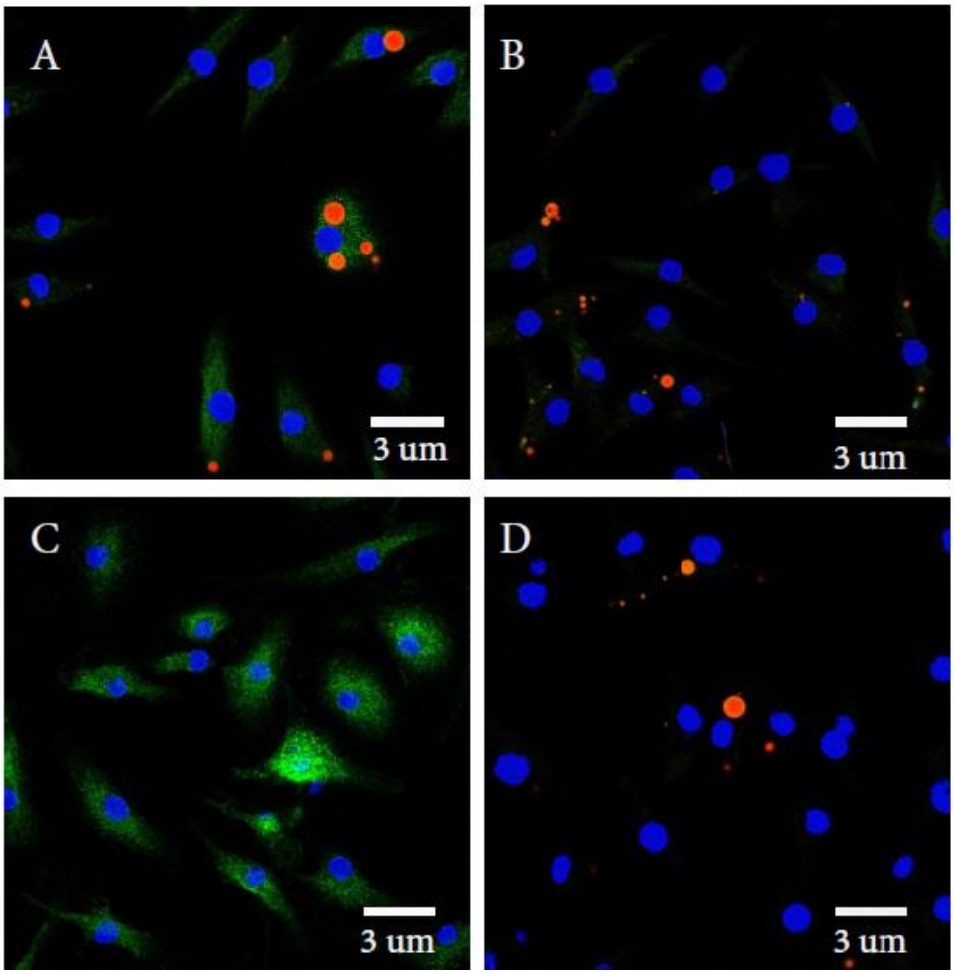

Figure 4.6: A) Primary macrophages treated with 20 µM PLGA-CFZ NP (Red) for 24 h. Late endosomes and lysosomes were labelled with LAMP-1 primary antibody and an Alexa488-coupled secondary antibody (Green). The cell nucleus was stained with DAPI (Blue). **B)** Primary macrophages treated with 20 µM PLGA-CFZ and secondary antibody without the LAMP-1 primary antibody. **C)** Macrophages treated with LAMP-1 antibody and secondary antibody without PLGA-CFZ treatment. **D)** Macrophages treated with PLGA-CFZ only.

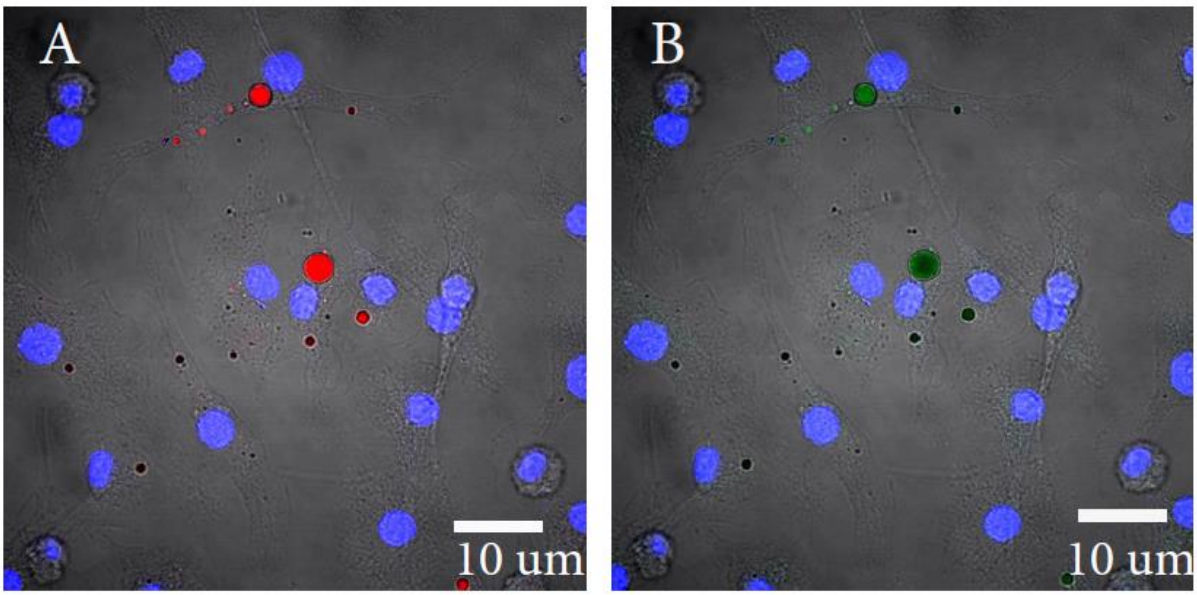

Figure 4.7: A) Primary macrophages treated with PLGA-CFZ NP imaged in the red fluorescence channel. **B)** The same cells as in A) imaged in the green fluorescence channel.

4.3.2. Uptake of PLGA-CFZ nanoparticles in macrophages

After analysis of NP localization within the cells, we sought to evaluate their uptake using flow cytometry, which is possible due to the fluorescence of the PLGA-CFZ NP. We therefore aimed at understanding how phagocytosis of PLGA CFZ NP would influence the drug's intracellular concentration as compared to delivery of the free compound.

To this end, macrophages were incubated for 3 hours with 10 µM or 40 µM of free or PLGA-encapsulated CFZ. After the incubation, we measured the intensity of the fluorescent signal from CFZ across the samples and counted the number of cells that had taken up drug. We defined cells positive for uptake to be cells with a fluorescence intensity that was higher than any fluorescence intensity measured in the untreated group. Thus, treated cells with a fluorescence intensity higher than the highest control value (CFZ-free) were denoted as CFZ-positive cells.

Figure 4.8 shows the median fluorescent intensity (MFI) and the percentage of positive macrophages for the 10 µM and 40 µM groups. For the 10 µM groups, free CFZ gave the highest MFI and the highest percentage of positive cells with 93.3 % positive, as compared to 7.9% for PLGA-CFZ NP. The high score for free CFZ may be due both to uptake of CFZ into the cells and to the lipophilic CFZ molecules sticking to the cell membranes; however we were not able to get a detailed picture of the free CFZ localization by fluorescence microscopy. The results were strikingly different when the cells were incubated with 40 µM CFZ in free or PLGA encapsulated form. At this concentration, only 18.4% of the cells incubated with free CFZ were positive while 52.0% of the PLGA-CFZ cells were positive. However, at 40 µM, free CFZ was toxic to the cells and the sample contained fewer cells. Most likely, only cells with limited uptake of CFZ survived the 3 hours of incubation, resulting in a low number of positive cells and low MFI in the cells available for analysis. In sharp contrast, the PLGA-NP were not toxic at this concentration and more NP in the solution led to an increase in uptake of CFZ, resulting in a larger fraction of positive cells, and to an almost 4 times increase in MFI, indicating a dose-dependent uptake of the PLGA-CFZ NP into the macrophages.

The uptake mechanism appears to be different between free drug and NP and we did not find any large accumulation of CFZ in the free drug incubated cells as we did for the PLGA-CFZ incubated cells (**Figure 4.10**).

Color	3 h Uptake group	MFI	% CFZ positive
A and B	Neg Ctrl	3,5	0
A	Free CFZ 10 µM	49,1	93,3
A	PLGA-CFZ 10 µM	6,7	7,9
B	Free CFZ 40 µM	12	18,4
B	PLGA-CFZ 40 µM	21,3	52

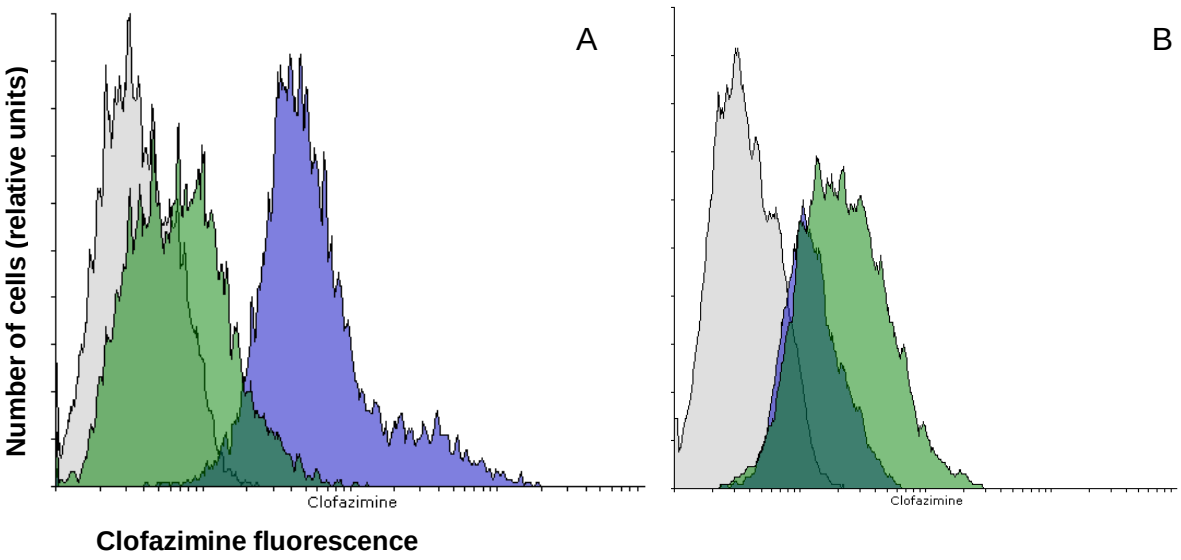

Figure 4.8: Histograms of cells analysed by flow cytometry after three hours of incubation with CFZ. The grey histograms correspond to untreated cells, the blue histograms correspond to cells treated with free CFZ and the green histograms correspond to cells treated with PLGA-CFZ NP. **A**) The histograms for cells exposed to 10 µM of CFZ B**)** The histograms of cells treated with 40 µM of CFZ. The table shows the corresponding median fluorescent intensity (MFI) for each group, and the percentage of CFZ positive cells.

4.3.3 Retention of PLGA-CFZ nanoparticles in macrophages.

Knowing that the PLGA-CFZ NP were taken up in cells, we next sought to assess their stability and the retention in the cells after uptake by the macrophages. In order to achieve a relatively high number of cells taking up NP, we incubated the macrophages for 3 hours with PLGA-CFZ NP, corresponding to 40 µM of CFZ. The MFI was measured by flow cytometry at day 0, 1, 2, 3 and 6 after incubation.

As seen in **(Figure 4.9)**, the MFI decreases for every time point. The decrease is steepest between day 0 and day 1 and flattens out at later time points. At the last time point, day 6, the MFI is still higher than the negative control indicating that there still are cells containing CFZ.

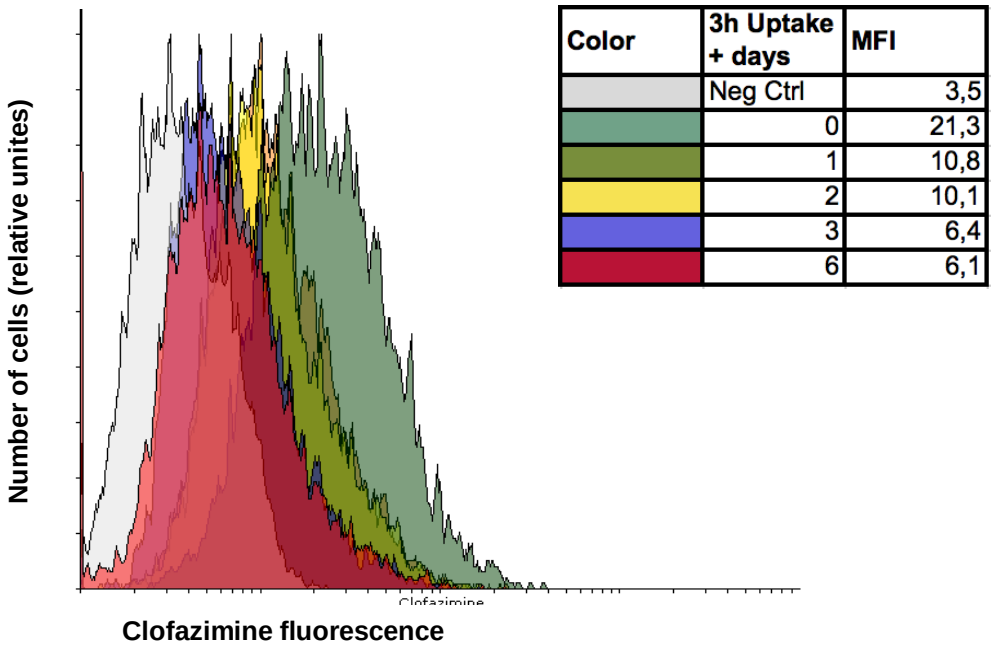

Color	3h Uptake + days	MFI
	Neg Ctrl	3,5
	0	21,3
	1	10,8
	2	10,1
	3	6,4
	6	6,1

Figure 4.9: Histograms of cells analyzed by flow cytometry after incubation for the indicated number of days, to follow the retention of the PLGA-CFZ NP in the cells. All groups were treated for 3 h with PLGA-CFZ NP (in an amount corresponding to a CFZ concentration of 40 µM), prior to the incubation. Untreated cells are shown in light grey, dark grey represents cells analyzed directly after the 3 h treatment, and green, yellow, blue and red corresponds to 1, 2, 3 and 6 days of incubation after treatment, respectively.
The table in the upper right corner shows the corresponding MFI values.

In parallel to the flow cytometry, we treated cells at the same concentration of either free or PLGA-encapsulated CFZ. We then fixed the cells at the same time points we used in the previous experiment, and looked at them in a fluorescence microscope.

As seen in **Figure 4.10,** there were still cells containing large accumulations of CFZ at day 6, confirming that they seem to be gradually, albeit slowly lost from the cells. Although we could not use our images as a quantitative method, the pictures taken suggest that there are less CFZ NP per cell at day 6 compared to day 0 or day 1 (**4.10** B vs D).

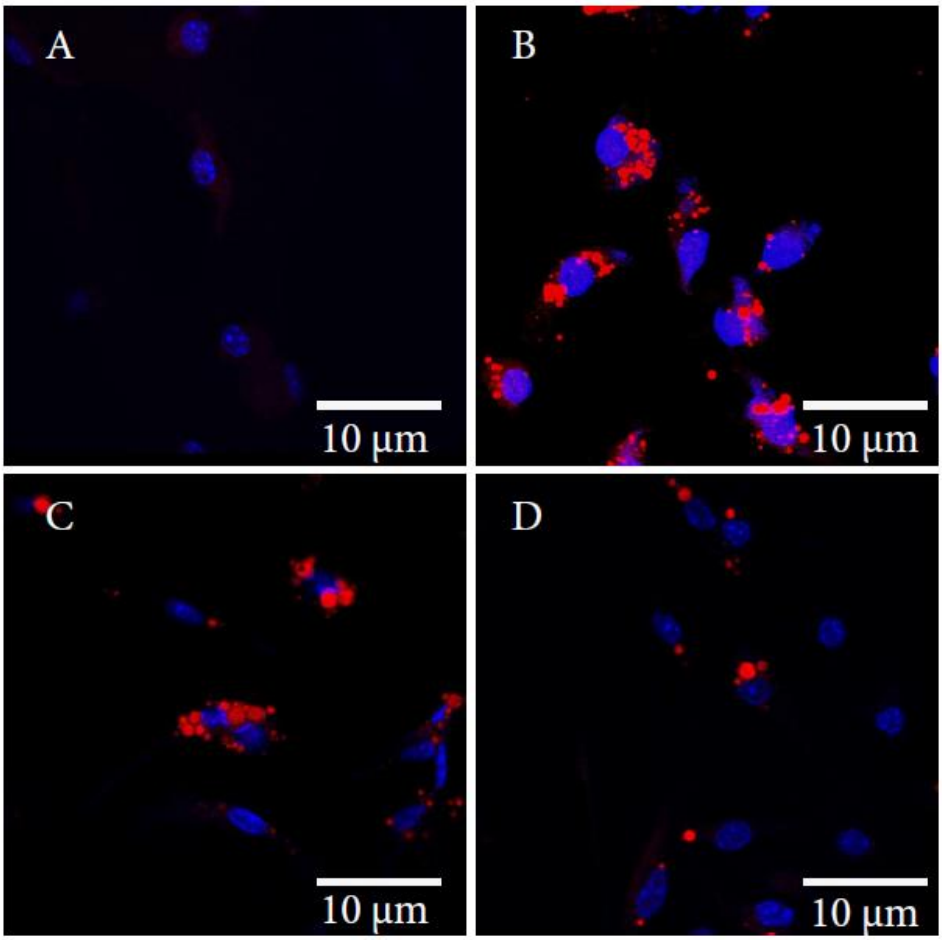

Figure 4.10: Representative images of macrophages from the uptake and retention experiment. CFZ is seen in red. Nuclei were Hoechst-stained and are seen in blue **A)** Primary macrophages treated with 10 µM free CFZ. **B)** Primary macrophages treated for 3 h with 40 µM PLGA-CFZ (Red). Uptake and accumulation of CFZ is apparent. **C)** Macrophages imaged 1 day after the 3 h treatment with 40 µM PLGA-CFZ. **D)** Macrophages imaged 6 days after incubation with PLGA-CFZ.

4.3.4 *In vitro* toxicity of PLGA-CFZ and free clofazimine

Our experiments with flow cytometry suggested that, at high concentrations, free clofazimine is toxic to cells, in line with what has be described by others (Yoon, Sud et al. 2015). It also seemed like the same amount of drug encapsulated in PLGA NP resulted in significantly lower cell death. We therefore decided to investigate with specific toxicity assays the impact of CFZ in the free and PLGA-encapsulated form. PLGA encapsulation of CFZ could potentially reduce the toxicity by keeping a larger fraction of the drug entrapped inside the NP and thereby preventing the cells from being exposed to the full dose at once. We compared the toxicity of free, and PLGA encapsulated, CFZ by using the CCK-8 and the crystal violet staining assays performed on macrophages that were given continuous treatment. The cell viability was evaluated at day 1, 3 and 6 after treatment with equal concentrations of free and PLGA-entrapped CFZ. Starting at 2.5 µM, the concentration was doubled for every group ending at 80 µM. CFZ was dissolved in DMSO before being added in the appropriate amount to the cell medium. The two highest concentrations of DMSO, 1% and 0.5% v/v (in the 80 µM and 40 µM samples respectively), were also tested for toxicity. Empty PLGA NP were given at a concentration of PLGA corresponding to that of the 80 µM PLGA-CFZ group.

Figure 4.11 and **Figure 4.12** shows the CCK-8 and crystal violet assays, respectively. The results with the two different assays corresponded nicely, and it is apparent that the toxicity was reduced when CFZ was encapsulated in PLGA. Thus, after day 1, there were no cells detected with concentrations of free CFZ higher than 10 µM in any of the assays. On the contrary, for PLGA-CFZ NP 80 µM of CFZ was well tolerated even after 6 days of continuous treatment in both assays. DMSO seemed to be slightly toxic at 1% v/v. It cannot be excluded that 0.5% of DMSO may also have toxic effects, but the detected toxicity of DMSO cannot solely explain the toxicity observed in the free CFZ treated groups.

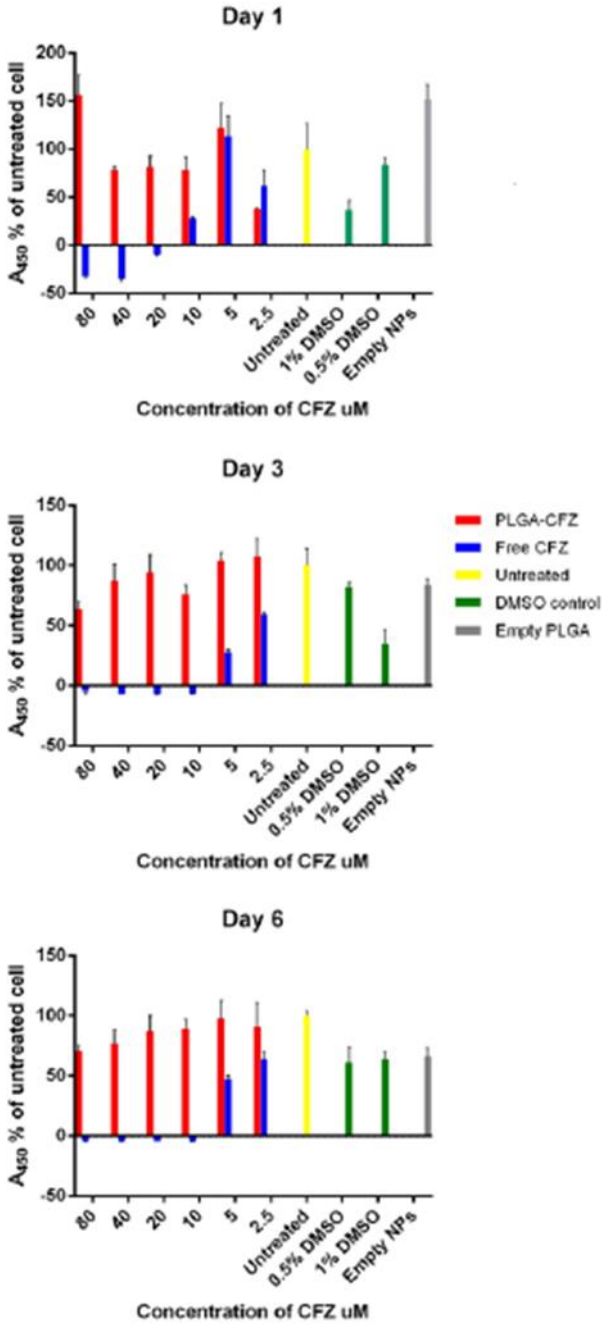

Figure 4.11: Cell viability after continuous treatment with CFZ was measured by absorbance at 450 nm using the CCK-8 assay (n=3). A_{450} values are presented as mean ± SD normalized to untreated control (100%). The background for each treatment was measured by incubating either CCK-8 reagent or CV-solution in empty wells. The background was then subtracted from each of the measurement. For some of the samples this led to negative value, meaning that the measured value was lower than the background. The experiment was performed in triplicate.

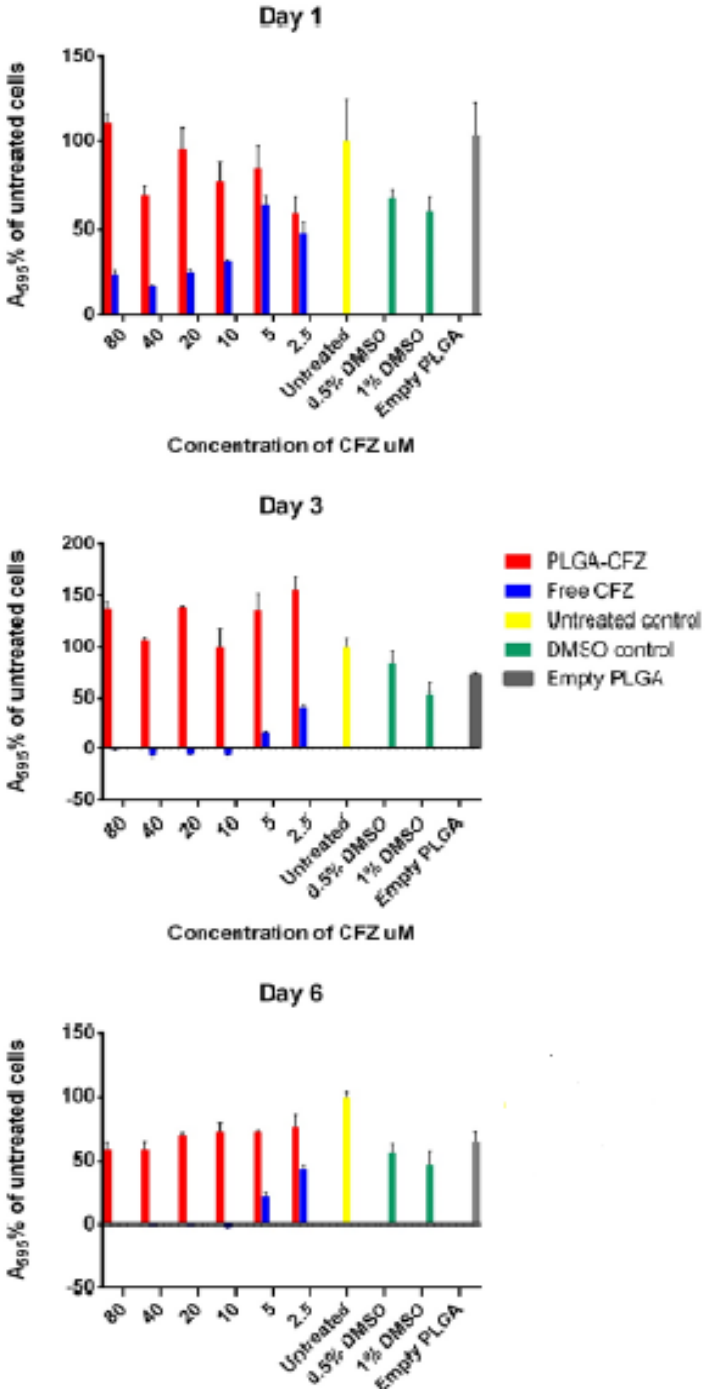

Figure 4.12: Cell viability measured by the Crystal Violet assay**.** Crystal violet staining was used to quantify the number of cells that remained attached to the dish surface during CFZ treatment (n=3). A_{595} values are expressed as mean ± SD, normalized to untreated cells for each time point.

4.4 Treatment experiments in zebrafish

4.4.1 Minimum inhibitory concentration of clofazimine against *M.m*

The final goal of this project was to test the therapeutic effect of CFZ NP in the zebrafish embryo model system. Before starting these experiments, it was important to find the minimum inhibitory concentration (MIC) of CFZ against *M.m* CFZ has an MIC of 0.15 µg/ml against *M.tb in vitro* (Lechartier and Cole 2015*)* and based on this information a dilution series of CFZ was prepared starting from 4.8 µg/ml and down to 0.075 µg/ml. MIC here is defined as the lowest concentration without any detectable bacterial growth. The first MIC experiment was done by measuring the OD_{600} of the bacterial culture. Bacteria were diluted to an OD_{600} of 0.0025 and incubated for 5 days. Before measuring the $OD_{600,}$ a blank sample of empty bacteria medium was tested against a solution of 5 µg/ml CFZ to verify that they had the same absorbance in the spectrophotometer. The results are shown in **Table 4.6** and suggest an MIC of around 0.15 µg/ml.

Concentration of CFZ (µg/mL)	**OD_{600}**
4.8	0
2.4	0
1.2	0
0.6	0
0.3	0
0.15	0.07
0.075	0.29
0	0.57

Table 4.6: OD_{600} measurements of *M.m* after treatment with different concentrations of free CFZ. The measurements were done after five days of incubation in bacteria growth medium containing the indicated concentrations of CFZ. All negative measurements are shown as 0.

Realising that OD measurements may not be always give correct results MIC experiments were also performed using the alamarBlue® assay that has been used to assess the MIC of CFZ against *M.tb* (Lechartier and Cole 2015). The cells received the same treatment as in the OD_{600}-experiment, but after five days of incubation, the bacterial solutions were added 10 % v/v of the alamarBlue® reagent rezasurin and then incubated for 12 hours. Rezasurin is a redox indicator that changes fluorescence emission when metabolised by active bacteria, and it has been used to determine the MIC of many of the most common anti-TB drugs against *M.tb* (Yajko, Madej et al. 1995). After incubation, the samples were analysed in a plate reader by measuring fluorescence at 585 nm. As seen in **Figure 4.13**, the alamarBlue® assay relates well to the OD_{600} measurement, again suggesting a MIC of CFZ against *M.m* of ~0.15 µg/ml. Thus, the two independent assessments are in agreement with each other and corresponds well with the reported MIC of CFZ against *M.tb* (Lechartier and Cole 2015).

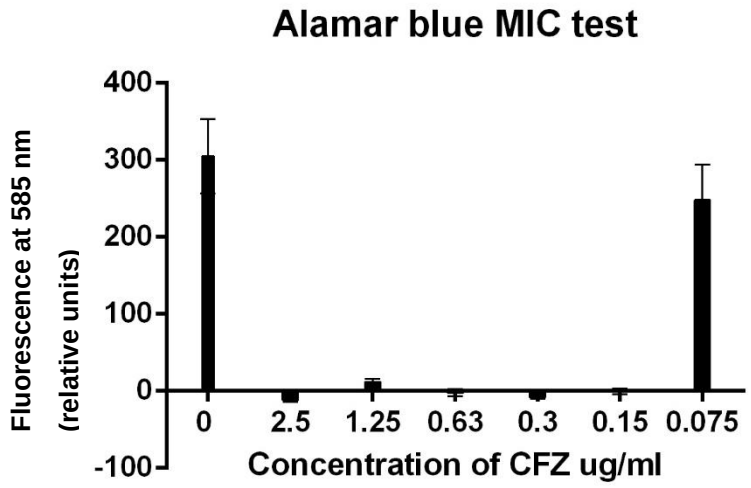

Figure 4.13: Fluorescence at 585 nm for *M.m* liquid cultures treated with the indicated concentrations of CFZ and then incubated for 12 hours with 10% alamarBlue® reagent as described in Materials and Methods.

4.4.2 Toxicity in zebrafish embryos

The zebrafish embryo is a very powerful indicator of toxicity of many compounds, and in our group the zebrafish embryo model had previously been used to demonstrate reduced toxicity of thioridazine when this compound was encapsulated in PLGA (Vibe, Fenaroli et al. 2015). Most CFZ animal studies are performed with oral administration of the drug and, and apart from skin and tissue discoloration, there are no reports of toxicity from these studies. Thus, the estimated LD_{50} of orally administered CFZ is >4 g/kg for mice, rabbits and guinea pig (Brennan 2008). However Mehta (Mehta 1996) found CFZ to be toxic at a concentration of 5 mg/ml when injected directly into the mouse vasculature and, in his experiments, liposome encapsulation of CFZ reduced the toxicity. We therefore wanted to test if CFZ was toxic towards zebrafish embryos when injected directly into the blood.

To assess the toxicity, 15 embryos were injected with 10 mg/ml of CFZ dissolved in 30% DMSO at 2 dpf. The injected embryos were compared to 15 un-injected embryos, and all embryos in both groups were inspected individually for toxicity indicators such as edemas and reduced heart rate or blood flow in a Leica M205 FA stereomicroscope (Leica microsystems, Wetzlar, Germany). There were no visible differences between the two groups and they both grew and developed normally over the 10 days they were controlled. At 12 dpf the experiment was terminated without any sign of toxicity.

We therefore concluded that even at the highest injectable concentration of 10 mg/ml, CFZ does not cause any evident signs of toxicity in the zebrafish embryo. Thus, we could not monitor whether encapsulation of the drug in PLGA would result in a reduced toxicity of CFZ in the embryos, like it was found for macrophages *in vitro*.

4.4.3 Monotherapy in zebrafish with 5 mg/kg clofazimine

Eventually, we wanted to test the therapeutic effect of PLGA-CFZ NP and see if they could perform better than free CFZ against *M.m in vivo*. The aggregations formed by the PLGA-CFZ NP limited the concentration of PLGA-encapsulated CFZ that could be injected to 0.7 ng/nl. We could inject around 7 nl in the zebrafish embryo and a zebrafish embryo 3 dpf has a body mass of ~1 mg. This meant that the maximum

treatment dose we could inject was 5 mg/kg, which is lower than the doses used in mice and humans. The first step of our experiment was the infection of zebrafish embryo using 180 cfu of *M.m*, which were injected at 2 dpf in a solution of 2% PVP in PBS. We then proceeded with the treatments at 3 dpf. PLGA-CFZ NP were dissolved in 2% PVP while free CFZ was dissolved in 30% DMSO in 2% PVP. The fish were controlled every 24 hours and dead fish were counted and removed. The results showed that that PLGA-CFZ NP gave a slightly better therapeutic effect than free CFZ, but the difference between these experimental groups was not statistically significant (**Figure 4.14)**. However, The PLGA-CFZ NP were significantly different (p=0.0478) from the *M.m*-infected untreated group, while the free CFZ treated group was not. This suggested that there could be an effect of treatment with PLGA-CFZ, and that this potential effect should be investigated further.

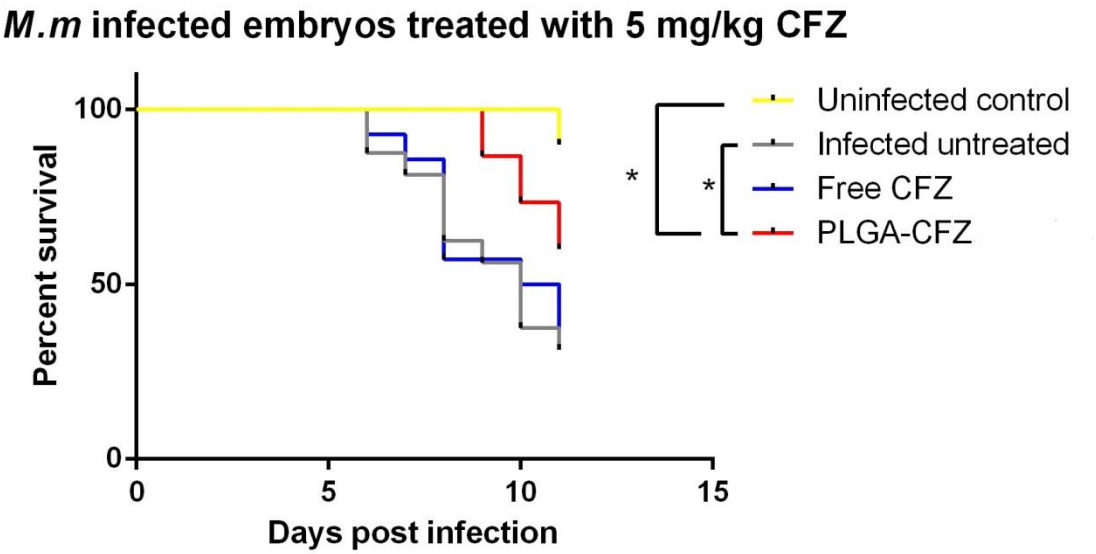

Figure 4.14: Survival of *M.m*-infected zebrafish embryos treated with free CFZ or PLGA-CFZ NP injected into to the embryo at 3 dpf in a solution of 2% PVP (n=15-17). Statistical significance is indicated by asterisks and was calculated by survival analysis in GraphPad Prism. * indicates p value<0.05.

Our inability to test the NP with a higher overall concentration of CFZ was an obvious limiting factor in this experiment. In the studies using PLGA-RIF treatment, effects were first seen at treatment doses of 15 mg/kg; and RIF is considered to be the most potent anti-TB drug together with isoniazid.

4.4.4 Monotherapy with 10 mg/kg clofazimine

It was important for our purposes to improve the experiment displayed in **Figure 4.14**, and therefore we tried repeatedly to increase the injected dose of CFZ. By dissolving PLGA-CFZ NP in PBS instead of 2% PVP in PBS, it was possible to raise the CFZ concentration of the NP solution to 1.6 ng/nl. This allowed us to inject a CFZ dose of 10 mg/kg, which potentially could improve the treatment. We also prepared empty PLGA NP by nanoprecipitation and tested whether they could be injected in the same concentration of PLGA as the PLGA-CFZ NP. The experiment was conducted as outlined for the previous experiment, and we managed to inject both the PLGA-CFZ NP and the empty PLGA NP reproducibly at the desired concentration. As shown in **Figure 4.15**, the increased concentration did not improve the therapy, and, although it again seemed that there was a tendency towards a treatment effect of PLGA-CFZ NP and free CFZ, there was no statistical difference between any of the 3 injected groups. All of the groups were significantly different from the uninfected control with p<0.0001. Due to a lack of suitable embryos when the experiment was conducted, this experiment was done without an only *M.m*-infected untreated control and the treatment effects were therefore compared to empty PLGA injected fish.

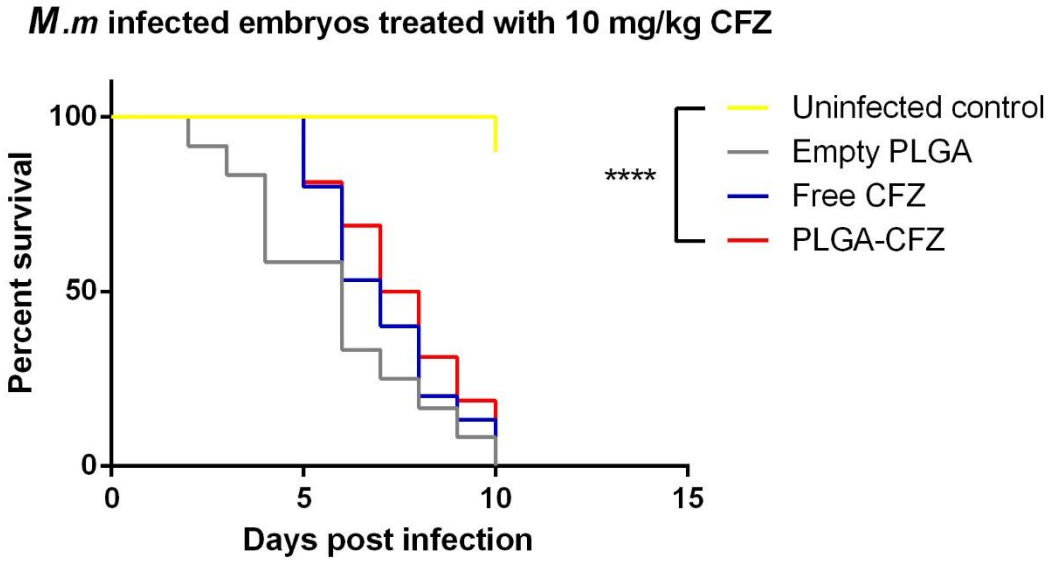

Figure 4.15: Survival of *M.m*-infected zebrafish embryos treated with 10 mg/kg free CFZ or PLGA-CFZ NP injected into to the embryo at 3 dpf in a solution of PBS (n=22-25). Statistical significance is indicated by asterisks and was calculated by survival analysis in GraphPad Prism. P value****<0.0001.

The two survival experiments were not conclusive and it was necessary to conduct an additional experiment to address the therapeutic potential of PLGA-CFZ NP. The embryos were injected with *M.m* at 2 dpf and treatments at 3 dpf. Three control groups were included; empty PLGA NP, untreated *M.m*-infected zebrafish embryos and PBS, mock-injected embryos.

The experimental results are displayed in **Figure 4.16.** In this experiment, all of the treatment groups were statistically indistinguishable from the untreated infected group. All of the treatment groups are significantly different from the uninfected control. Hence, we could not observe any effect of the CFZ treatment in this experiment either. We continued the effort to raise the treatment dose, but none of these attempts were successful and we concluded that 10 mg/kg was the maximum treatment dose that could be injected with our NP.

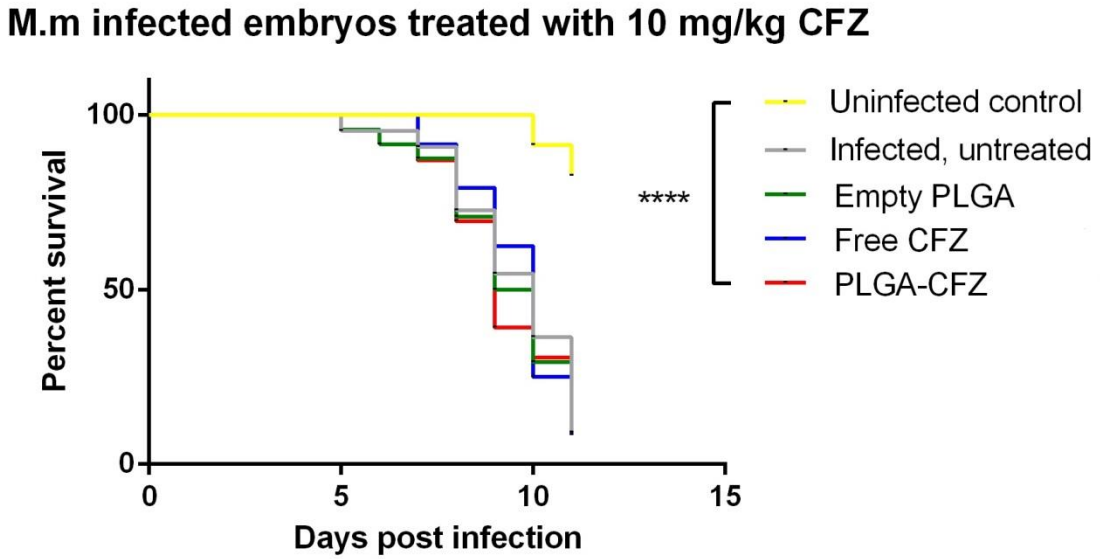

Figure 4.16: Survival of *M.m*-infected zebrafish embryos treated with 10 mg/kg free CFZ or PLGA-CFZ NP injected into to the embryo at 3 dpf in a solution of PBS (n=22-25). Statistical significance is indicated by asterisks and was calculated by survival analysis in GraphPad Prism. P value****<0.0001.

4.4.5 Combinatorial treatment with clofazimine and rifampicin

Because we could not inject enough CFZ to see a clear effect on embryo survival, we decided to test combinatorial treatment of CFZ and RIF. The lack of therapeutic effect during monotherapy had also been observed with thioridazine NP that were made and tested in our group. However, when these NP were tested together with RIF, they enhanced the therapeutic effect and significantly increased the survival of the zebrafish embryos as compared to embryos treated with only RIF. It is quite common that two drugs given together have an additive effect and, in some cases, two drugs may even have synergistic effects that exceed the additive effect. Because the injection dose could not be increased further and because making new NP with a higher CFZ loading was likely to exceed the time limits of this project, we continued the treatment experiments in zebrafish by trying combinatorial treatment with CFZ and RIF.

The CFZ was injected as before, but the treated zebrafish were additionally put in a bath containing 200 µg/ml of free RIF. The treatment groups in this experiment showed higher survival rates than the untreated *M.m*-injected group (**Figure 4.17**). Thus, the group with fish treated with PLGA-CFZ/RIF-bath was significantly different from the *M.m*-injected group ($p=0.0007$). This was also the case for the embryos treated with free CFZ/RIF-bath ($p=0.0368$) and empty PLGA/RIF bath ($p=0.002$). The embryos treated only with RIF-bath were not statistically different from the infected untreated embryos, suggesting the additional injections had an effect. However, none of the CFZ treated groups were statistically different from the embryos treated with RIF bath alone. There was a small difference in survival between embryos injected with free CFZ and embryos injected with PLGA-CFZ NP, with the latter resulting in a slightly increased survival. PLGA-CFZ/RIF treatment was not statistically different from the uninfected control, while the free CFZ was, with $p=0.0318$. PLGA-CFZ/RIF-bath was however not statistically different from empty-PLGA/RIF, thereby questioning the contribution of CFZ.

Nevertheless, the results indicate that there was a hint of an additional effect of CFZ based on an increased effect observed for both free CFZ and PLGA-CFZ NP

compared to only RIF treated fish. The additional effect of encapsulating CFZ in PLGA is however not that convincing and the experiment should be repeated.

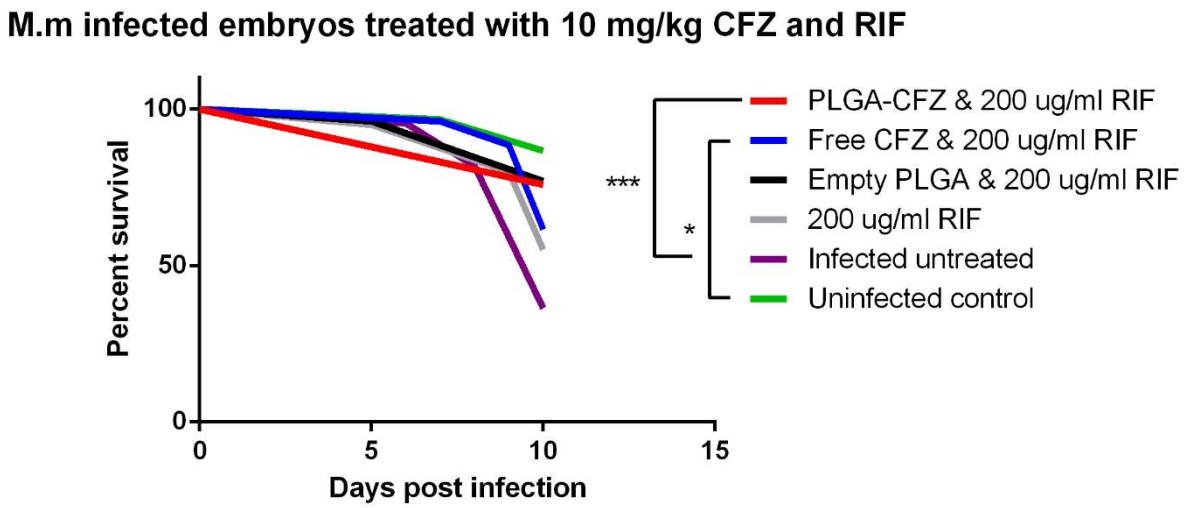

Figure 4.17: Survival of zebrafish embryos treated as indicated in the figure. CFZ treated fish received a CFZ dose of 10 mg/kg, either as free or encapsulated drug; and the fish were in addition treated with 200 µg/ml RIF in bath (n=23-25). P-values *<0.05, and ***<0.001.

5 Discussion

The emergence of MDR-TB has emphasized the need for the development of new TB drug therapies, and at the same time highlighted the limitations of the current standard TB treatment; especially the long duration of the treatments and the problems with patient compliance. Several studies have shown that nanoparticle encapsulation of TB drugs can increase their effect compared to free administered drugs (Pandey and Khuller 2004, Griffiths, Nystrom et al. 2010). This can potentially dramatically increase the effect of the therapy and reduce the dosing frequency. In particular, the loading of hydrophobic drugs into PLGA polymers have given promising therapeutic results in mammalian models (Dutt and Khuller 2001, Sharma, Sharma et al. 2004) and, in some studies, the use of antibiotic loaded PLGA-NP has even achieved complete eradication of *M.tb* (Pandey, Zahoor et al. 2003). Our group has established a unique zebrafish embryo model to test NP therapy against TB (Fenaroli, Westmoreland et al. 2014). The low cost and high fertility of zebrafish means that it is well suited for fast and efficient *in vivo* testing of NP treatments. Even more importantly, the zebrafish embryo model provides direct visual access to the treatment. Hence, using fluorescent probes the NPs can be tracked and analysed in real-time during the treatment.

Clofazimine is a drug used for leprosy treatment that has shown great promise against MDR-TB (Van Deun, Maug et al. 2010). Although the complicated biodistribution profile and the variable effect of CFZ have limited its use, several studies are now investigating ways to improve CFZ-based treatments. These new studies include synthesis of new CFZ-analogs with a more favourable chemistry (Cholo, Steel et al. 2012). The fact that CFZ is a red fluorescent, hydrophobic drug with a complicated biodistribution made it an interesting candidate for testing with NP in our zebrafish embryo model. Building on previous knowledge from zebrafish studies in our group, we hypothesized that PLGA-encapsulation of CFZ could prevent the massive off-target accumulation and direct the CFZ to the infection site by macrophage uptake and transportation. Thus, this study aimed at encapsulating CFZ into NP and test the therapeutic potential of the CFZ-NP. This work was divided into three parts: (i) Formulation and characterization of PLGA-CFZ NP; (ii) Testing of the

PLGA-CFZ NP in cell culture; (iii) Testing the PLGA-CFZ NP in the zebrafish embryo TB model.

5.1 Nanoparticle preparation and characterization

A precondition for our ability to test clofazimine NP *in vivo* was to develop methods for reproducibly encapsulating the antibiotic in polymeric NP. There are no polymeric CFZ-NP reported in the literature so we started with minimal preliminary knowledge. Previously in our group, other hydrophobic drugs such as RIF and thioridazine had been successfully encapsulated by the single emulsion solvent evaporation method (Kalluru, Fenaroli et al. 2013, Vibe, Fenaroli et al. 2015), but in our hands this method unfortunately proved unsuited for encapsulation of CFZ. CFZ has a notoriously difficult chemistry, with a very low water solubility, and it turned out to be very difficult to encapsulate CFZ in NP. Thus, under most conditions tested in this work, CFZ was not encapsulated in the polymer and no NP were formed. Rather, most of the attempts to encapsulate CFZ led to crystal formation, most likely caused by CFZ's low solubility in the preparation solution.

To successfully encapsulate CFZ in PLGA, it was necessary to find a NP preparation method that increased the solubility of CFZ to avoid crystal formation, and that at the same time allowed for PLGA-particle formation. This could only be done by empirical testing of different combinations of solvents and surfactants, a tedious, time-consuming and complicated undertaking. Nanoprecipitation proved to be a method suited for this kind of screening because it allows for testing of multiple conditions in a relatively short time. The chemistry of CFZ limited the potential solvents we could use to THF and DMSO. During pre-testing these were the only two solvents that could dissolve CFZ at a concentration that would be useful for nanoprecipitation. Other solvents such as acetone and acetonitrile were also tested, but were excluded due to poor solubility of CFZ.

The initial nanoprecipitation screening lead to the identification of one condition where PLGA-CFZ NP could be formed. Thus, by using Tween 80 as a surfactant and THF as a solvent it was possible to encapsulate CFZ into PLGA. However, to progress from mere encapsulation of CFZ, i.e. to make NP suited for biological

testing it was necessary to further optimize the PLGA-CFZ NP formulation. We aimed at establishing a formulation that could give uniform NP, in a size-range that would allow for uptake by macrophages and injection into zebrafish embryos. It was also necessary to formulate NP in a manner that did not create any aggregates or crystals, as these were often observed as bi-products during the PLGA-CFZ NP formulation. To be able to investigate the effect of the PLGA-CFZ NP in biological systems, it was also necessary to have NP that remained stable during and after freeze-drying, and that could subsequently be re-suspended in water.

For the use in *in vivo* therapeutic studies, it was also important that the drug loading was sufficiently high to give a meaningful biological effect. To be able to accurately determine the amount of encapsulated CFZ the NP therefore also had to be washable, so that any non-encapsulated drug molecules could be removed before HPLC-analysis.

These requirements were somewhat in conflict with each other. To reduce the formation of aggregates and crystals it was necessary to increase the concentration of Tween 80 and thereby increase the solubility of CFZ in the solution. This resulted in much of the CFZ being retained in the solution and later lost in the supernatant during the washing steps of NP-formulation. This probably would affect the drug loading, and for this reason, we wished to keep the solvent:water ratio as high as possible. However, the size of the NP formed by nanoprecipitation is also affected by the solvent:water ratio; thus it is often observed that reducing the solvent:water ratio gives smaller NPs (Cheng, Teply et al. 2007). The size of the NP is also dependent on the PLGA concentration, and lower PLGA concentration gives smaller NP (Cheng, Teply et al. 2007). During the optimization, we frequently saw microparticles up to 3-5 µm, and often even larger aggregates of NP; these were obviously too big for our needs. To reduce the size of the PLGA-CFZ NP and eliminate the aggregates it was necessary to decrease the solvent:water ratio, and also the PLGA and CFZ concentration. By doing this, we observed fewer aggregated PLGA-CFZ NP, and also fewer larger microparticles, in accordance with what could be expected (Cheng, Teply et al. 2007).

Hence, the final PLGA-CFZ NP formulation procedure was necessarily a compromise between several conflicting criteria. Still, by trial and error we managed to settle on a set of conditions for making CFZ NP that both gave reproducible results, and that

yielded NP sufficiently good in all the key criteria for the use in subsequent biological experiments.

The further physical and chemical characterization of the NP confirmed the microscopic observations we had performed during the nanoprecipitation screening. The Dynamic Light Scattering (DLS) analysis showed that the NP size we obtained with the final formulation was around 350 nm, and that the NP size was fairly monodispersed. This demonstrated that we had managed to minimize the number of aggregates and microparticles that we often observed during the earlier stages of PLGA-CFZ NP formulation. This may be very important with regard to some forms of *in vivo* applications of the NP, because particles smaller than 400 nm can cross epithelial barriers non-invasively and can therefore be suited for aerosol delivery (Hussain 2001). Aerosol delivery is a potentially important aspect of TB treatments with particle formulated drugs; e.g. Verma *et al*. showed that inhaled CFZ microparticles reduced the CFU counts in *M.tb*-infected mice lungs significantly, relative to regular oral CFZ administration (Verma, Germishuizen et al. 2013). Aerosol delivery using other drugs has also demonstrated good therapeutic effects in guinea pigs (Sharma, Sharma et al. 2004). The DLS also confirmed that the PLGA-CFZ NP was in the optimal size range for phagocytosis (0.2-3μm) (Desjardins and Griffiths 2003). This is another critical parameter in TB treatment since the passive targeting to macrophages is the core feature of TB NP treatment. DLS measurements were performed both before and after freeze-drying and the data showed that the size of the NP was largely unaffected by freeze-drying, although a slight shrinking could be observed (**Table 4.5**). This is likely caused by evaporation of either water or solvent from the NP during freeze-drying. However, the PLGA-CFZ NP size was still within the optimal size range for macrophage uptake and TB treatment.

The measured zeta-potential revealed that the PLGA-CFZ NP had a slightly negative surface charge (-1.7 ± 0.3) (**Table 4.5**). The negative charge was less than what has been measured for other PLGA-NP made in our lab. E.g. PLGA-RIF (2% PVA) had a charge of -3.14 ± 0.2 (Kalluru, Fenaroli et al. 2013), and for PLGA-TZ (4% PVA) the charge was -14.2 ± 0.8 (Vibe, Fenaroli et al. 2015). Both the change of surfactant from PVA to Tween 80 and the loading of CFZ may play a role in the reduced charge. A high surface charge may be advantageous because it causes the NP to repel each

other in solution, whereas a low surface charge can cause aggregation. Aggregations were frequently observed with the PLGA-CFZ NP although they could be re-suspended in water. However, aggregation of the NP became a challenge during the treatment experiments, limiting the concentration of NP that could be injected because of clogging of the injection needle. Importantly, a negative surface charge of the NP is favourable for TB nanotherapy because a negative surface charge leads to a more selective uptake by specialized phagocytic cells such as macrophages.

The HPLC analysis showed that the drug loading we achieved for CFZ in PLGA was 14% was lower than the drug loading that had previously been achieved for thioridazine (26.7%) and RIF (31.8%) in PLGA (Vibe, Fenaroli et al. 2015) (Fenaroli, Westmoreland et al. 2014). This rather low drug loading represented a problem for the *in vivo* studies because, together with the aggregation of NP described above, it further limited the dose of CFZ that could be injected.

During this first part of this study, we managed to find a way to encapsulate CFZ that could meet our criteria in a sufficient way. However, there is still room for improvement, especially there is a need for higher drug loading combined with a more negative surface charge, to make CFZ-NP that are potentially better suited for *in vivo* TB treatment. Apart from some few attempts using TPP-Chitosan, which were inconclusive, we did not test other polymers than 50:50 PLGA. Plenty of different polymers are available (Couvreur and Vauthier 2006) and given the progress we had made in identifying formulation conditions for CFZ-NP it would be very interesting to continue testing other polymers to improve the critical parameters and thereby improve the properties of the CFZ NP.

5.2 PLGA encapsulation changes CFZ cell interactions

The main purpose of encapsulating CFZ into NP was to change the unmanageable chemistry of CFZ into a nanoparticle that would allow for a better biodistribution and more controlled and specific delivery to macrophages. Although this must ultimately be studied *in vivo,* cell culture studies can also give valuable information about NP behaviour. Efficient NP uptake by macrophages is very important in the context of TB treatment and it was necessary to see if, and to what extent PLGA-CFZ NP could be

taken up by macrophages, and what impact the uptake would have on the cellular response to CFZ, especially with regard to possible cytotoxicity of CFZ. Because CFZ is fluorescent, we could study this directly using microscopy and flow cytometry, an important advantage of this drug.

Our first observation was that PLGA-encapsulation of CFZ leads to large, spherical, intracellular accumulations of the drug inside the macrophages. We observed none of these accumulations in cells that were treated with free CFZ (**Figure 4.10)**. Similar accumulations have been observed for macrophages treated with PLGA encapsulated Coumarin-6. These coumarin-6 accumulations were found to co-localize with a variety of lysosomal markers, clearly indicating that the PLGA-Coumarin-6 were phagocytosed and brought to lysosomes through the endocytic pathways (Kalluru, Fenaroli et al. 2013)

It is interesting to compare the CFZ accumulations we found *in vitro* to what has been observed in macrophages *in vivo* when mice were treated with free CFZ. In several studies Baik and Rosania have demonstrated that CFZ treatment of mice leads to large CFZ accumulations inside macrophages (Baik and Rosania 2012). These accumulations look like needle-shaped crystals and consist of sheets of CFZ closely associated with intracellular membranes. These crystal-like drug inclusions (CLDIs) are often surrounded by a double membrane, suggesting that autophagy may play a role in their formation (Baik and Rosania 2012). CLDIs are found mostly in the liver and spleen and in their work these authors speculated that CLDI formation serves to protect the body from the toxic effects of CFZ. *In vitro* CFZ is toxic to cells, while isolated CLDIs are not (Yoon, Sud et al. 2015). The therapeutic implications the CLDIs may have are not known, but they appear to represent a non-active version of the drug and may play a role in the long half-life (70 days in humans) and slow therapeutic activity *in vivo*.

The lysosomes are the default intracellular destination for phagocytosed NP (Desjardins and Griffiths 2003, Flannagan, Cosio et al. 2009, Schliehe, Schliehe et al. 2011) . Thus, based on the observed intracellular accumulations and their similarity to what had been observed for PLGA-Coumarin-6, it seemed probable that the PLGA-CFZ NP were also taken up by phagocytosis and delivered to lysosomes. CFZ can be fluorescent at different wavelengths, but the fluorescence properties can vary depending on how CFZ molecules are organized (Keswani, Yoon et al. 2015).This

meant that there were some uncertainties in visualizing the CFZ NP together with other fluorescent markers inside cells. We nevertheless tried to localise the NP by comparison to the late endosomal/lysosomal marker LAMP 1 by immunofluorescence microscopy, using the fluorophore Alexa 488. We tried this since excitation of Alexa 488 does not lead to excitation of dissolved CFZ or CFZ CLDIs according to the work of Keswani et al. Chemically pure CFZ-crystals are however excited at the same wavelength as Alexa 488 (Keswani, Yoon et al. 2015).

The experiments we performed were inconclusive and there was no obvious overlap between the LAMP-1 antibody and the CFZ accumulations. For one thing, the size of the observed NP aggregations made it difficult to see a possible co-localisation of the NP and the LAMP-1 antibody that would be expected to localise in a thin layer of lysosomal membrane around the aggregations. This was further complicated by the realization that PLGA-CFZ NP also are slightly green fluorescent, thereby interfering with the signal of the Alexa-488 fluorophore we used (**Figure 4.7**). Up until the cell experiments were conducted, we had not detected green fluorescence from the PLGA-CFZ NP. The green fluorescence was mostly seen in the largest CFZ accumulations, but nevertheless complicated the interpretation of the localisation experiments. As seen in **Figure 4.6** C the primary macrophages were also very dense with lysosomes making co-localization hard to analyse regardless. We were therefore not able to conclude where the PLGA-CFZ NP localizes after uptake by macrophages.

It was also interesting to see what impact the PLGA encapsulation had on the CFZ uptake in macrophages. We tested two concentrations (10 µM and 40 µM) of free and PLGA-encapsulated CFZ, and analysed the cellular uptake by flow cytometry. When macrophages were treated with a CFZ concentration of 10 µM, the measured median fluorescent intensity was much higher for free CFZ than for PLGA encapsulated CFZ (**Figure 4.8**). Accordingly, the number of CFZ-positive cells (i.e. cells with a fluorescent intensity that was higher than any measured auto-fluorescence) was also higher for the free CFZ treated cells (**Figure 4.8**). Thus, by these criteria, for the PLGA-CFZ NP-treated cells the percentage of CFZ-positive cells was only 7.9 %. However, it is clear from the histograms in **Figure 4.8 A** that the way we defined CFZ-positive cells in our experiment leads to an underestimation of the uptake of PLGA-CFZ NP. The MFI is clearly higher for the PLGA-CFZ NP treated

cells compared to the untreated cells (6.7 and 3.5 respectively), but a large fraction of the PLGA-CFZ NP histogram overlaps with the small, right-most fraction of the untreated cells histogram (**Figure 4.8**), indicating that when detecting fluorescence a low uptake of PLGA-CFZ NP may be indistinguishable from the high auto-fluorescence found in a small fraction of the non-treated cells.

Despite the lack of visible CFZ accumulation by fluorescence microscopy, the MFI of the free CFZ treated cells was much higher than the measured auto-fluorescence, and 93.3% of free CFZ treated cells scored as CFZ-positive. This demonstrates that, despite the lack of visible accumulations, free CFZ was associated with a large fraction of the cells. It is likely that this is due to CFZ sticking to the plasma membrane and possibly also to intracellular membrane systems in the macrophages. CFZ is very lipophilic and it has been shown that free CFZ is incorporated into the mitochondrial membrane of macrophages. In the same study it was shown that free CFZ was toxic and that incorporation into the mitochondrial membrane led to membrane disruption and was associated with the cells showing sign of apoptosis, such as membrane blebbing (Yoon, Sud et al. 2015).

Increasing the CFZ dose to 40 µM gave strikingly different results. For the PLGA-CFZ NP the MFI and the percentage of positive cells increased nearly proportionally to the dose, indicating a dose-dependent uptake of the NP. In contrast, for the cells treated with free CFZ both the MFI and the number of positive cells were substantially reduced at the higher dose (**Figure 4.8**). The most probable explanation for this is CFZ cytotoxicity (see below). Thus, we observed that at 40 µM of free CFZ the samples contained very few cells and the majority of the cells were CFZ-negative. Most likely, the cells that were analysed from the 40 µM free CFZ sample were cells with low, or no uptake of CFZ, while cells with a higher uptake had been killed. We observed no such effect on the cells treated with PLGA-CFZ NP at 40 µM. This suggested that PLGA-encapsulation could reduce the toxicity of CFZ and that cells can be treated with substantially higher doses of CFZ when the drug is encapsulated.

We therefore wanted to test the toxicity of free CFZ compared to the PLGA-CFZ NP to directly assess the extent to which encapsulation of CFZ in NP could reduce toxicity. With this aim, we conducted a toxicity experiment using mouse macrophages. The experiment was adapted from Yoon *et al.* (Yoon, Sud et al. 2015) who compared the toxicity of free CFZ to CLDIs using an XTT assay, which is similar

in concept to the CCK-8 assay used in our experiment. According to the CCK-8 user manual WST-8, the reagent used in the CCK-8 assay, may be influenced by reducing agents such as CFZ. To make sure that we had reliable results we therefore combined the CCK-8 assay with a crystal violet assay that measures the number of cells that remains attached to the culture plate during treatment. Thus, the crystal violet assay is not dependent on the activity of the dehydrogenases and is not influenced by reducing agents in the solution. This gave us two independent measurement of the toxicity of CFZ and provided added experimental robustness.

The CFZ concentrations tested were based on Yoon *et al.* (Yoon, Sud et al. 2015) and these concentrations also span the blood serum concentration that has been reported in mice, from ~16 µM reported in Baik *et al.* (Baik, Stringer et al. 2013) down to 2.8 µM reported in Swanson *et al.* (Swanson, Adamson et al. 2015). The highest dose we used was 80 µM, and this is higher than any reported serum concentration during CFZ administration in mice. The results shown in **Figure 4.11** and **4.12** demonstrated that the PLGA encapsulation strongly reduced the toxicity of CFZ. From day 3 onwards, neither the CCK-8 assay nor the crystal violet staining assay could detect living cells in the dishes treated with concentrations of 10 µM or above of free CFZ. In contrast, PLGA-CFZ was well tolerated even in doses as high as 80 µM given continuously for 6 days. This clearly shows that CFZ can be given in higher doses when it is encapsulated.

Lastly, we investigated the retention of the PLGA-CFZ NP in macrophages after uptake. Obviously, the retention time of the PLGA-CFZ NP plays a significant role in understanding both the toxicity and the potential therapeutic effect of the particles. The NP retention was measured by flow cytometry, following cell fluorescence over a period of 6 days. From the results in (**Figure 4.9**) it is clear that the MFI decreases sharply for the first 24 hours, before the decrease seems to slow down. The fluorescence kinetics in our experiment resembles what was reported for PLGA-Coumarin-6 NP (Kalluru, Fenaroli et al. 2013). Drug-loaded NP are often not completely stable and may contain a fraction of loosely attached drug. This fraction will often be released shortly after NP administration and result in a rapid burst release, giving a kinetic profile similar to the one we observed in our experiments. Burst release is frequently observed for PLGA NP and it has the negative effect of reducing the amount of drug that can be targeted to the diseased site (Sun, Sui et al.

2010). Nevertheless, it is clear from fluorescence microscopy images that after 6 days CFZ accumulations were still frequent inside the cells, although the amount in the cells seems to be reduced with increasing time of incubation (**Figure 4.10 D**). We also noted that in Kalluru *et al.* the fluorescence of Coumarin-6 could still be detected after 13 days, showing that drugs delivered by NP may have a long retention time in cells (Kalluru, Fenaroli et al. 2013).

The *in vitro* experiments show that PLGA-CFZ NP are taken up by the cells in a way that is very different from the free drug and it is very likely that this contributes to the reduced cytotoxicity observed. The uptake of PLGA-CFZ NP also leads to large spherical accumulations of CFZ that seemed to be stable over the period of time these experiments were conducted. Based on previous studies with CFZ and PLGA we hypothesize that free CFZ is mostly associated with the cells' plasma membrane, while the PLGA-CFZ NP are taken up by phagocytosis. However, further experiments are needed to substantiate this hypothesis.

Future experiments should aim at identifying the CFZ-accumulations we observed in the macrophage culture experiments and analyse the effect of PLGA-CFZ NP *in vitro* in more detail. Transmission electron microscopy could be particularly useful in this regard. Using TEM in combination with gold-coupled antibodies it should be possible to assess the subcellular localization of CFZ without relying on its fluorescence. In addition, this methodology could also give information about the ultrastructure of the CFZ-accumulations. E.g. it would be very interesting to investigate if the NP are associated with the putative autophagy-related double membranes that have been proposed for the CLDI observed by Baik and Rosania (Baik and Rosania 2012). Assessing the uptake and retention of CFZ quantitatively by performing HPLC analysis on macrophage cell lysates would be a better and more direct way to compare the behaviour of CFZ when delivered as PLGA-CFZ NP or free drug in cells.

Testing the effect of the PLGA-CFZ NP in an *in vitro* infection model would also give very valuable information about the therapeutic potential of encapsulated CFZ. Thus, we also tried to set up a macrophage infection model using BCG. Due to the slow growth of BCG, such an experiment takes 5-6 week to do and we only managed to do the experiment once, with very inconclusive data. The experiment is described in the supplementary data **section 8.1.1**. Continuing the work to set up an *in vitro*

infection model would be very important to get a more complete understanding of the PLGA-CFZ NP behaviour in cells, and it would also give valuable information about these NP therapeutic potential.

5.3 Therapeutic experiments with PLGA-CFZ nanoparticles in the zebrafish embryo model

5.3.1 Monotherapy with clofazimine

We estimated that PLGA-CFZ NP with 14% drug loading were in the lower range of what would be suitable for testing a therapeutic effect of the PLGA-CFZ NP against *M.m* in zebrafish embryos *in vivo*. However, the effective treatment dose of CFZ against TB is not well established (Gopal, Padayatchi et al. 2013). In addition, recent data from mouse studies have questioned the therapeutic effect of high CFZ doses, as the investigators saw no differences in bactericidal effect between doses of 6.25 mg/kg/day and 25 mg/kg/day (Swanson, Adamson et al. 2015). Also data from Gopal Khuller's group showed that when encapsulated in PLGA the doses of RIF, PZA and INH administered could be at 2/3rd of their respective therapeutic doses without any loss in therapeutic effect (Sharma, Pandey et al. 2004). Taken together, this made it reasonable to continue with testing our NP in zebrafish, despite our worries about the low drug loading.

The first *in vivo* experiment, using a CFZ dose of 5 mg/kg, indicated that there could be a therapeutic effect of PLGA-CFZ NP and suggested a better therapeutic effect of the PLGA-CFZ NP as compared to free CFZ. The difference between these groups was not statistically significant, but while the PLGA-CFZ group was significantly different from the infected untreated group, the free CFZ group was not.

Based on the result from this first treatment experiment we expected that an increased treatment dose would give a more pronounced effect of the CFZ-treatment and possibly would make it easier to see differences between PLGA-CFZ NP and free CFZ. In the first experiment the NP were re-suspended in 2% PVP, but using this re-suspension medium it was not possible to inject an increased concentration of

PLGA-CFZ NP. Re-suspension in PBS however partly solved this problem making it possible to increase the injection dose to 10 mg/kg. Two more treatment experiments were conducted with this treatment dose. Despite the increased dosing we observed no significant treatment effect in these experiments; although in one of the experiments there was again a slight indication of a better effect with the PLGA-CFZ NP, seen from the observation that the CFZ injected embryos started dying later than the empty PLGA injected embryos. However, taken together these three experiments suggest that, at the doses we could inject, there seemed at most to be only a miniscule effect of CFZ monotherapy, both with PLGA-CFZ NP and with free CFZ.

Nonetheless, 10 mg/kg is still not a very high treatment dose in a zebrafish TB survival experiment. Treatment with PLGA-RIF had an effect in treatment doses at 12 mg/kg (Fenaroli, Westmoreland et al. 2014), and RIF is generally considered the most potent TB drug *in vivo*, together with INH (Sarkar and Suresh 2011). Also, for PLGA-TZ, a treatment effect was first observed at 32 mg/kg in zebrafish embryo Vibe *et al*. (Vibe, Fenaroli et al. 2015), and although not fully comparable to an experiment using liposome encapsulated CFZ in mice, Adams *et al.* found encapsulated CFZ to be effective at 50 mg/kg against *M.tb* (Adams, Sinha et al. 1999).

While the low injection dose is a potential culprit for the lack of treatment effect, it should also be kept in mind that the monotherapeutic effect of CFZ against *M.tb* is disputed. While Swanson *et al.* showed a good therapeutic effect of CFZ against TB in mice (Swanson, Adamson et al. 2015); Irwin *et al.* (Irwin, Gruppo et al. 2014) found only a limited effect of CFZ monotherapy, testing it in a different mouse model.

5.3.2 Combinatorial treatment

Because we saw only a very limited effect from CFZ treatment in the monotherapy experiments and since the injection dose of CFZ in these experiments could not be increased, we continued testing the PLGA-CFZ NP as part of a combinatorial treatment, together with RIF. This is in many ways also a more relevant experiment because CFZ is unlikely to be given as monotherapy in any TB treatment. Also, in a recent treatment study in mice, using CFZ instead of ETH in the standard four drug regimen shortened the duration of the treatment by 2 months (Tyagi, Ammerman et al. 2015).

Our combinatorial treatment experiment is interesting because it clearly differentiates the treatment groups and it is the only the treatment that showed an effect with free CFZ compared to the infected, untreated control. When combined with RIF, free CFZ, empty PLGA NP and PLGA-CFZ NP all improved survival significantly as compared to *M.m*-infected embryos that received no treatment, while treatment in only a RIF-bath did not. The fact that also the effect with empty PLGA NP was significantly different from the infected untreated group demonstrates the importance of including this control in the experiment. A slight treatment effect of empty PLGA NP has been observed before (Fenaroli, Westmoreland et al. 2014) and it should be pointed out that the results with empty PLGA NP are not significantly different from the RIF bath-treated embryos. It is therefore not possible to draw any clear conclusion about the treatment effect of CFZ in this experiment, and clearly it should be repeated. The differentiation between the treatment groups suggests that future experiment with PLGA-CFZ NP should include combinatorial treatments, and that this may increase the chance of finding an effect of PLGA-CFZ NP, as well as with CFZ alone.

5.3.3 Zebrafish treatment: Summary and considerations

The treatment results in this thesis fits well into the existing contention about the potential of CFZ in TB treatment. The effect of CFZ against bacteria in culture is clear and undisputed, while the effect in cells and animal models is much less convincing.

Although very advantageous in many respects, the zebrafish embryo model also puts some limitations to the treatment experiments that are worth considering. Zebrafish injections are technically difficult and it takes a trained and experienced investigator to produce reliable injections. As seen from **Figure 3.4** small variations is droplet size can change the injection volume quite significantly and this technical variation should always be considered when evaluating zebrafish embryo treatment effects. It is particularly hard to inject NP because they easily clog the needle, and this also limits the treatment dose that can be injected reliably.

The experiments also contain two biological variables, the embryos and the bacteria. During the work with this thesis, several planned survival experiments had to be cancelled either due to poor embryo quality or to non-virulent bacteria. The non-virulent bacteria was detected because we observed low mortality rates across all the infected groups, including the infected untreated control group, where the embryos

usually start to die at 4 dpi. We therefore had to change the ds:Red-*M.m* frozen stock we used during the treatment experiments because the old frozen stock had lost its virulence.

It is also important to keep in mind the limitations the short time frame put on the treatment experiments, with the zebrafish embryo survival studies lasting for a maximum of 10 days post-treatment. Treatment experiments in mice have shown that CFZ is a slow-acting drug and, despite the overall effect of CFZ monotherapy found by Swanson *et al.,* there was no effect of CFZ on CFU counts from the *M.tb*-infected mice during the first week of administration (Swanson, Adamson et al. 2015). In Tyagi *et al.,* where CFZ was given together with RIF, INH and PZA the first additional effect of CFZ was observed first after 2 weeks (Tyagi, Ammerman et al. 2015). It is not clear whether the lack of early bactericidal effect in mice should be attributed to the poor biodistribution of CFZ or to a possible slow metabolic activation of the drug. If the latter alternative is the case, our treatment experiments might have been too short to see the real effect of CFZ treatment.

We were not able to assess the biodistribution of PLGA-CFZ NP in this study. Even though the PLGA-CFZ NP were red fluorescent, the signal was not very strong and we were not able to distinguish PLGA-CFZ NP from auto-fluorescence from the zebrafish embryo. This meant that we could not tell how the PLGA encapsulation influenced the distribution of CFZ during treatment. The zebrafish embryo has a large yolk sac during the first week of embryonal development and our impression is that some of the CFZ NP get stuck in the yolk sac. This would, of course influence the treatment outcome. However, the yolk sac is the part of zebrafish embryo with the strongest auto-fluorescence and it was not possible to conclude on the localisation of the PLGA-CFZ NP.

However, despite of the above-mentioned limitations, the zebrafish model was very useful in this study. During the relatively short time frame of a master thesis we managed to do several treatment experiments that have given us very useful information for the continued pursuit of developing CFZ NP treatment. This would not have been possible using any other nanoparticle *in vivo* model and it underlines the unique ability of efficient nanoparticle screening that the zebrafish model provides.

6 Conclusions

During the work with this thesis, we established a method for making PLGA-clofazimine (PLGA-CFZ) NP by nanoprecipitation. By testing multiple conditions, it was possible to identify a combination of parameters that consistently gave NP that were suitable for testing in biological systems. Thus, physical and chemical characterization demonstrated that the PLGA-CFZ NP had properties well within the critical parameters for size, surface charge and drug-loading, for testing in *in vitro* and *in vivo* models. This was the first main goal for the work in this thesis.

The second main goal was to analyse the PLGA-CFZ NP *in vitro* in macrophage culture. Firstly, it was established that free CFZ was toxic to macrophages, while PLGA encapsulation of CFZ protected the cells from this toxicity, even at the highest drug doses we tested. Further analyses revealed that PLGA encapsulation of CFZ led to a change in the uptake of CFZ into the cells, as compared to what was observed for the free drug. Especially, delivery of the PLGA-CFZ NP led to accumulation of large spherical intracellular CFZ-containing structures. After uptake, the CFZ accumulations stayed in the cells for several days, but seemed to disappear slowly from the cells. Thus, the fluorescent signal from CFZ in the cells decreases in a similar manner to what has previously been observed for other NP (e.g. PLGA-Coumarin-6 NP (Kalluru, Fenaroli et al. 2013).

The third main goal was to test the therapeutic effect of PLGA-CFZ NP *in vivo* using the zebrafish embryo model. Although early experiments gave indications that there might be some therapeutic effect of the PLGA-CFZ NP, the experiments were not conclusive. Thus, taken together there appeared to be at most a very modest effect of CFZ monotherapy at the doses we were able to inject into the embryos. A combinatorial treatment experiment, where the PLGA-CFZ NP were combined with the anti-TB first-line drug RIF suggested there might be a therapeutic effect from combining CFZ and RIF, but given that this experiment has only been performed once, no clear conclusion can yet be drawn. However, using PLGA-CFZ NP in combination with other drugs seems like a promising approach for future therapeutic studies.

7 Future perspectives

Clofazimine is still an elusive and under-characterized drug and a continued effort is necessary to increase the understanding of CFZ's potential in treatment of MDR-TB. However, the results from the "Bangladesh study" indicates that CFZ could play a major part in MDR-TB treatment, and it demonstrates that despite its unclear contribution, the use CFZ should not be overlooked in the future treatment of TB (Van Deun, Maug et al. 2010).

CFZ therapy is usually associated with massive skin and tissue accumulations of the coloured drug, and this is very inconvenient for patients. Such off-target accumulation of CFZ also means that only a small fraction of the administered drug dose will be available for therapy at the infections sites in the body.

Nanoparticle encapsulation of CFZ seems like an attractive potential way to alleviate both these problems. The main obstacle for making successful CFZ NP is the difficult chemistry of CFZ, which has been thoroughly discussed in this thesis. Identifying new polymers or encapsulation techniques that can increase the drug loading should be the first aim in further CFZ NP studies.

Further investigation of the *in vitro* cellular response to CFZ NP should also be a part of future studies. Uptake and degradation of CFZ should be measured in a more direct way than was done in this thesis, e.g. by lysing the cells and measuring the intracellular concentration of CFZ by HPLC. It would also be very important to set up *in vitro* infection experiment of CFZ NP using macrophages and preferentially *M.tb*. As a part of the *in vitro* PLGA-CFZ NP experiments, we tried to set up a CFU time-kill assay using BCG-infection in primary macrophages (see supplementary methods and results). Due to the large variability in the results of this experiment, it was not included in the main part of the thesis.

Continuing treatment experiments in the zebrafish embryo model using PLGA-CFZ NP in combination with other drugs seems like a promising avenue for assessing and possibly realizing the potential of CFZ NP in TB treatment. Eventually, if CFZ NP with a higher drug-loading can be made, new experiments testing the effect of monotherapy at higher doses of CFZ should also be pursued. If the drug loading can be increased it is also likely that the fluorescence of the NP will be stronger, and this

may allow for better localisation experiments using CFZ NP. Our group is also planning to test a silica-CFZ nanoparticle recently provided to us by our collaborators Sabrina Valetti and Adam Feiler in the Swedish company Nanologica. The silica-CFZ has a drug loading of 50% and could therefore solve many of the challenges we had in the present study due to the low drug loading.

CFZ is a clinically approved, affordable and well-tolerated drug that has already been used to treat more than two million leprosy patients world-wide. This makes CFZ a quite unique alternative for treatment of MDR-TB, compared to the often toxic and expensive alternatives that are mostly used today. Finding ways to potentiate CFZ by making it more bio-available and identifying drug combinations that works in synergy witch could therefore have great impact on the future MDR-TB therapy and should be a main target for further CFZ studies.

8 Supplementary

8.1 Supplementary experiments

8.1.1 Primary macrophage infection and treatment assay

During the cell work in this thesis, we found that PLGA-encapsulation of CFZ made it possible to treat cells with much higher doses of CFZ without causing toxicity. To further investigate this potential we wanted to establish an *in vitro* macrophage infection model for testing of PLGA-CFZ NP. Our group has previously used an *in vitro* infection model were primary macrophages are infected with *Mycobacterium bovis* (BCG) (Kalluru, Fenaroli et al. 2013). Thus, alongside the zebrafish embryo infection experiments, we started testing the effect of PLGA-CFZ NP in this macrophage infection model.

Primary bone marrow derived macrophages were thawed, grown and seeded as described for the other cell experiments. We seeded $2x10^5$ macrophages in 96 wells dishes overnight. The next day the cells were infected with dsRed-BCG in the exponential growth phase (OD_{600} 0.4-0.9). The BCG bacteria were grown and prepared by Jon Hildahl in our group at University of Oslo. To infect the cells, the bacteria were first collected by centrifugation at 3000 x g for 10 minutes and the bacterial medium was removed. The bacteria were then washed twice in PBS, before being re-suspended in RPMI cell medium and sonicated to make sure the suspension was homogeneous. The BCG suspension was then diluted to $2x10^6$ CFU/ml to give a multiplicity of infection (MOI) of 10. The cells were infected with BCG for 3 hours and after removal of the bacterial medium the cells were thoroughly washed in 3 times PBS to remove all extracellular bacteria. Just after infection, the cells were added treatment media of either free or PLGA encapsulated CFZ and in addition groups of untreated and empty PLGA treated cells were prepared.

For PLGA-CFZ NP we used the MIC that we had previously been determined for free CFZ (0.15 µg/mL, see section **4.4.1**), and prepared groups of 1x, 10x and 100x MIC. PLGA-CFZ NP were carefully weighed, diluted in RPMI medium to the desired concentration and sonicated for 3 minutes to break all clumps. Free CFZ was

prepared in a concentration of 1x MIC in 0.05% DMSO in RPMI medium. Treatment lasted for 3 hours before the cells were washed 3 times in PBS and added fresh RPMI medium. At the time points, 0 hours, 3 days and 6 days the macrophages were lysed using 0.005% SDS in Milli-Q water. The lysates were then diluted 100 times and 20 µl of this lysate was plated on 7H10 agar plates supplemented with OADC and 50 µg/mL hygromycin. The plates were incubated in sealed plastic bags at 37 ^{o}C for 20 days, before the BCG colonies were counted.

The results are shown in **Figure 8.1**. This experiment was excluded from the result part of the thesis for two reasons. The initial experiment was planned with an extra time point at day 9, but because of improper lysing of these cells, this time point had to be excluded. In addition, the colony counting revealed great variation within the individual treatment groups. This variation made it hard to use the data for further analysis. Except possibly for the day 3 sample in 100x MIC PLGA-CFZ NP group we did not observe any bacterial killing is this experiment. Given more time, a new experiment should have been conducted and based on what we observed in the presented experiment a few changes should be done. Firstly, it is important to make sure the experiment last longer than 6 days to see if we can observe any killing. Secondly, based on what we observed for the toxicity and uptake studies the concentration of PLGA-CFZ should be increased even more to see if there is an effect of the treatment. It is interesting that the 100 x MIC grows slower for the first three days and faster for the last three days of this experiment, but the implication of this observation is so far unclear.

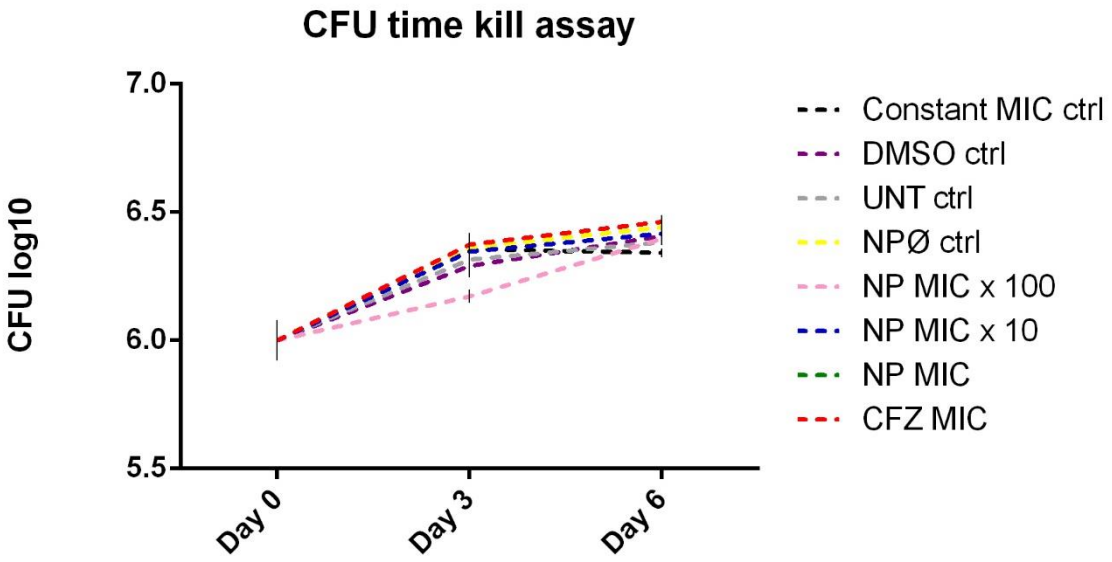

Figure 8.1: CFU time kill assay using free and PLGA encapsulated CFZ. Values are shown as mean log_{10} CFU ± SEM (n=3).

8.2 Supplementary recipes

Tricaine stock solution

The recipe was adapted from Cosma *et al.* (Cosma, Swaim et al. 2006) and gave 100 mL tricaine 20x stock solution. 400 mg Tricaine methanosulfate MS-222 (Argent laboratories group Inc., Redmond, WA, USA) was dissolved in 97.9 mL water then and added 2.1 mL 1 M TrisCl (pH 9). The pH was measured and then adjusted to 7.4 by adding water or TrisCl. 1 mL of the tricaine stock solution was added to 19 mL of embryo water to give the final embryo tricaine sedation solution. For sedation, the zebrafish embryos were put in the sedation solution for 1-5 minutes.

7H10 agar plates

The protocol was adapted from Cosma *et al.* (Cosma, Swaim et al. 2006). 19 mg 7H10 Difco Middlebrook agar powder and 10 mL 50% glycerol were dissolved in 900 mL sterile Milli-Q water. The solution was autoclaved, left to cool and then added 100 mL OADC and 1 mL 50 mg/mL hygromycin. Working completely aseptically, ~ 20 mL was poured into 10 mm petri dishes and left to let the agar solidify. Plates were put together in sealed plastic bags and stored at 4 ^{o}C until used.

ADC/OADC growth supplement

The recipe was adapted from Gao and Manoranjan (Gao and Manoranjan 2005). 4.5 g NaCl, 25 g BSA, 10 g dextrose and 15 mg catalase was added to 400 mL sterilized Milli-Q water and dissolved under stirring at room temperature. More sterilized Milli-Q was added to make the final volume 500 mL and the pH was adjusted to 6.8-7.0 by adding 1 M NaOH. The solution was stored at 4 ^{o}C until use.

Zebrafish embryo water

The recipe was taken from Cosma *et al.* (Cosma, Swaim et al. 2006). To make 100 mL embryo water 1.0 mL of Hanks' stock solution #1, 0.1 mL of Hanks' stock solution #2, 1 mL of Hanks' stock solution #4, 1 mL of Hanks' stock solution #5 and 1 mL of Hanks' stock solution #6 were mixed in 95.9 mL of Milli-Q water. The pH was adjusted 7.2 and the embryo water was autoclaved. The embryo water was stored at 4 ^{o}C until use.

Hanks' stock #1

8.0 g NaCl
0.4 g KCl
100 mL H_2O

Hanks' stock #2

0.358 g Na_2HPO_4 anhydrous
0.60 g KH_2PO_4
100 mL H_2O

Hanks' stock #4

0.72 g $CaCl_2$
50 mL H_2O

Hanks' stock #5

1.23 g $MgSO_4 \cdot H_2O$
50 mL H_2O

Hanks' stock #6

0.35 g $NaHCO_3$
10 mL H_2O

Store at 4 ^oC

Full RPMI medium

RPMI-1640 Medium (Sigma-Aldrich, St. Louis, MO, USA)

10% Heat inactivated Fetal Calf Serum (Sigma-Aldrich, St. Louis, MO, USA)

20% L929

50 µM β-mercaptoethanol

8.3 Supplementary method information

Settings for Olympus Fluoview 1000, inverted confocal laser scanning microscope IX81

Channel 1: (DAPI)
Excitation DM name: DM 405/473/559/635 (multi-edge main dichroic element)
Excitation wavelength: 405 nm
Emission DM (DM=dichroic mirror) name: SDM473 (this is a beam splitter)
Emission wavelength: 461 nm
BF position: 425 nm
BF range: 35 nm

Channel 2: (Alexa Fluor 488)
Excitation DM name: DM 405/473/559/635 (multi-edge main dichroic element)
Excitation wavelength: 473 nm
Emission DM (DM=dichroic mirror) name: SDM560
Emission wavelength: 520 nm
BF position: 485 nm
BF range: 60 nm

Channel 3: (Alexa Fluor 568)
Excitation DM name: DM 405/473/559/635 (multi-edge main dichroic element)
Excitation wavelength: 559 nm
Emission filter name: BA575-675
Emission wavelength: 603 nm

References

(British research council, 1948). "Streptomycin treatment of pulmonary tuberculosis." Br Med J **2**(4582): 769-782.

Adams, K. N., K. Takaki, L. E. Connolly, H. Wiedenhoft, K. Winglee, O. Humbert, P. H. Edelstein, C. L. Cosma and L. Ramakrishnan (2011). "Drug Tolerance in Replicating Mycobacteria Mediated by a Macrophage-Induced Efflux Mechanism." Cell **145**(1): 39-53.

Adams, L. B., I. Sinha, S. G. Franzblau, J. L. Krahenbuhl and R. T. Mehta (1999). "Effective treatment of acute and chronic murine tuberculosis with liposome-encapsulated clofazimine." Antimicrob Agents Chemother **43**(7): 1638-1643.

Alexis, F., E. Pridgen, L. K. Molnar and O. C. Farokhzad (2008). "Factors affecting the clearance and biodistribution of polymeric nanoparticles." Mol Pharm **5**(4): 505-515.

Allen, T. M. and P. R. Cullis (2013). "Liposomal drug delivery systems: from concept to clinical applications." Adv Drug Deliv Rev **65**(1): 36-48.

Andrews, J. R., F. Noubary, R. P. Walensky, R. Cerda, E. Losina and C. R. Horsburgh (2012). "Risk of progression to active tuberculosis following reinfection with Mycobacterium tuberculosis." Clin Infect Dis **54**(6): 784-791.

Anisimova, Y. V., S. I. Gelperina, C. A. Peloquin and L. B. Heifets (2000). "Nanoparticles as antituberculosis drugs carriers: effect on activity against Mycobacterium tuberculosis in human monocyte-derived macrophages." Journal of Nanoparticle Research **2**(2): 165-171.

Baik, J. and G. R. Rosania (2012). "Macrophages sequester clofazimine in an intracellular liquid crystal-like supramolecular organization." PLoS One **7**(10): e47494.

Baik, J., K. A. Stringer, G. Mane and G. R. Rosania (2013). "Multiscale distribution and bioaccumulation analysis of clofazimine reveals a massive immune system-mediated xenobiotic sequestration response." Antimicrob Agents Chemother **57**(3): 1218-1230.

Barry, C. E., H. I. Boshoff, V. Dartois, T. Dick, S. Ehrt, J. Flynn, D. Schnappinger, R. J. Wilkinson and D. Young (2009). "The spectrum of latent tuberculosis: rethinking the biology and intervention strategies." Nat Rev Micro **7**(12): 845-855.

Barry, V. C., J. G. Belton, M. L. Conalty, J. M. Denneny, D. W. Edward, J. F. O'Sullivan, D. Twomey and F. Winder (1957). "A new series of phenazines (rimino-compounds) with high antituberculosis activity." Nature **179**(4568): 1013-1015.

Barry, V. C. and M. L. Conalty (1965). "THE ANTIMYCOBACTERIAL ACTIVITY OF B 663." Lepr Rev **36**: 3-7.

Barry, V. C., M. L. Conalty and E. E. Gaffney (1956). "Antituberculosis activity in the phenazine series; isomeric pigments obtained by oxidation of o-phenylenediamine derivatives." J Pharm Pharmacol **8**(12): 1089-1096.

Berne, B.J.; Pecora, R. Dynamic Light Scattering. Courier Dover Publications (2000)

Brennan, P. J. and H. Nikaido (1995). "The envelope of mycobacteria." Annu Rev Biochem **64**: 29-63.

Brennan, Y. (2008). "Handbook of anti-tuberculosis agents. Introduction." Tuberculosis (Edinb) **88**(2): 85-86.

Capuano, S. V., 3rd, D. A. Croix, S. Pawar, A. Zinovik, A. Myers, P. L. Lin, S. Bissel, C. Fuhrman, E. Klein and J. L. Flynn (2003). "Experimental Mycobacterium tuberculosis infection of cynomolgus macaques closely resembles the various manifestations of human M. tuberculosis infection." Infect Immun **71**(10): 5831-5844.

Cheng, J., B. A. Teply, I. Sherifi, J. Sung, G. Luther, F. X. Gu, E. Levy-Nissenbaum, A. F. Radovic-Moreno, R. Langer and O. C. Farokhzad (2007). "Formulation of functionalized PLGA-PEG nanoparticles for in vivo targeted drug delivery." Biomaterials **28**(5): 869-876.

Chertok, B., M. J. Webber, M. D. Succi and R. Langer (2013). "Drug Delivery Interfaces in the 21st Century: From Science Fiction Ideas to Viable Technologies." Mol Pharm.

Cholo, M. C., H. C. Steel, P. B. Fourie, W. A. Germishuizen and R. Anderson (2012). "Clofazimine: current status and future prospects." J Antimicrob Chemother **67**(2): 290-298.

Comas, I., M. Coscolla, T. Luo, S. Borrell, K. E. Holt, M. Kato-Maeda, J. Parkhill, B. Malla, S. Berg, G. Thwaites, D. Yeboah-Manu, G. Bothamley, J. Mei, L. Wei, S. Bentley, S. R. Harris, S. Niemann, R. Diel, A. Aseffa, Q. Gao, D. Young and S. Gagneux (2013). "Out-of-Africa migration and Neolithic coexpansion of Mycobacterium tuberculosis with modern humans." Nat Genet **45**(10): 1176-1182.

Converse, P. J., A. M. Dannenberg, Jr., T. Shigenaga, D. N. McMurray, S. W. Phalen, J. L. Stanford, G. A. Rook, T. Koru-Sengul, H. Abbey, J. E. Estep and M. L. Pitt (1998). "Pulmonary bovine-type tuberculosis in rabbits: bacillary virulence, inhaled dose effects, tuberculin sensitivity, and Mycobacterium vaccae immunotherapy." Clin Diagn Lab Immunol **5**(6): 871-881.

Cooper, A. M. (2009). "Cell-mediated immune responses in tuberculosis." Annu Rev Immunol **27**: 393-422.

Cosma, C. L., D. R. Sherman and L. Ramakrishnan (2003). "The secret lives of the pathogenic mycobacteria." Annu Rev Microbiol **57**: 641-676.

Cosma, C. L., L. E. Swaim, H. Volkman, L. Ramakrishnan and J. M. Davis (2006). "Zebrafish and frog models of Mycobacterium marinum infection." Curr Protoc Microbiol **Chapter 10**: Unit 10B.12.

Couvreur, P. and C. Vauthier (2006). "Nanotechnology: intelligent design to treat complex disease." Pharm Res **23**(7): 1417-1450.

Daniel, T. M. (2006). "The history of tuberculosis." Respir Med **100**(11): 1862-1870.

Dannenberg, A. M. (2006). Pathogenesis of Human Pulmonary Tuberculosis: Insights from the Rabbit Model, ASM Press.

Dartois, V. (2014). "The path of anti-tuberculosis drugs: from blood to lesions to mycobacterial cells." Nat Rev Microbiol **12**(3): 159-167.

Davis, J. M., H. Clay, J. L. Lewis, N. Ghori, P. Herbomel and L. Ramakrishnan (2002). "Real-time visualization of mycobacterium-macrophage interactions leading to initiation of granuloma formation in zebrafish embryos." Immunity **17**(6): 693-702.

Davis, J. M. and L. Ramakrishnan (2009). "The Role of the Granuloma in Expansion and Dissemination of Early Tuberculous Infection." Cell **136**(1): 37-49.

Desjardins, M. and G. Griffiths (2003). "Phagocytosis: latex leads the way." Curr Opin Cell Biol **15**(4): 498-503.

Dheda, K., T. Gumbo, N. R. Gandhi, M. Murray, G. Theron, Z. Udwadia, G. B. Migliori and R. Warren (2014). "Global control of tuberculosis: from extensively drug-resistant to untreatable tuberculosis." The Lancet Respiratory Medicine **2**(4): 321-338.

DiMasi, J. A., R. W. Hansen and H. G. Grabowski (2003). "The price of innovation: new estimates of drug development costs." J Health Econ **22**(2): 151-185.

Dutt, M. and G. K. Khuller (2001). "Chemotherapy of Mycobacterium tuberculosis infections in mice with a combination of isoniazid and rifampicin entrapped in Poly (DL-lactide-co-glycolide) microparticles." J Antimicrob Chemother **47**(6): 829-835.

Egen, J. G., A. G. Rothfuchs, C. G. Feng, M. A. Horwitz, A. Sher and R. N. Germain (2011). "Intravital imaging reveals limited antigen presentation and T cell effector function in mycobacterial granulomas." Immunity **34**(5): 807-819.

Egen, J. G., A. G. Rothfuchs, C. G. Feng, N. Winter, A. Sher and R. N. Germain (2008). "Macrophage and T cell dynamics during the development and disintegration of mycobacterial granulomas." Immunity **28**(2): 271-284.

Ernst, J. D. (1998). "Macrophage receptors for Mycobacterium tuberculosis." Infect Immun **66**(4): 1277-1281.

Fenaroli, F., D. Westmoreland, J. Benjaminsen, T. Kolstad, F. M. Skjeldal, A. H. Meijer, M. van der Vaart, L. Ulanova, N. Roos, B. Nystrom, J. Hildahl and G. Griffiths (2014). "Nanoparticles as Drug Delivery System against Tuberculosis in Zebrafish Embryos: Direct Visualization and Treatment." ACS Nano **8**(7): 7014-7026.

Flannagan, R. S., G. Cosio and S. Grinstein (2009). "Antimicrobial mechanisms of phagocytes and bacterial evasion strategies." Nat Rev Microbiol **7**(5): 355-366.

Flynn, J. L., S. V. Capuano, D. Croix, S. Pawar, A. Myers, A. Zinovik and E. Klein (2003). "Non-human primates: a model for tuberculosis research." Tuberculosis **83**(1-3): 116-118.

Flynn, J. L., J. Chan and P. L. Lin (2011). "Macrophages and control of granulomatous inflammation in tuberculosis." Mucosal Immunol **4**(3): 271-278.

Fox, W., G. A. Ellard and D. A. Mitchison (1999). "Studies on the treatment of tuberculosis undertaken by the British Medical Research Council tuberculosis units, 1946-1986, with relevant subsequent publications." Int J Tuberc Lung Dis **3**(10 Suppl 2): S231-279.

Frohlich, E. (2012). "The role of surface charge in cellular uptake and cytotoxicity of medical nanoparticles." Int J Nanomedicine **7**: 5577-5591.

Gao, L. Y. and J. Manoranjan (2005). "Laboratory maintenance of Mycobacterium marinum." Curr Protoc Microbiol **Chapter 10**: Unit 10B.11.

Gaware, V. S., M. Hakerud, K. Leosson, S. Jonsdottir, A. Hogset, K. Berg and M. Masson (2013). "Tetraphenylporphyrin tethered chitosan based carriers for photochemical transfection." J Med Chem **56**(3): 807-819.

Gopal, M., N. Padayatchi, J. Z. Metcalfe and M. R. O'Donnell (2013). "Systematic review of clofazimine for the treatment of drug-resistant tuberculosis." Int J Tuberc Lung Dis **17**(8): 1001-1007.

Grant, S. S., B. B. Kaufmann, N. S. Chand, N. Haseley and D. T. Hung (2012). "Eradication of bacterial persisters with antibiotic-generated hydroxyl radicals." Proc Natl Acad Sci U S A **109**(30): 12147-12152.

Gref, R., Y. Minamitake, M. T. Peracchia, V. Trubetskoy, V. Torchilin and R. Langer (1994). "Biodegradable long-circulating polymeric nanospheres." Science **263**(5153): 1600-1603.

Griffiths, G., B. Nystrom, S. B. Sable and G. K. Khuller (2010). "Nanobead-based interventions for the treatment and prevention of tuberculosis." Nat Rev Microbiol **8**(11): 827-834.

Grosset, J. (2003). "Mycobacterium tuberculosis in the Extracellular Compartment: an Underestimated Adversary." Antimicrobial Agents and Chemotherapy **47**(3): 833-836.

Grosset, J. H., S. Tyagi, D. V. Almeida, P. J. Converse, S. Y. Li, N. C. Ammerman, W. R. Bishai, D. Enarson and A. Trebucq (2013). "Assessment of clofazimine activity in a second-line regimen for tuberculosis in mice." Am J Respir Crit Care Med **188**(5): 608-612.

Herbomel, P., B. Thisse and C. Thisse (1999). "Ontogeny and behaviour of early macrophages in the zebrafish embryo." Development **126**(17): 3735-3745.

Hu, Y., A. R. Coates and D. A. Mitchison (2006). "Sterilising action of pyrazinamide in models of dormant and rifampicin-tolerant Mycobacterium tuberculosis." Int J Tuberc Lung Dis **10**(3): 317-322.

Hunter, R. L. (2011). "Pathology of post primary tuberculosis of the lung: an illustrated critical review." Tuberculosis (Edinb) **91**(6): 497-509.

Hunter, R. L., C. Jagannath and J. K. Actor (2007). "Pathology of postprimary tuberculosis in humans and mice: contradiction of long-held beliefs." Tuberculosis (Edinb) **87**(4): 267-278.

Irwin, S. M., V. Gruppo, E. Brooks, J. Gilliland, M. Scherman, M. J. Reichlen, R. Leistikow, I. Kramnik, E. L. Nuermberger, M. I. Voskuil and A. J. Lenaerts (2014). "Limited activity of clofazimine as a single drug in a mouse model of tuberculosis exhibiting caseous necrotic granulomas." Antimicrob Agents Chemother **58**(7): 4026-4034.

Ishiyama, M., H. Tominaga, M. Shiga, K. Sasamoto, Y. Ohkura and K. Ueno (1996). "A combined assay of cell viability and in vitro cytotoxicity with a highly water-soluble tetrazolium salt, neutral red and crystal violet." Biol Pharm Bull **19**(11): 1518-1520.

Jarlier, V. and H. Nikaido (1994). "Mycobacterial cell wall: structure and role in natural resistance to antibiotics." FEMS Microbiol Lett **123**(1-2): 11-18.

Kalluru, R., F. Fenaroli, D. Westmoreland, L. Ulanova, A. Maleki, N. Roos, M. Paulsen Madsen, G. Koster, W. Egge-Jacobsen, S. Wilson, H. Roberg-Larsen, G. K. Khuller, A. Singh, B. Nystrom and G. Griffiths (2013). "Poly(lactide-co-glycolide)-rifampicin nanoparticles efficiently clear Mycobacterium bovis BCG infection in macrophages and remain membrane-bound in phago-lysosomes." J Cell Sci **126**(Pt 14): 3043-3054.

Kamaly, N., Z. Xiao, P. M. Valencia, A. F. Radovic-Moreno and O. C. Farokhzad (2012). "Targeted polymeric therapeutic nanoparticles: design, development and clinical translation." Chem Soc Rev **41**(7): 2971-3010.

Keswani, R. K., G. S. Yoon, S. Sud, K. A. Stringer and G. R. Rosania (2015). "A far-red fluorescent probe for flow cytometry and image-based functional studies of xenobiotic sequestering macrophages." Cytometry A **87**(9): 855-867.

Kjellsson, M. C., L. E. Via, A. Goh, D. Weiner, K. M. Low, S. Kern, G. Pillai, C. E. Barry, 3rd and V. Dartois (2012). "Pharmacokinetic evaluation of the penetration of antituberculosis agents in rabbit pulmonary lesions." Antimicrob Agents Chemother **56**(1): 446-457.

Koch, R. (1932). "Die Aetiologie der Tuberkulose." Klinische Wochenschrift **11**(12): 490-492.

Kumari, A. and S. K. Yadav (2011). "Cellular interactions of therapeutically delivered nanoparticles." Expert Opin Drug Deliv **8**(2): 141-151.

Langenau, D. M., A. A. Ferrando, D. Traver, J. L. Kutok, J.-P. D. Hezel, J. P. Kanki, L. I. Zon, A. T. Look and N. S. Trede (2004). "In vivo tracking of T cell development, ablation, and engraftment in transgenic zebrafish." Proceedings of the National Academy of Sciences of the United States of America **101**(19): 7369-7374.

Langer, R. and J. Folkman (1976). "Polymers for the sustained release of proteins and other macromolecules." Nature **263**(5580): 797-800.

Lechartier, B. and S. T. Cole (2015). "Mode of Action of Clofazimine and Combination Therapy with Benzothiazinones against Mycobacterium tuberculosis." Antimicrob Agents Chemother **59**(8): 4457-4463.

Leong, F. J., V. Dartois and T. Dick (2010). A Color Atlas of Comparative Pathology of Pulmonary Tuberculosis, Taylor & Francis.

Li, H. H., P. Huang, W. Dong, Z. Y. Zhu and D. Liu (2013). "[A brief history of zebrafish research--toward biomedicine]." Yi Chuan **35**(4): 410-420.

Liu, J., C. E. Barry, 3rd, G. S. Besra and H. Nikaido (1996). "Mycolic acid structure determines the fluidity of the mycobacterial cell wall." J Biol Chem **271**(47): 29545-29551.

Lugo-Villarino, G., K. M. Balla, D. L. Stachura, K. Banuelos, M. B. F. Werneck and D. Traver (2010). "Identification of dendritic antigen-presenting cells in the zebrafish." Proceedings of the National Academy of Sciences of the United States of America **107**(36): 15850-15855.

McDermott, W. (1958). "Microbial persistence." Yale J Biol Med **30**(4): 257-291.

McKinney, J. D., K. Honer zu Bentrup, E. J. Munoz-Elias, A. Miczak, B. Chen, W. T. Chan, D. Swenson, J. C. Sacchettini, W. R. Jacobs, Jr. and D. G. Russell (2000). "Persistence of Mycobacterium tuberculosis in macrophages and mice requires the glyoxylate shunt enzyme isocitrate lyase." Nature **406**(6797): 735-738.

Mehta, R. T. (1996). "Liposome encapsulation of clofazimine reduces toxicity in vitro and in vivo and improves therapeutic efficacy in the beige mouse model of disseminated Mycobacterium avium-M. intracellulare complex infection." Antimicrob Agents Chemother **40**(8): 1893-1902.

Meijer, A. H. and H. P. Spaink (2011). "Host-Pathogen Interactions Made Transparent with the Zebrafish Model." Current Drug Targets **12**(7): 1000-1017.

Mitchison, D. and G. Davies (2012). "The chemotherapy of tuberculosis: past, present and future." Int J Tuberc Lung Dis **16**(6): 724-732.

Nicolas, J., S. Mura, D. Brambilla, N. Mackiewicz and P. Couvreur (2013). "Design, functionalization strategies and biomedical applications of targeted biodegradable/biocompatible polymer-based nanocarriers for drug delivery." Chem Soc Rev **42**(3): 1147-1235.

Noordeen, S. K. (2016). "History of chemotherapy of leprosy." Clin Dermatol **34**(1): 32-36.

Padilla-Carlin, D. J., D. N. McMurray and A. J. Hickey (2008). "The guinea pig as a model of infectious diseases." Comp Med **58**(4): 324-340.

Panchagnula, R. and N. S. Thomas (2000). "Biopharmaceutics and pharmacokinetics in drug research." Int J Pharm **201**(2): 131-150.

Pandey, R. and G. K. Khuller (2004). "Polymer based drug delivery systems for mycobacterial infections." Curr Drug Deliv **1**(3): 195-201.

Pandey, R., A. Sharma, A. Zahoor, S. Sharma, G. K. Khuller and B. Prasad (2003). "Poly (DL-lactide-co-glycolide) nanoparticle-based inhalable sustained drug delivery system for experimental tuberculosis." J Antimicrob Chemother **52**(6): 981-986.

Pandey, R., A. Zahoor, S. Sharma and G. K. Khuller (2003). "Nanoparticle encapsulated antitubercular drugs as a potential oral drug delivery system against murine tuberculosis." Tuberculosis (Edinb) **83**(6): 373-378.

Parikka, M., M. M. Hammaren, S. K. Harjula, N. J. Halfpenny, K. E. Oksanen, M. J. Lahtinen, E. T. Pajula, A. Iivanainen, M. Pesu and M. Ramet (2012). "Mycobacterium marinum causes a latent infection that can be reactivated by gamma irradiation in adult zebrafish." PLoS Pathog **8**(9): e1002944.

Peterson, R. T. and C. A. Macrae (2012). "Systematic approaches to toxicology in the zebrafish." Annu Rev Pharmacol Toxicol **52**: 433-453.

Peyron, P., J. Vaubourgeix, Y. Poquet, F. Levillain, C. Botanch, F. Bardou, M. Daffe, J. F. Emile, B. Marchou, P. J. Cardona, C. de Chastellier and F. Altare (2008). "Foamy macrophages from tuberculous patients' granulomas constitute a nutrient-rich reservoir for M. tuberculosis persistence." PLoS Pathog **4**(11): e1000204.

Ramakrishnan, L. (2012). "Revisiting the role of the granuloma in tuberculosis." Nat Rev Immunol **12**(5): 352-366.

Rohde, K. H., D. F. Veiga, S. Caldwell, G. Balazsi and D. G. Russell (2012). "Linking the transcriptional profiles and the physiological states of Mycobacterium tuberculosis during an extended intracellular infection." PLoS Pathog **8**(6): e1002769.

Russell, D. G. (2001). "Mycobacterium tuberculosis: here today, and here tomorrow." Nat Rev Mol Cell Biol **2**(8): 569-577.

Russell, D. G. (2007). "Who puts the tubercle in tuberculosis?" Nat Rev Microbiol **5**(1): 39-47.

Russell, D. G. (2013). "The evolutionary pressures that have molded Mycobacterium tuberculosis into an infectious adjuvant." Curr Opin Microbiol **16**(1): 78-84.

Russell, D. G., P. J. Cardona, M. J. Kim, S. Allain and F. Altare (2009). "Foamy macrophages and the progression of the human tuberculosis granuloma." Nature Immunology **10**(9): 943-948.

Rustad, T. R., A. M. Sherrid, K. J. Minch and D. R. Sherman (2009). "Hypoxia: a window into Mycobacterium tuberculosis latency." Cell Microbiol **11**(8): 1151-1159.

Sacchettini, J. C., E. J. Rubin and J. S. Freundlich (2008). "Drugs versus bugs: in pursuit of the persistent predator Mycobacterium tuberculosis." Nat Rev Microbiol **6**(1): 41-52.

Sarkar, S. and M. R. Suresh (2011). "An overview of tuberculosis chemotherapy - a literature review." J Pharm Pharm Sci **14**(2): 148-161.

Savoia, D. (2015). "New antimicrobial approaches: reuse of old drugs." Curr Drug Targets.

Schliehe, C., C. Schliehe, M. Thiry, U. I. Tromsdorf, J. Hentschel, H. Weller and M. Groettrup (2011). "Microencapsulation of inorganic nanocrystals into PLGA microsphere vaccines enables their intracellular localization in dendritic cells by electron and fluorescence microscopy." Journal of Controlled Release **151**(3): 278-285.

Schluger, N. W. (2005). "The pathogenesis of tuberculosis: the first one hundred (and twenty-three) years." Am J Respir Cell Mol Biol **32**(4): 251-256.

Sharma, A., R. Pandey, S. Sharma and G. K. Khuller (2004). "Chemotherapeutic efficacy of poly (DL-lactide-co-glycolide) nanoparticle encapsulated antitubercular drugs at sub-therapeutic dose against experimental tuberculosis." Int J Antimicrob Agents **24**(6): 599-604.

Sharma, A., S. Sharma and G. K. Khuller (2004). "Lectin-functionalized poly (lactide-co-glycolide) nanoparticles as oral/aerosolized antitubercular drug carriers for treatment of tuberculosis." J Antimicrob Chemother **54**(4): 761-766.

Shim, T. S. and K. W. Jo (2013). "Medical treatment of pulmonary multidrug-resistant tuberculosis." Infect Chemother **45**(4): 367-374.

Shive, M. S. and J. M. Anderson (1997). "Biodegradation and biocompatibility of PLA and PLGA microspheres." Adv Drug Deliv Rev **28**(1): 5-24.

Sturgill-Koszycki, S., P. H. Schlesinger, P. Chakraborty, P. L. Haddix, H. L. Collins, A. K. Fok, R. D. Allen, S. L. Gluck, J. Heuser and D. G. Russell (1994). "Lack of acidification in Mycobacterium phagosomes produced by exclusion of the vesicular proton-ATPase." Science **263**(5147): 678-681.

Sun, F., C. Sui, L. Teng, X. Liu, L. Teng, Q. Meng and Y. Li (2010). "Studies on the preparation, characterization and pharmacological evaluation of tolterodine PLGA microspheres." Int J Pharm **397**(1-2): 44-49.

Swaim, L. E., L. E. Connolly, H. E. Volkman, O. Humbert, D. E. Born and L. Ramakrishnan (2006). "Mycobacterium marinum infection of adult zebrafish causes caseating granulomatous tuberculosis and is moderated by adaptive immunity." Infect Immun **74**(11): 6108-6117.

Swanson, R. V., J. Adamson, C. Moodley, B. Ngcobo, N. C. Ammerman, A. Dorasamy, S. Moodley, Z. Mgaga, A. Tapley, L. A. Bester, S. Singh, J. H. Grosset and D. V. Almeida (2015). "Pharmacokinetics and pharmacodynamics of clofazimine in a mouse model of tuberculosis." Antimicrob Agents Chemother **59**(6): 3042-3051.

Szumowski, J. D., K. N. Adams, P. H. Edelstein and L. Ramakrishnan (2013). "Antimicrobial efflux pumps and Mycobacterium tuberculosis drug tolerance: evolutionary considerations." Curr Top Microbiol Immunol **374**: 81-108.

Tobin, D. M. and L. Ramakrishnan (2008). "Comparative pathogenesis of Mycobacterium marinum and Mycobacterium tuberculosis." Cellular Microbiology **10**(5): 1027-1039.

Tonjum, T., D. B. Welty, E. Jantzen and P. L. Small (1998). "Differentiation of Mycobacterium ulcerans, M. marinum, and M. haemophilum: mapping of their relationships to M. tuberculosis by fatty acid profile analysis, DNA-DNA hybridization, and 16S rRNA gene sequence analysis." J Clin Microbiol **36**(4): 918-925.

Tyagi, S., N. C. Ammerman, S. Y. Li, J. Adamson, P. J. Converse, R. V. Swanson, D. V. Almeida and J. H. Grosset (2015). "Clofazimine shortens the duration of the first-line treatment regimen for experimental chemotherapy of tuberculosis." Proc Natl Acad Sci U S A **112**(3): 869-874.

Van Deun, A., A. K. Maug, M. A. Salim, P. K. Das, M. R. Sarker, P. Daru and H. L. Rieder (2010). "Short, highly effective, and inexpensive standardized treatment of multidrug-resistant tuberculosis." Am J Respir Crit Care Med **182**(5): 684-692.

Van Rensburg, C. E., G. K. Joone, J. F. O'Sullivan and R. Anderson (1992). "Antimicrobial activities of clofazimine and B669 are mediated by lysophospholipids." Antimicrob Agents Chemother **36**(12): 2729-2735.

Verma, I. and A. Grover (2009). "Antituberculous vaccine development: a perspective for the endemic world." Expert Rev Vaccines **8**(11): 1547-1553.

Verma, R. K., W. A. Germishuizen, M. P. Motheo, A. K. Agrawal, A. K. Singh, M. Mohan, P. Gupta, U. D. Gupta, M. Cholo, R. Anderson, P. B. Fourie and A. Misra (2013). "Inhaled microparticles containing clofazimine are efficacious in treatment of experimental tuberculosis in mice." Antimicrob Agents Chemother **57**(2): 1050-1052.

Via, L. E., P. L. Lin, S. M. Ray, J. Carrillo, S. S. Allen, S. Y. Eum, K. Taylor, E. Klein, U. Manjunatha, J. Gonzales, E. G. Lee, S. K. Park, J. A. Raleigh, S. N. Cho, D. N.

McMurray, J. L. Flynn and C. E. Barry, 3rd (2008). "Tuberculous granulomas are hypoxic in guinea pigs, rabbits, and nonhuman primates." Infect Immun **76**(6): 2333-2340.

Vibe, C. B., F. Fenaroli, D. Pires, S. R. Wilson, V. Bogoeva, R. Kalluru, M. Speth, E. Anes, G. Griffiths and J. Hildahl (2015). "Thioridazine in PLGA nanoparticles reduces toxicity and improves rifampicin therapy against mycobacterial infection in zebrafish." Nanotoxicology: 1-9.

Wang, J. J., Z. W. Zeng, R. Z. Xiao, T. Xie, G. L. Zhou, X. R. Zhan and S. L. Wang (2011). "Recent advances of chitosan nanoparticles as drug carriers." Int J Nanomedicine **6**: 765-774.

Wayne, L. G. (1976). "Dynamics of submerged growth of Mycobacterium tuberculosis under aerobic and microaerophilic conditions." Am Rev Respir Dis **114**(4): 807-811.

Wayne, L. G. and H. A. Sramek (1994). "Metronidazole is bactericidal to dormant cells of Mycobacterium tuberculosis." Antimicrob Agents Chemother **38**(9): 2054-2058.

Wells, W. F., H. L. Ratcliffe and C. Crumb (1948). "On the mechanics of droplet nuclei infection: II. Quantitative experimental air-borne tuberculosis in rabbits." American Journal of Epidemiology **47**(1): 11-28.

White, R., K. Rose and L. Zon (2013). "Zebrafish cancer: the state of the art and the path forward." Nat Rev Cancer **13**(9): 624-636.

White, R. M., A. Sessa, C. Burke, T. Bowman, J. LeBlanc, C. Ceol, C. Bourque, M. Dovey, W. Goessling, C. E. Burns and L. I. Zon (2008). "Transparent adult zebrafish as a tool for in vivo transplantation analysis." Cell Stem Cell **2**(2): 183-189.

WHO (2013). "WHO (2013) Global Tuberculosis Report 2013 (Geneva:WHO Press)

".

Wyart, C. and F. Del Bene (2011). "Let there be light: zebrafish neurobiology and the optogenetic revolution." Rev Neurosci **22**(1): 121-130.

Xu, J., Y. Lu, L. Fu, H. Zhu, B. Wang, K. Mdluli, A. M. Upton, H. Jin, M. Zheng, W. Zhao and P. Li (2012). "In vitro and in vivo activity of clofazimine against Mycobacterium tuberculosis persisters." Int J Tuberc Lung Dis **16**(8): 1119-1125.

Yajko, D. M., J. J. Madej, M. V. Lancaster, C. A. Sanders, V. L. Cawthon, B. Gee, A. Babst and W. K. Hadley (1995). "Colorimetric method for determining MICs of antimicrobial agents for Mycobacterium tuberculosis." J Clin Microbiol **33**(9): 2324-2327.

Yano, T., S. Kassovska-Bratinova, J. S. Teh, J. Winkler, K. Sullivan, A. Isaacs, N. M. Schechter and H. Rubin (2011). "Reduction of clofazimine by mycobacterial type 2 NADH:quinone oxidoreductase: a pathway for the generation of bactericidal levels of reactive oxygen species." J Biol Chem **286**(12): 10276-10287.

Yoon, G. S., S. Sud, R. K. Keswani, J. Baik, T. J. Standiford, K. A. Stringer and G. R. Rosania (2015). "Phagocytosed Clofazimine Biocrystals Can Modulate Innate Immune Signaling by Inhibiting TNFalpha and Boosting IL-1RA Secretion." Mol Pharm **12**(7): 2517-2527.

Yoshida, A., M. Matumoto, H. Hshizume, Y. Oba, T. Tomishige, H. Inagawa, C. Kohchi, M. Hino, F. Ito, K. Tomoda, T. Nakajima, K. Makino, H. Terada, H. Hori and G.-I. Soma (2006). "Selective delivery of rifampicin incorporated into poly(dl-lactic-co-glycolic) acid microspheres after phagocytotic uptake by alveolar macrophages, and the killing effect against intracellular Mycobacterium bovis Calmette–Guérin." Microbes and Infection **8**(9–10): 2484-2491.

Zhang, Y. (2014). "Persisters, persistent infections and the Yin–Yang model." Emerging Microbes & Infections **3**(1): e3.

Zhang, Y., W. W. Yew and M. R. Barer (2012). "Targeting persisters for tuberculosis control." Antimicrob Agents Chemother **56**(5): 2223-2230.

Zumla, A., P. Nahid and S. T. Cole (2013). "Advances in the development of new tuberculosis drugs and treatment regimens." Nat Rev Drug Discov **12**(5): 388-404.

Zumla, A. I., S. H. Gillespie, M. Hoelscher, P. P. J. Philips, S. T. Cole, I. Abubakar, T. D. McHugh, M. Schito, M. Maeurer and A. J. Nunn (2014). "New antituberculosis drugs, regimens, and adjunct therapies: needs, advances, and future prospects." The Lancet Infectious Diseases **14**(4): 327-340.